

4 FSRU Chlorine Discharge

4.1 Model Set-up

The FSRU produces chlorine in the seawater used for cooling and other purposes by electrolysis of the sodium chloride in the seawater drawn into the vessel. There is rapid decay of the chlorine as it passes through the pipes and heat exchangers. At the discharge ports, the chlorine level will be a maximum of 100 µg/L. Almost all of the chlorine will actually be replaced by bromine (CEE, 2018c), but by convention, the modelling below is undertaken assuming the discharge still contains the residual chlorine.

The same 28-day simulations discussed in Chapter 3 was used to assess the concentration of chlorine at the seabed. A conservative numerical tracer with a concentration of 100 µg/L in the pre-diluted discharge was injected into the far-field mapping of the cool water discharge. This was repeated for peak and average FSRU discharge rates.

Consistent with CSIRO's report (Batley and Simpson, 2019), CEE has adopted CPO (chlorine produced oxidants) guideline value of 6 µg Cl/L for 99% species protection for assessing potential impacts at Crib Point where strong tidal reversals in currents result in intermittent exposure of biota to the dispersing discharge.

Contours of chlorine concentrations of less than 6 µg/L have been illustrated in the sections that follow to provide a context for the shape and extent of the more diluted portions of the plume.

4.2 Model Results

4.2.1 Peak FSRU Discharge

Median chlorine concentration at the seabed was less than 2 µg/L (Figure 4.1). The 95th percentile map (Figure 4.2) shows a patch on the seabed (approx. 200 m N-S by 150m E-W) where the discharge plume plunges and chlorine concentrations at the seabed are higher than 6 µg/L.

The time series and 24-hour time-weighted average timeseries of chlorine concentration at locations near the FSRU (Figure 4.3 and Figure 4.4 respectively) show intermittent periods of chlorine concentrations above 6 µg/L and time-averaged concentrations of less than 2 µg/L, below the guideline value of 6 µg/L recommended by the CSIRO (illustrated by the green line). In addition, the results show no cumulative build-up of chlorine concentrations in the project area over the simulation period.

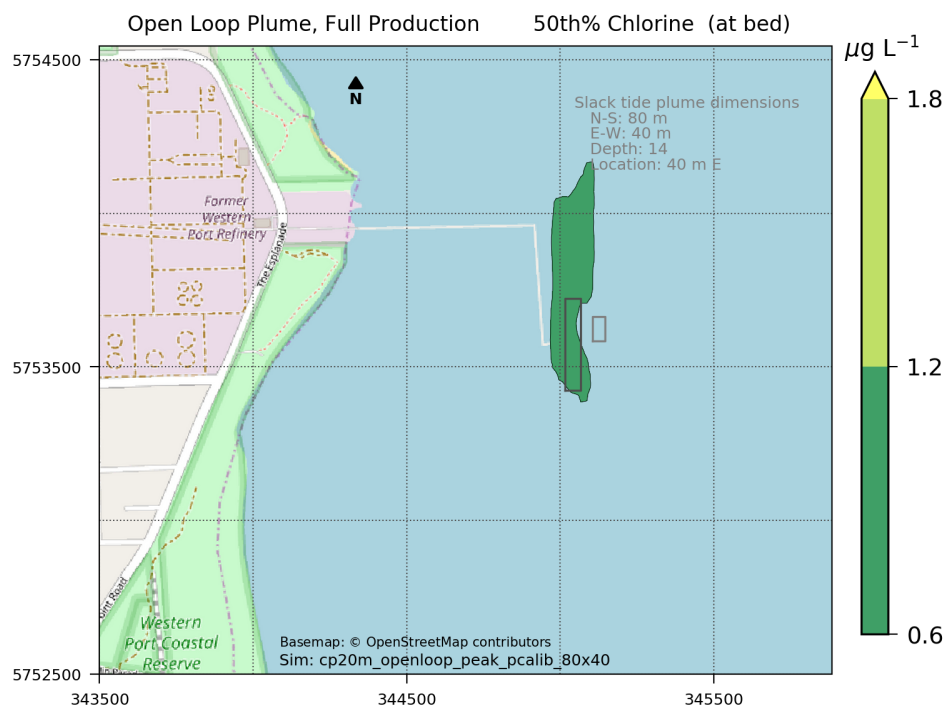


Figure 4.1 50th percentile of chlorine concentration at the seabed during over a 28-day simulation at peak FSRU discharge.

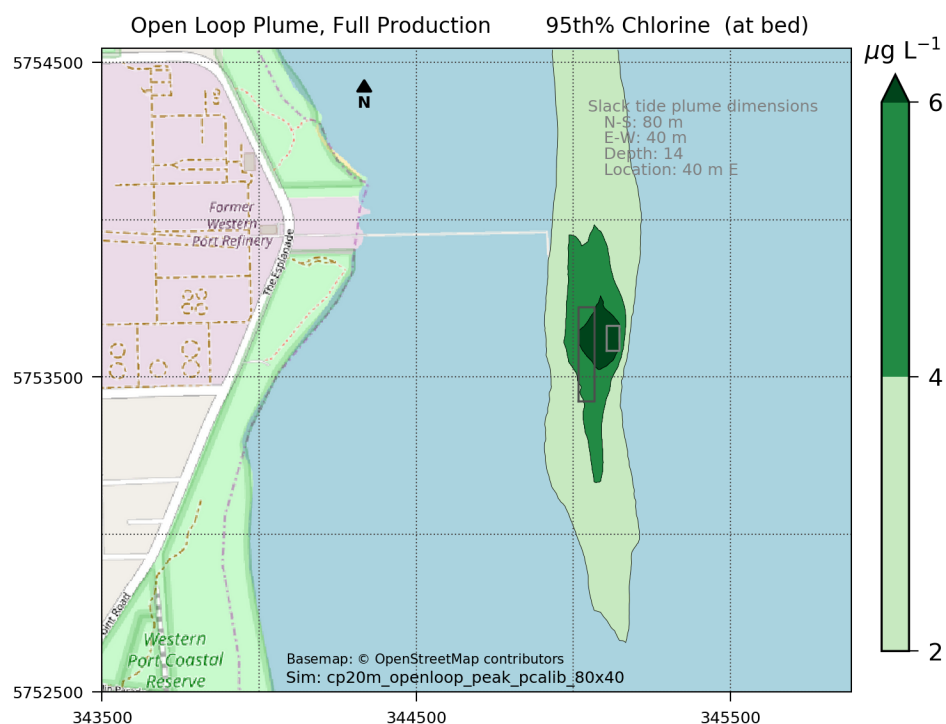


Figure 4.2 95th percentile of chlorine concentration at the seabed during over a 28-day simulation at peak FSRU discharge.

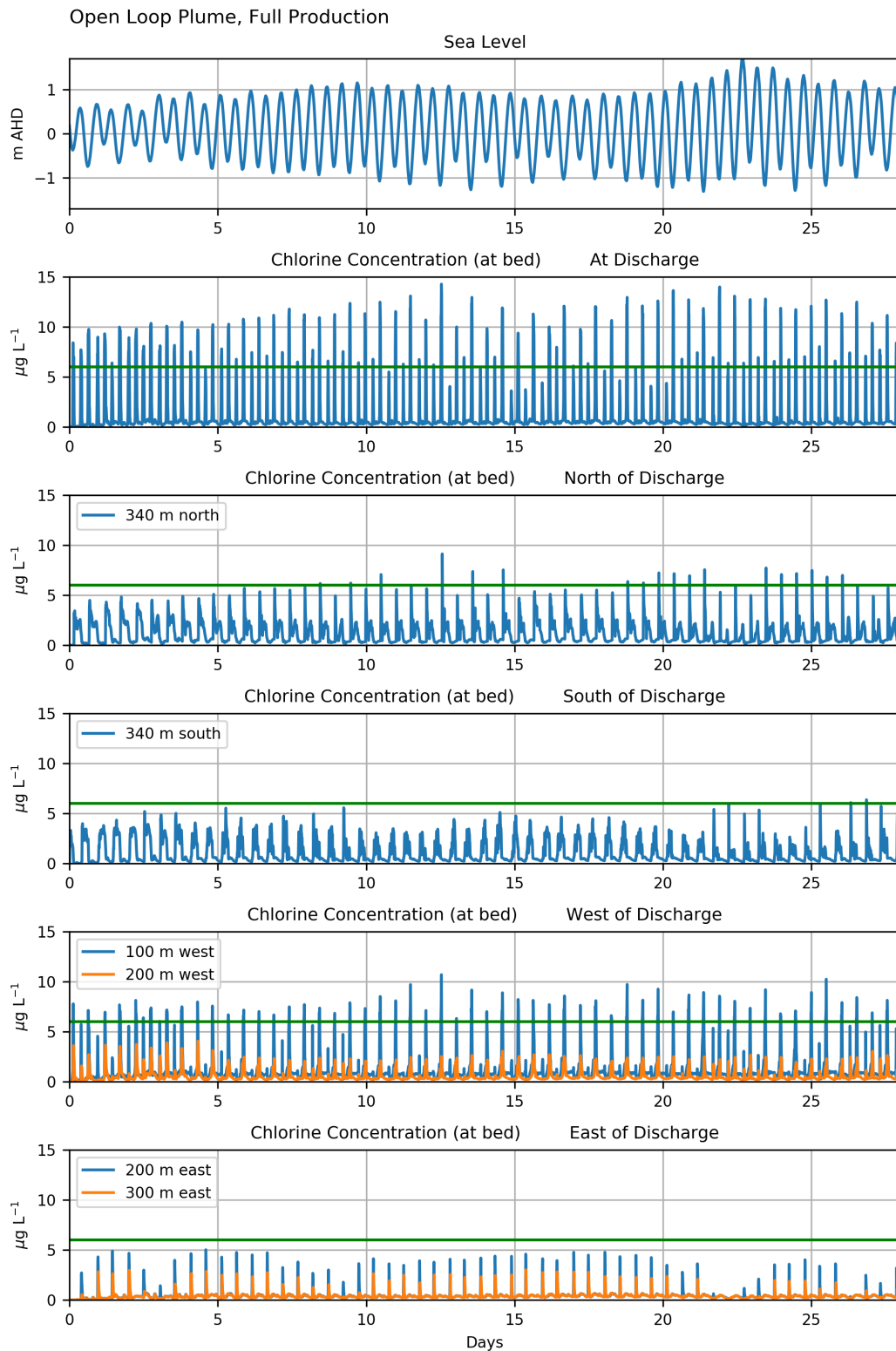


Figure 4.3 Time series of sea level (top panel) and (running down the page) chlorine concentration at the seabed below the plume and north, south, west and east of the FSRU during peak discharge.

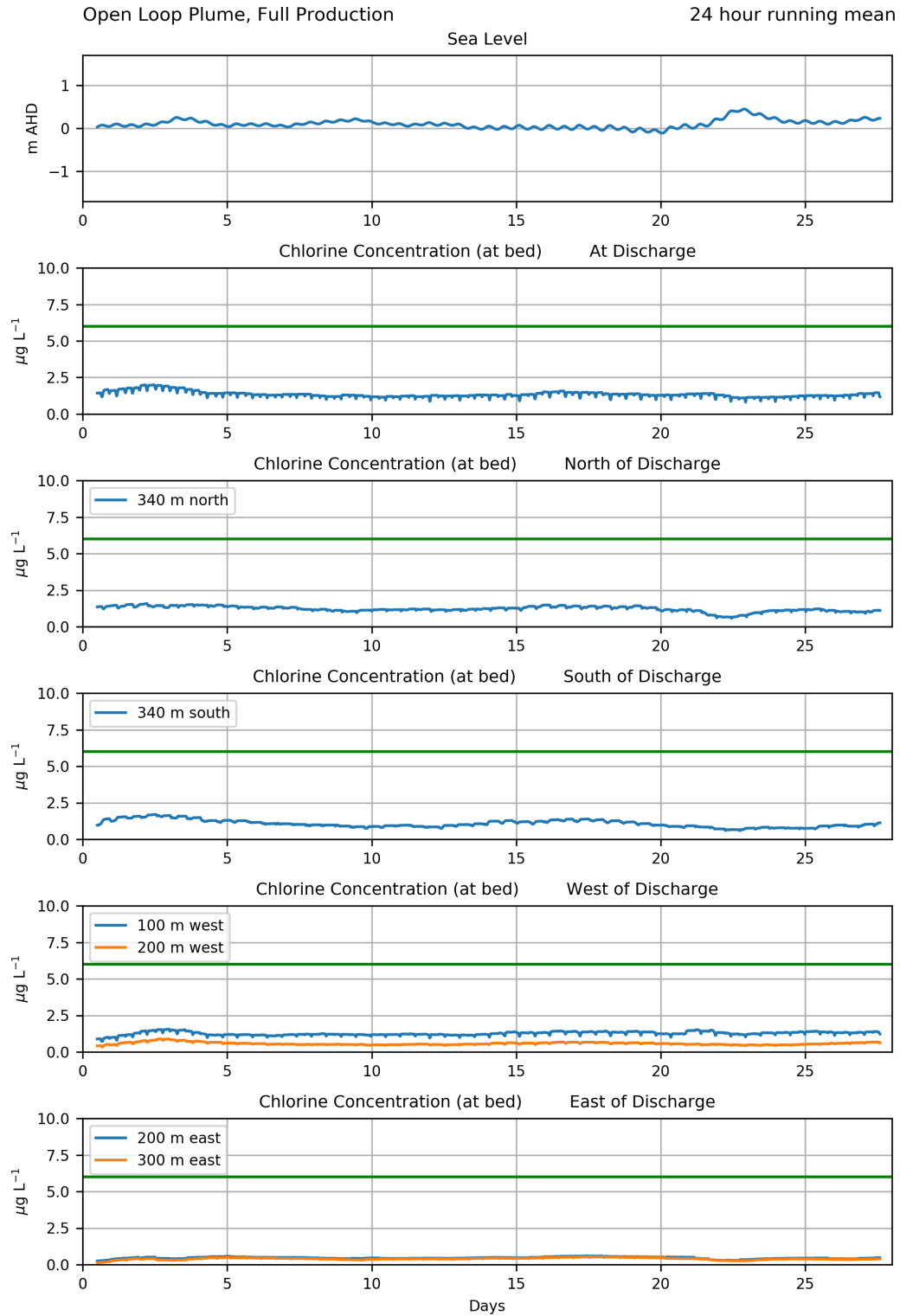


Figure 4.4 24-hr moving average time series of sea level (top panel) and (running down the page) chlorine concentration at the seabed below the plume and north, south, west and east of the FSRU during peak discharge.

4.2.2 Average FSRU Discharge

For a reduced FSRU discharge rate of two-thirds of that at peak production (i.e. $3.6 \text{ m}^3/\text{s}$) the median of chlorine concentration at the seabed were less than 2 µg/L (Figure 4.5). The 95th

percentile map shows concentrations above 6 $\mu\text{g/L}$ occur only in a small area of less than 100 m by 100 m below the discharge ports (Figure 4.6).

The 24-hour time-weighted average timeseries of chlorine concentration at locations near the FSRU (Figure 4.7) time-averaged concentrations of less than 2 $\mu\text{g/L}$, below the guideline value of 6 $\mu\text{g/L}$ recommended by the CSIRO (illustrated by the green line). In addition, the results show no cumulative build-up of chlorine concentrations in the project area over the simulation period.

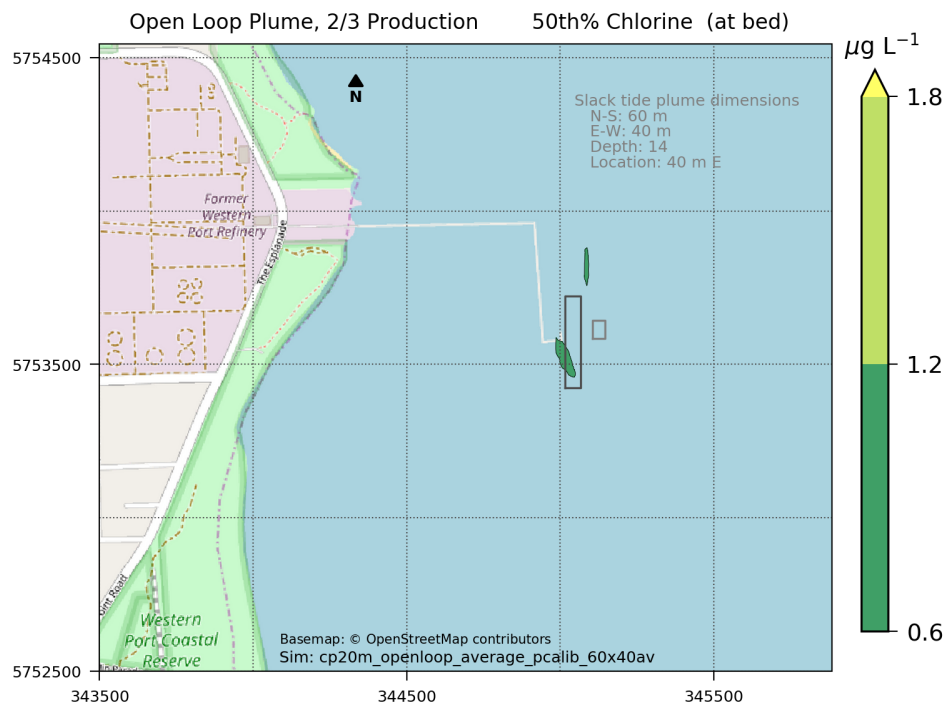


Figure 4.5 50th percentile of chlorine concentration at the seabed during over a 28-day simulation at average FSRU discharge.

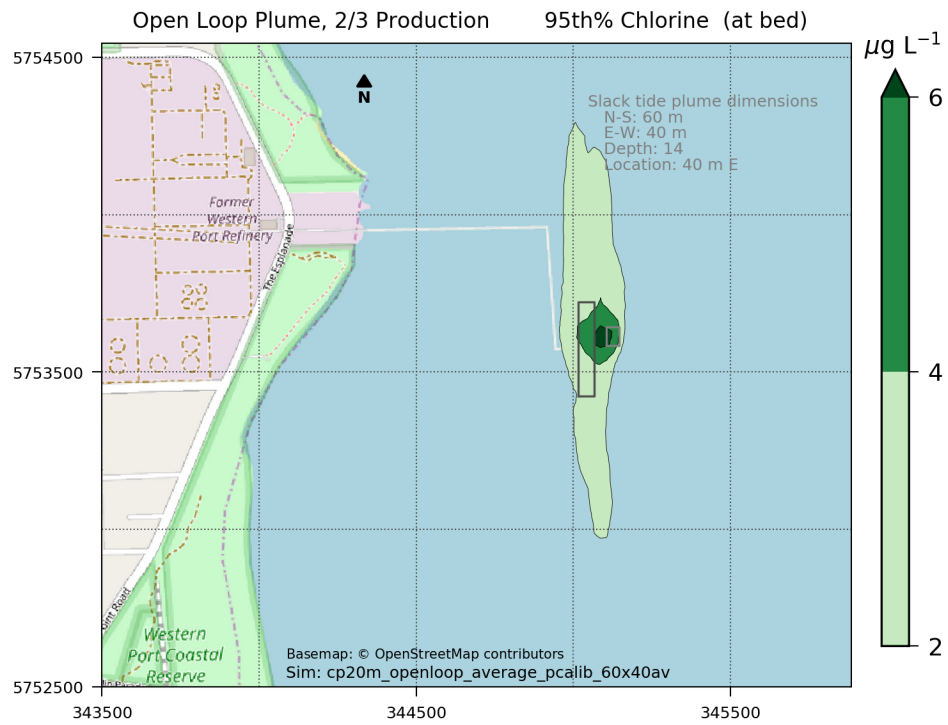


Figure 4.6 95th percentile of chlorine concentration at the seabed during over a 28-day simulation at average FSRU discharge.

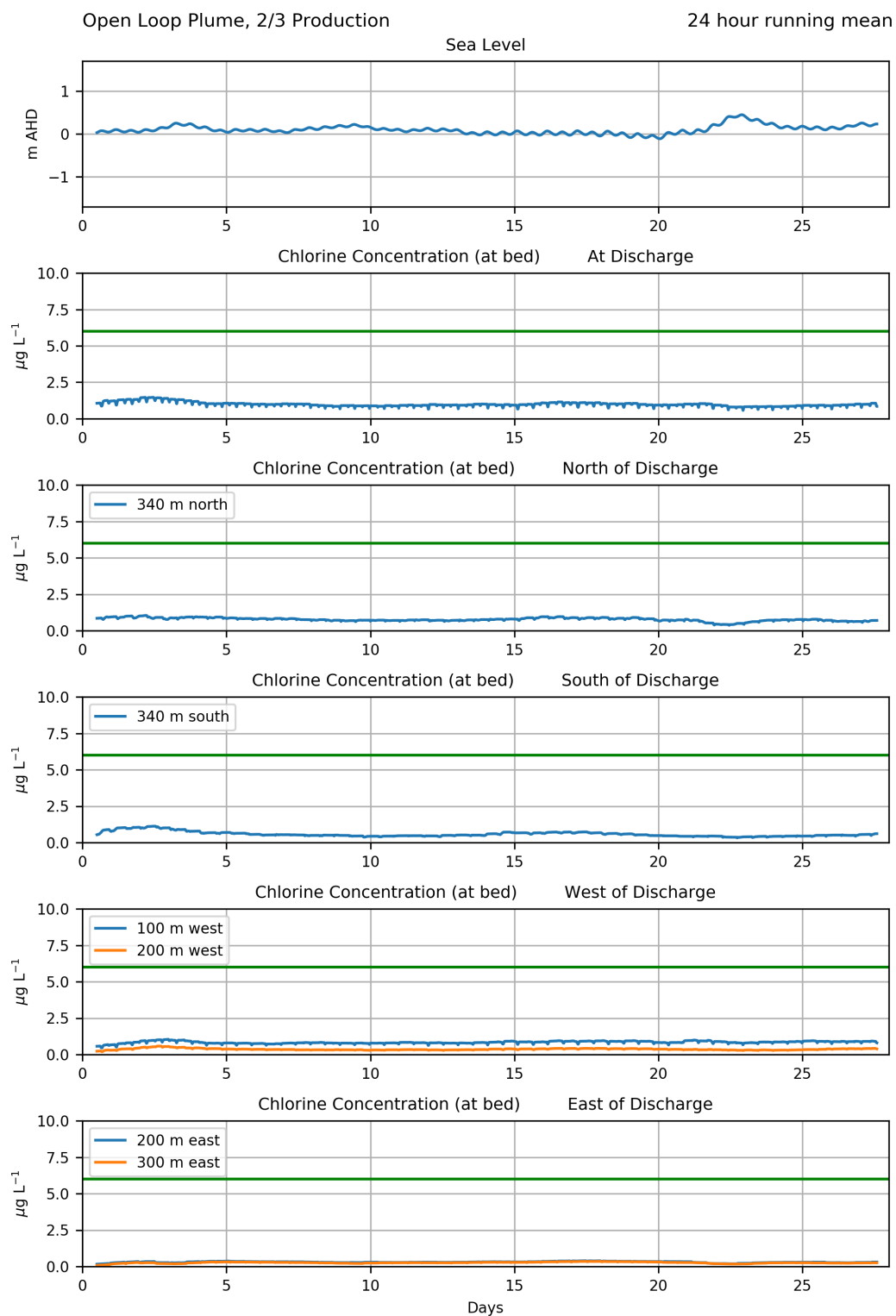


Figure 4.7 24-hr moving average time series of sea level (top panel) and (running down the page) chlorine concentration at the seabed below the plume and north, south, west and east of the FSRU during average discharge.

4.3 Chlorine Outcomes

The FSRU produces chlorine in the seawater used for cooling and other purposes by electrolysis of the sodium chloride in the seawater drawn into the vessel. There is rapid decay of the chlorine as it passes through the pipes and heat exchangers. At the discharge ports, the chlorine level will be a maximum concentration of 100 µg/L. Over the same March 2019 28-day simulation for cool-water discharge the concentrations of chlorine at the seabed were assessed.

For the great majority of the time the chlorine is dispersed and diluted to concentrations less than 6 µg/L in the vicinity of the FSRU and lower concentrations beyond the project area.

The modelling indicated for the peak FSRU discharge rate of 5.4 m³/s:

- For 5% of the time there is a patch on the seabed (approx. 200 m N-S by 150m E-W) where the discharge plume plunges and chlorine concentrations at the seabed are higher than 6 µg/L; and

The modelling indicated for average discharge of 3.6 m³/s:

- For 5% of the time there is a patch on the seabed (approx. 50 m N-S by 50m E-W) where the discharge plume plunges and chlorine concentrations at the seabed are higher than 6 µg/L.

These percentile results reflect short-duration concentration peaks. The time-weighted average chlorine concentration at the seabed near the FSRU is below 2 µg/L which is below the guideline value of 6 µg/L recommended by CSIRO.

Cumulative Impacts

For most of the time the chlorine is dispersed and diluted to concentrations less than 6 µg/L in the vicinity of the FSRU and to lower concentrations beyond the project area. Because there is rapid chemical change, and because of exchange of waters between the project area and the remainder of the bay (and ultimately with the ocean), the cumulative effects of the FSRU on chlorine concentrations in the project area and more broadly over the remainder of the bay are expected to be negligible. The chlorine created by electrolysis of seawater returns to the chloride (as part of sodium chloride) in seawater in a day or so, so there is no long-term accumulation of chlorine in the bay (CEE 2018d).

5 FSRU Intake of Plankton

5.1 Model Set-up

5.1.1 Particle Release

The model was applied to assess the fate of particles that were released from different zones within WPB. The selected zones are illustrated in Figure 5.1. Note that Zone 1 immediately around the FSRU was included as a test case for the model configuration only and was not used for the analysis. In addition, Zone 4 was not defined in the set-up.

The model was run for a spin-up period of 10 days prior to the release of particles in each of the zones. The particles were configured to be neutrally buoyant and spaced evenly within each zone with one particle in each corner of a 50 m by 50 m cartesian mesh. The number of particles released ranged from 3137 to 63921 depending on the size of the zone (i.e. the larger the zones started with more particles than the smaller zones). The particles were tracked for a range of initial starting conditions that are listed below. The mixed distributions were achieved by running the model for two tidal cycles after a uniform distribution of particles at the surface.

- Uniform distribution at the surface during a spring rising tide (all zones);
- Mixed distribution (lateral and vertical) during spring rising tide (all zones);
- Mixed distribution (lateral and vertical) during spring falling tide (all zones);
- Uniform distribution at the seabed released during a spring rising tide (zones 2, 3 and 7);
- Uniform distribution at the surface released during a neap rising tide (zones 2, 3 and 7);
- Mixed distribution (lateral and vertical) during neap rising tide (zones 2, 3 and 7); and
- Mixed distribution (lateral and vertical) during neap falling tide (zone 2, 3 and 7).

The tracking period was for 28 days starting in 11 November 2018 (see Section 2.2.4) with the position of each particle recorded every 10 minutes. To allow for longer run times, the 50 x 50 m model grid was used for the particle release and capture simulations. An additional simulation period at a different time of year (June 2018) was undertaken as part of a model sensitivity analysis (see Section 9.2.2)

Figure 5.2 provides an example of the movement of particles released in zone 2 as the simulation progresses.

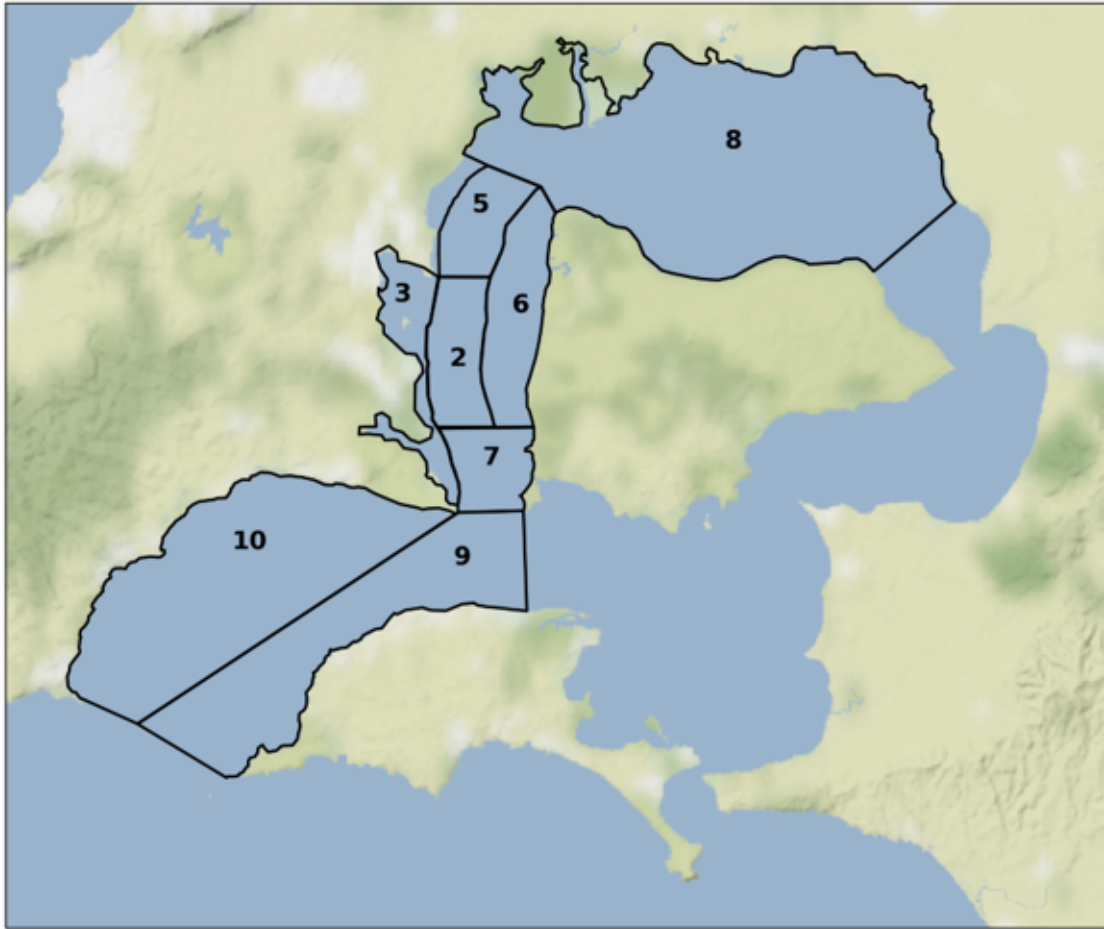


Figure 5.1 Particle release zones based on description from CEE (pers. comms, 2019).

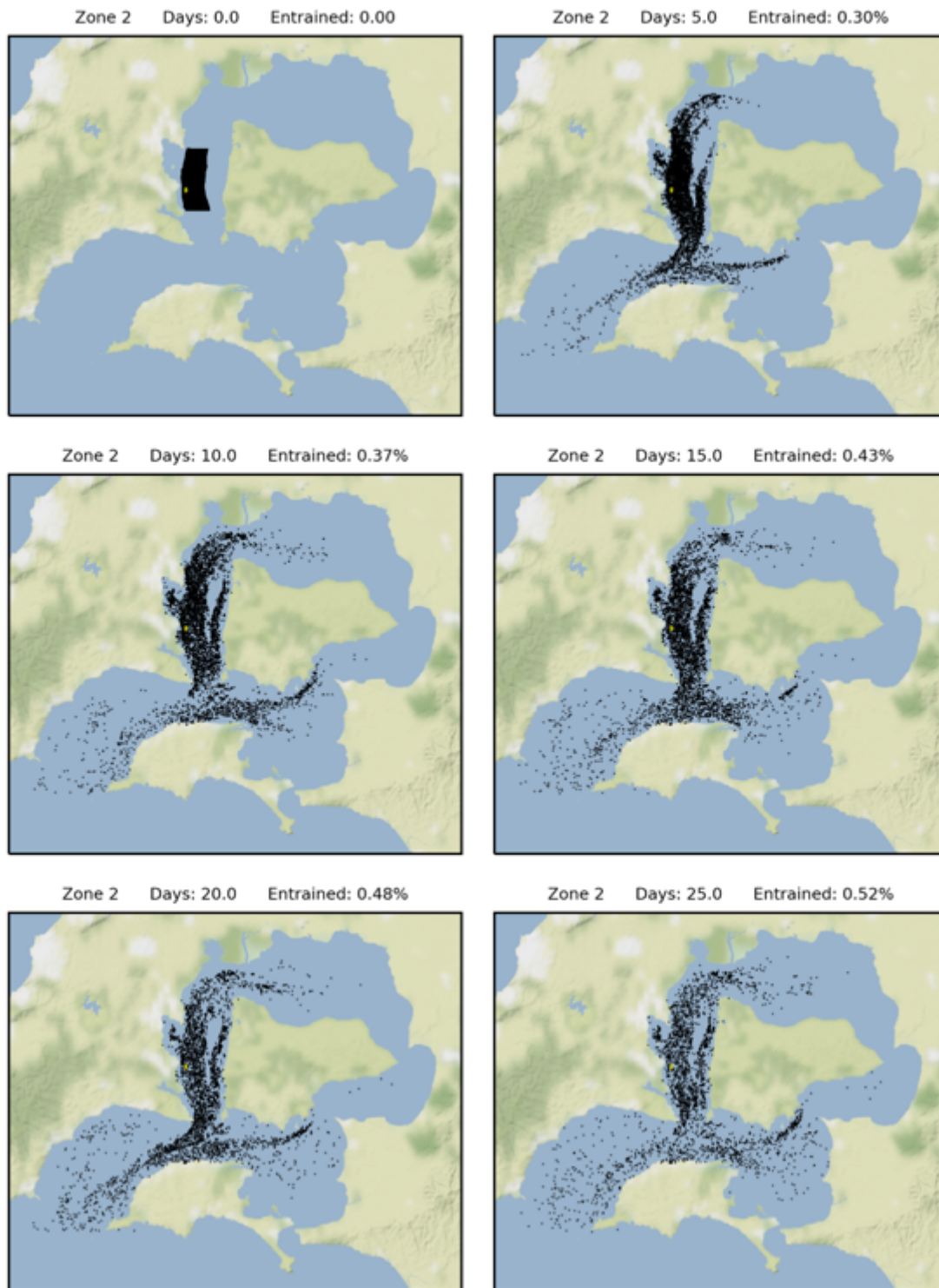


Figure 5.2 Distribution of Zone 2 particles over 25 days.

5.1.2 Particle Entrainment into FSRU Intake

The FSRU intake chests are assumed to have a north-south length of 14.5 m, depth of 3 m (from 5.5 to 8.5 m below the water surface) and located on the port and starboard side 42.5

to 57 m from stern of the FSRU vessel (CEE, pers. comms, 2019). The dimensions of the entrainment volume associated with each sea chest were determined as a function of the current speed as shown in Table 5.1 (CEE, pers. comms, 2019).

These dimensions were applied to determine the number of released particles from each zone that travelled into the intake entrainment area over the duration of the simulation. Particles that pass through this zone are added to the count of entrained particles and removed from further analysis. This process was repeated for each of the initial distributions and times of the tide cycle.

Table 5.1 Dimensions of entrainment zone from the FSRU sea chest. Vertical distances are from the surface, lateral distances are from the side of the vessel.

Current speed, m/s	Top of entry zone, m	Base of entry zone, m	Width of entry zone, m
0.03	3	11	21.7
0.1	4	10	8.7
0.15	4.1	9.9	6.0
0.2	4.3	9.7	4.8
0.3	4.7	9.3	3.8
0.4	4.9	9.1	3.1
0.5	5.1	8.9	2.7
0.6	5.2	8.8	2.5
0.7	5.4	8.6	2.3
0.8	5.5	8.5	2.2
0.9	5.5	8.5	1.9
1	5.5	8.5	1.7

5.2 Model Results

5.2.1 FSRU Entrainment

The simulation results are discussed below in terms of the highest entrainment percentage (i.e. $100 \times \text{number captured} / \text{number released}$) for a peak FSRU intake rate of $5.2 \text{ m}^3/\text{s}$ and average FSRU intake rate of $3.5 \text{ m}^3/\text{s}$ recorded over 28-day simulations.

The highest level of entrainment into the FSRU after 28 days of simulations are shown in Table 5.2 for peak and average intake rates. These values are mapped in Figure 5.3 and Figure 5.4.

Timeseries for peak production are shown in Figure 5.5 to Figure 5.12. The timeseries include a running count of the percentage that is entrained into the FSRU, the percentage that is flushed out to the ocean, and the percentage that remains in the zone. The percentage not accounted for are elsewhere in the bay.

The highest entrainment into the FSRU of 0.75% occurs for zone 2 particles. For the zones either side of the main channel at Crib Point, the closer zone 3 had a higher entrainment of 0.41%, compared to 0.10% for zone 6. This indicates the disconnect between the main and eastern channel of the north arm that is created by the shallow bank running north-south between zone 2 and 6.

Zones 5 and 7, immediately north and south of zone 2, have similar entrainment of 0.27% and 0.37% respectively. Further north for the tidal flats of zone 8, the entrainment decreases to 0.13%. Zones 9 and 10 to the south have the lowest entrainment of 0.05% and 0.06% respectively. Hydrodynamically these regions are in the western entrance to the bay and exchange directly and rapidly with Bass Strait.

Using the highest entrainment rates during peak production there are 0.38% of particles released in the north arm that are entrained into the FSRU during the 28-day simulation. This is equivalent to approximately 0.014 % of particles being entrained each day. These numbers reduce to 0.26% over 28 days, or 0.009% per day at average production rate.

During peak production 35% of the particles released in the North Arm are flushed from the bay in 28 days, which is equivalent to 1.2% per day, a rate this is approximately 85 times greater than entrainment of particles into the FSRU.

For the range of simulations that were undertaken an average of 81% of the entrainment into the FSRU occurred through the starboard (eastern) sea chest. This occurs because there is greater flow past the eastern side of the vessel that transports more particles through the entrainment window. A starboard-side bias of less than 77% only occurred consistently for entrainment of those particles originating from zone 5.

The entrainment results from each simulation are tabulated in Appendix C.

Table 5.2 Percentage of particles entrained during 28 days at peak and annual average intake (maximum percentage from scenarios is shown here).

Zone	Entrained into FSRU after 28 days (%)	
	During Peak FSRU Production	During Annual Average FSRU Production
2	0.75	0.47
3	0.41	0.29
5	0.27	0.20
6	0.10	0.07
7	0.37	0.25
8	0.13	0.09
9	0.05	0.03
10	0.06	0.04

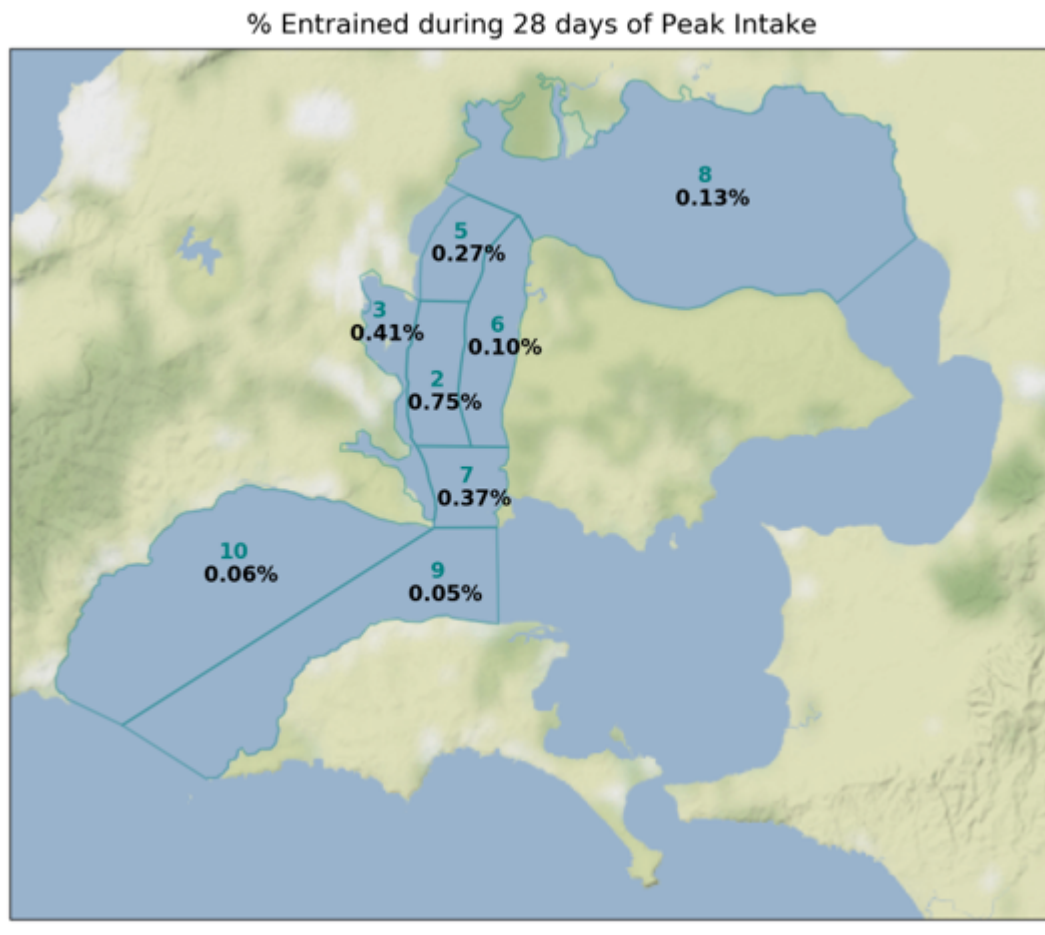


Figure 5.3 Percentage of particles entrained during 28 days at peak intake (maximum percentage from scenarios is shown here). The average for North Arm at peak production is approximately 0.38 % per 28 days.

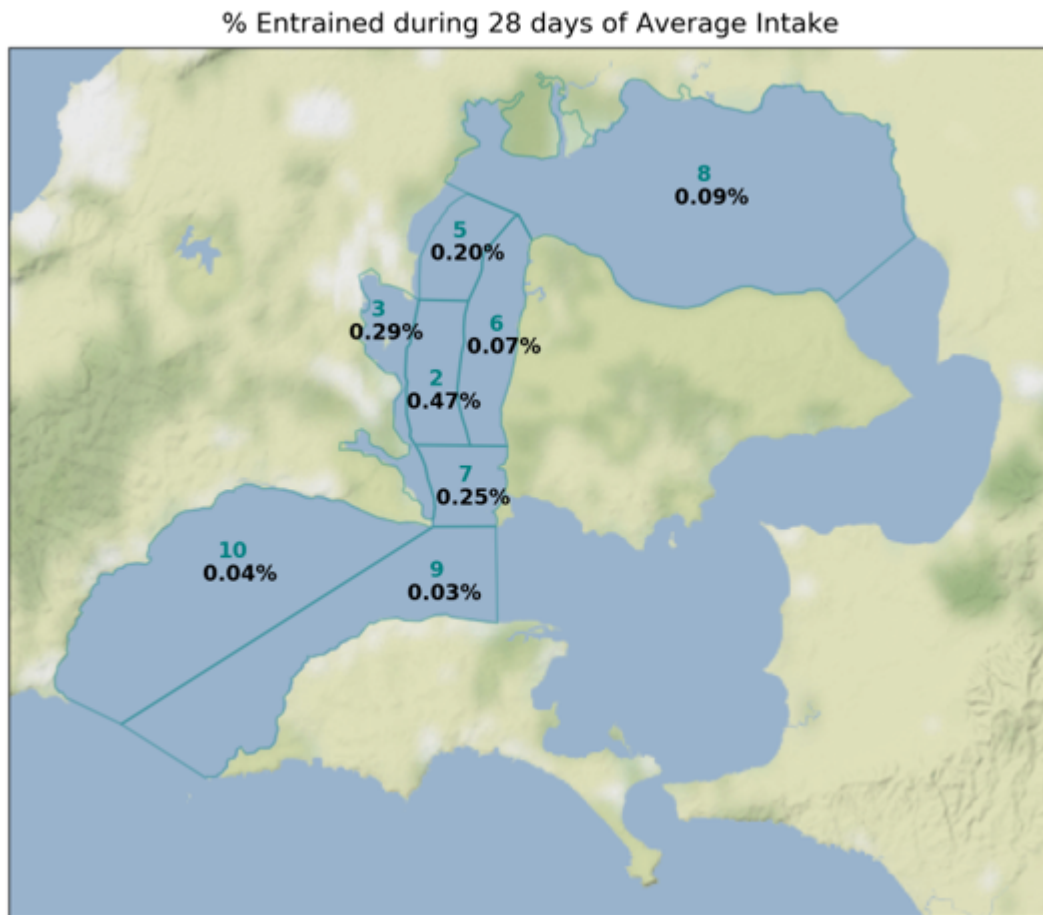


Figure 5.4 Percentage of particles entrained during 28 days at annual average intake (maximum percentage from scenarios is shown here). The average for North Arm at average production is approximately 0.26 % per 28 days.

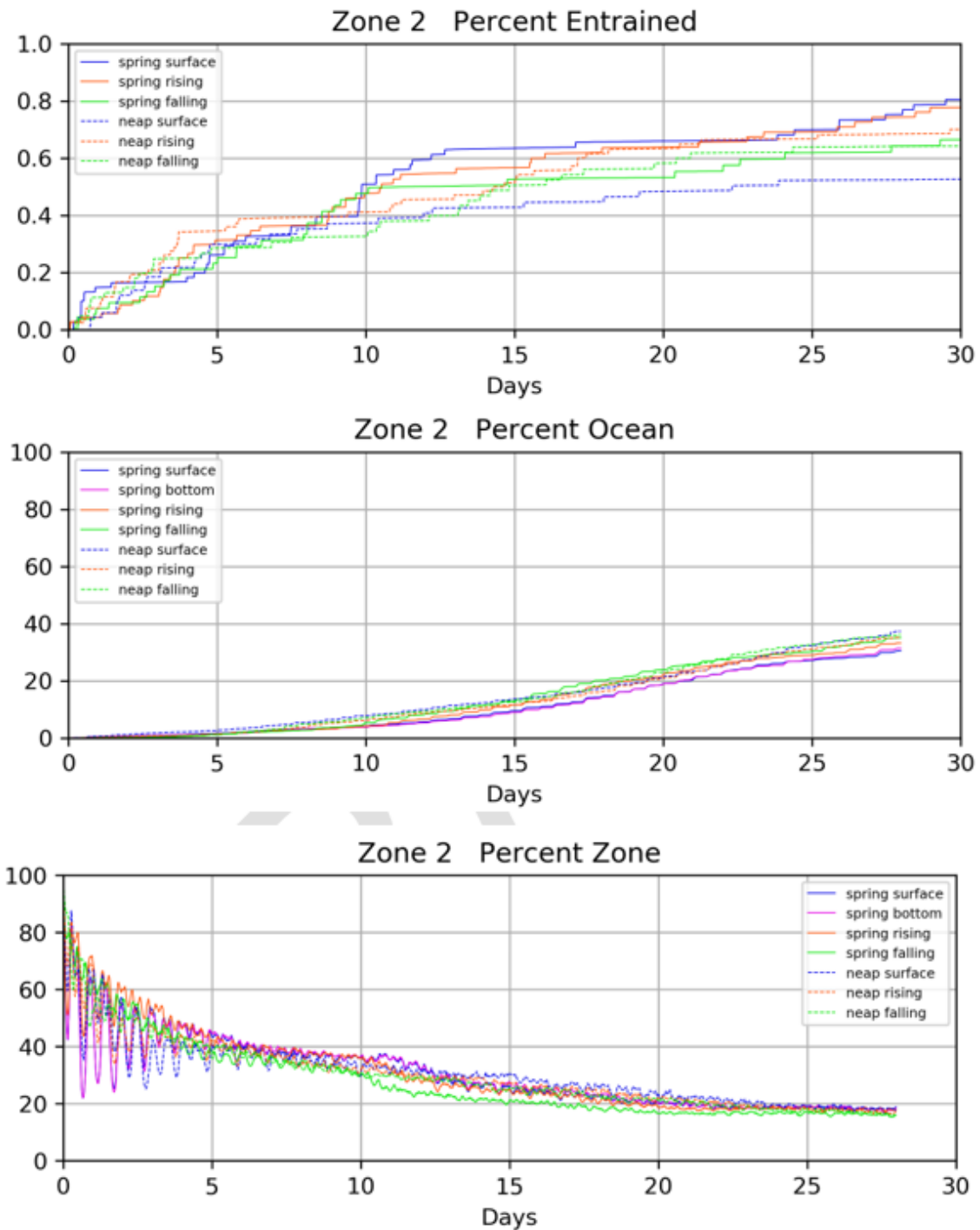


Figure 5.5 Fate of Zone 2 particles over 28 days (top: percentage entrained; centre: percentage leaving to Bass Strait; bottom: percentage remaining in zone region).

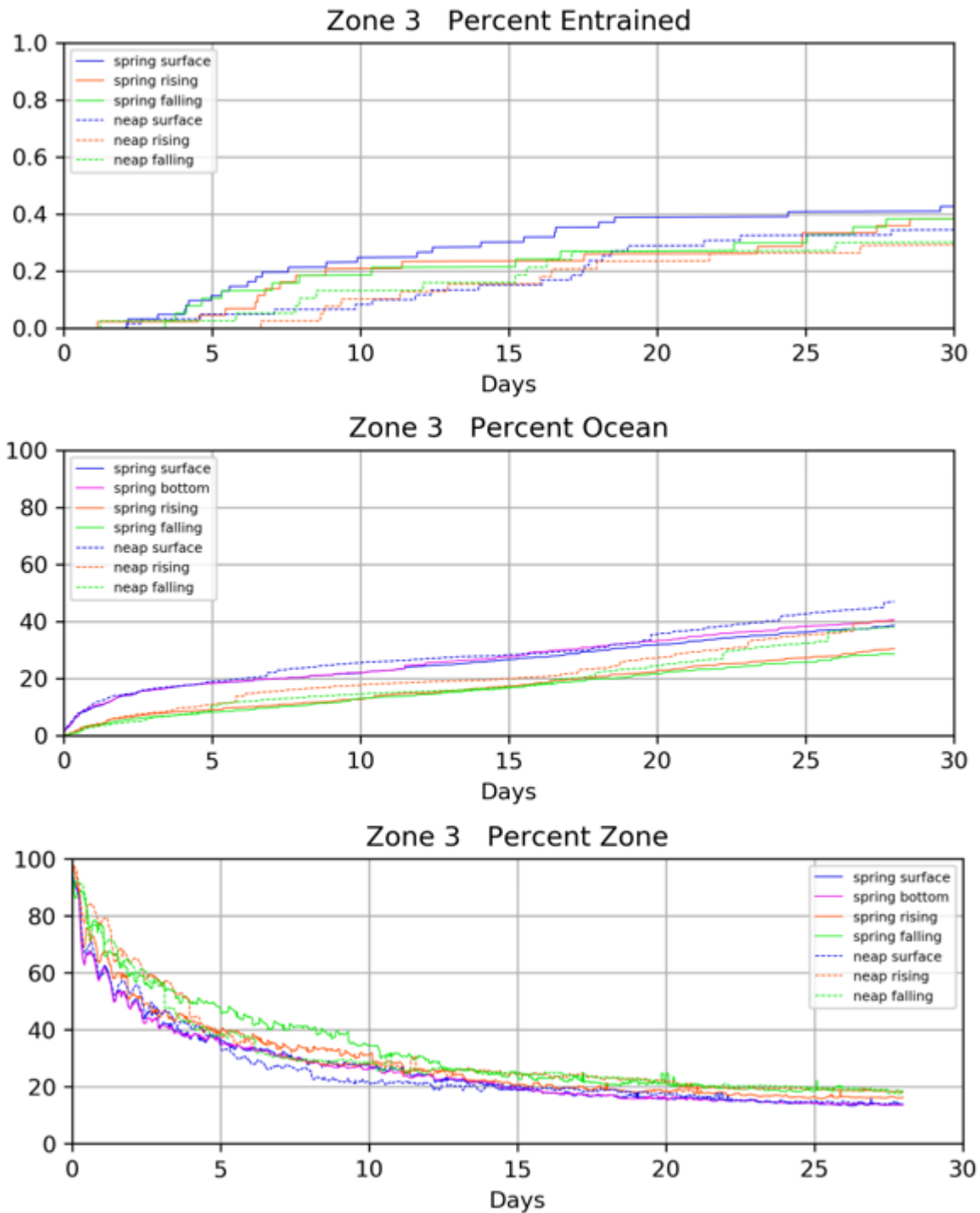


Figure 5.6 Fate of Zone 3 particles over 28 days: percentage entrained into FSRU (top); percentage leaving to Bass Strait (middle); and percentage remaining in zone (bottom).

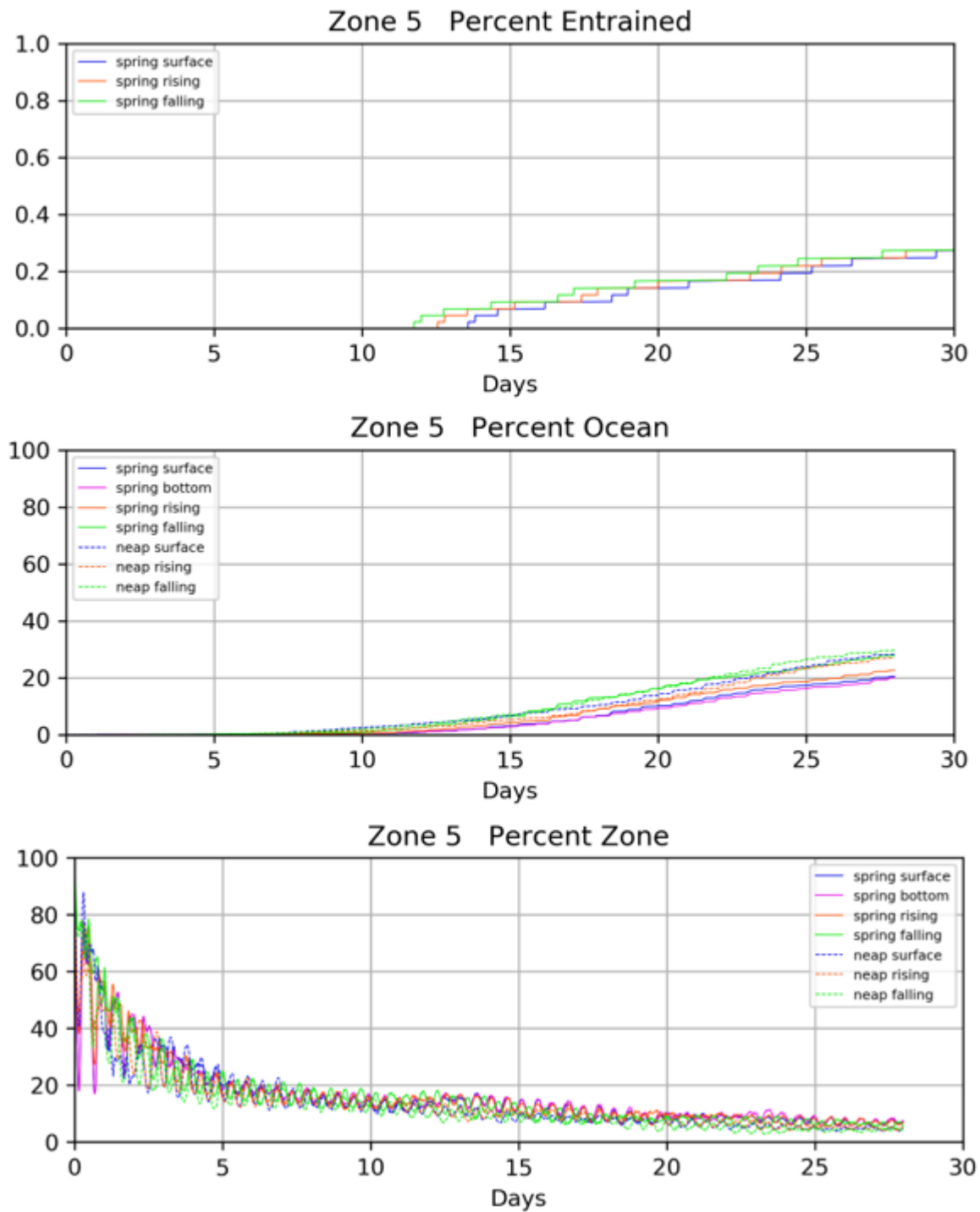


Figure 5.7 Fate of Zone 5 particles over 28 days: percentage entrained into FSRU (top); percentage leaving to Bass Strait (middle); and percentage remaining in zone (bottom).

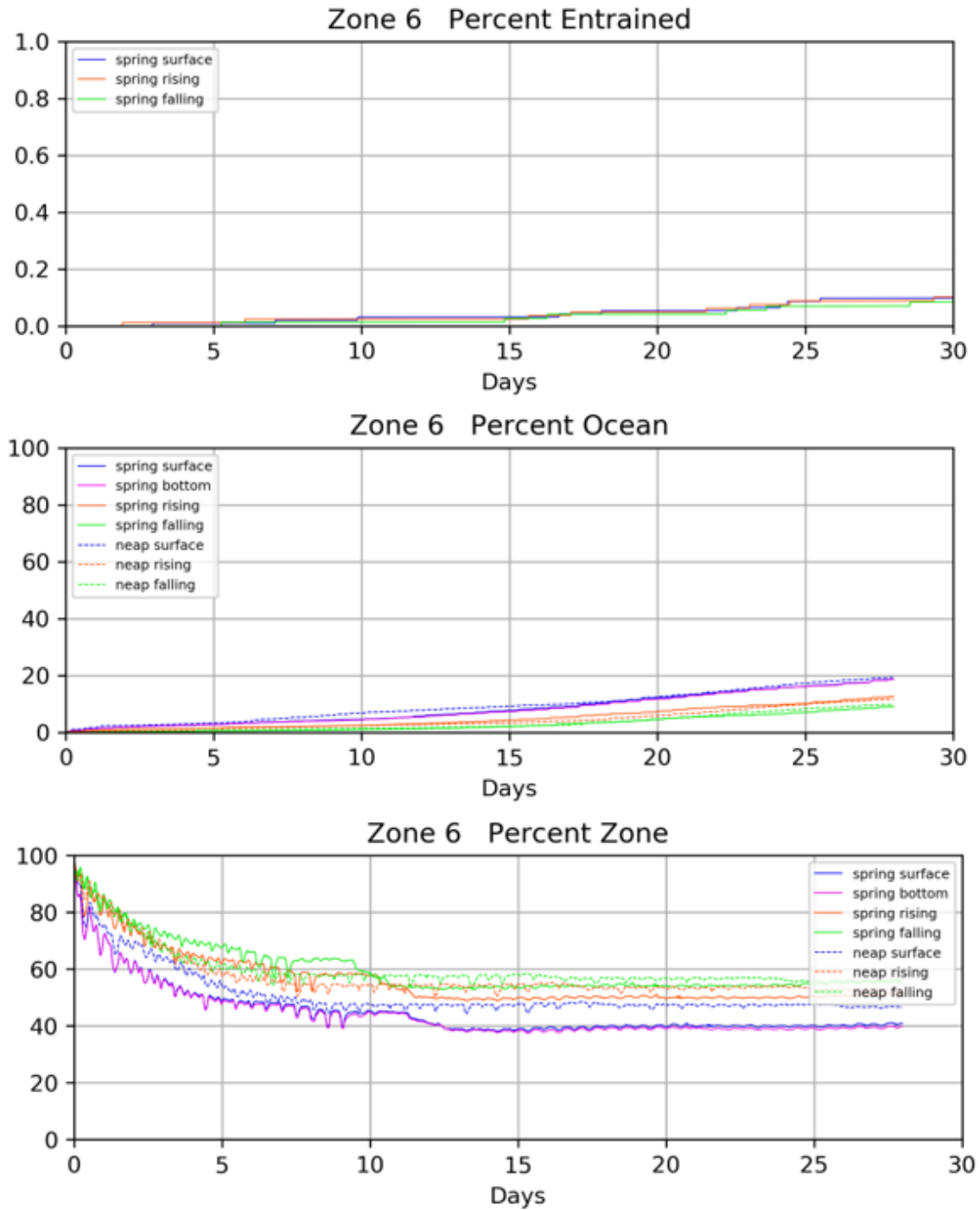


Figure 5.8 Fate of Zone 6 particles over 28 days: percentage entrained into FSRU (top); percentage leaving to Bass Strait (middle); and percentage remaining in zone (bottom).

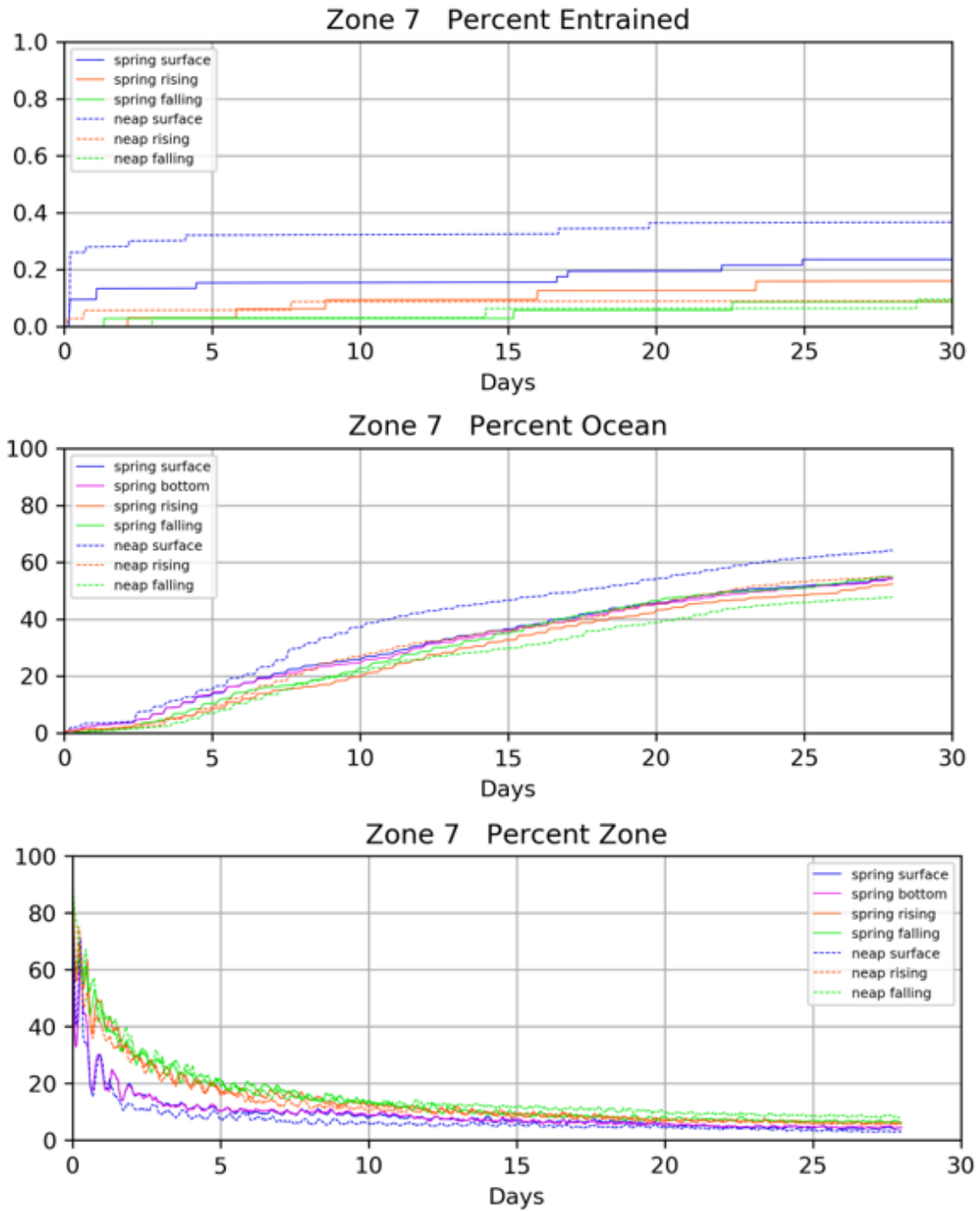


Figure 5.9 Fate of Zone 7 particles over 28 days: percentage entrained into FSRU (top); percentage leaving to Bass Strait (middle); and percentage remaining in zone (bottom).

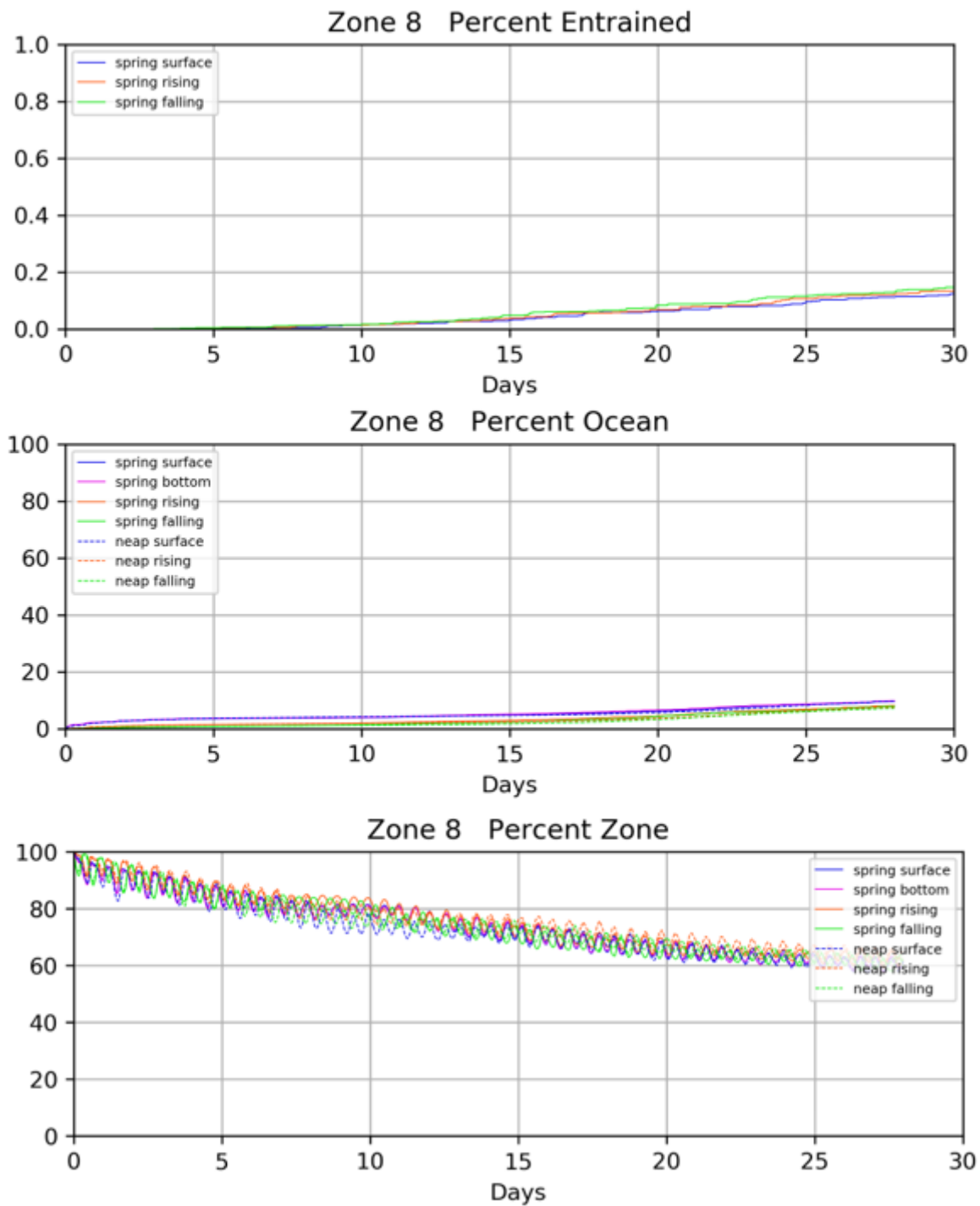


Figure 5.10 Fate of Zone 8 particles over 28 days: percentage entrained into FSRU (top); percentage leaving to Bass Strait (middle); and percentage remaining in zone (bottom).

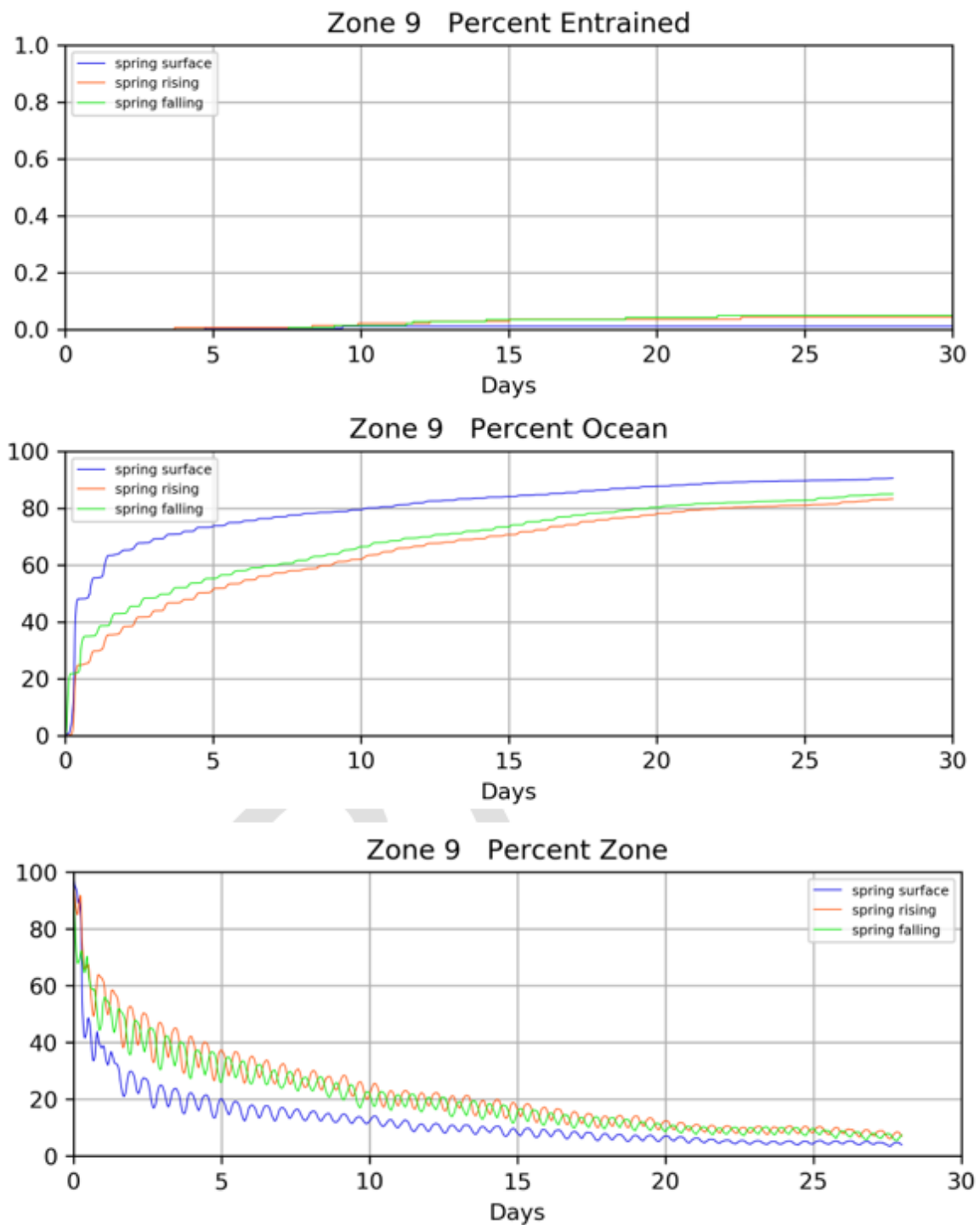


Figure 5.11 Fate of Zone 9 particles over 28 days: percentage entrained into FSRU (top); percentage leaving to Bass Strait (middle); and percentage remaining in zone (bottom).

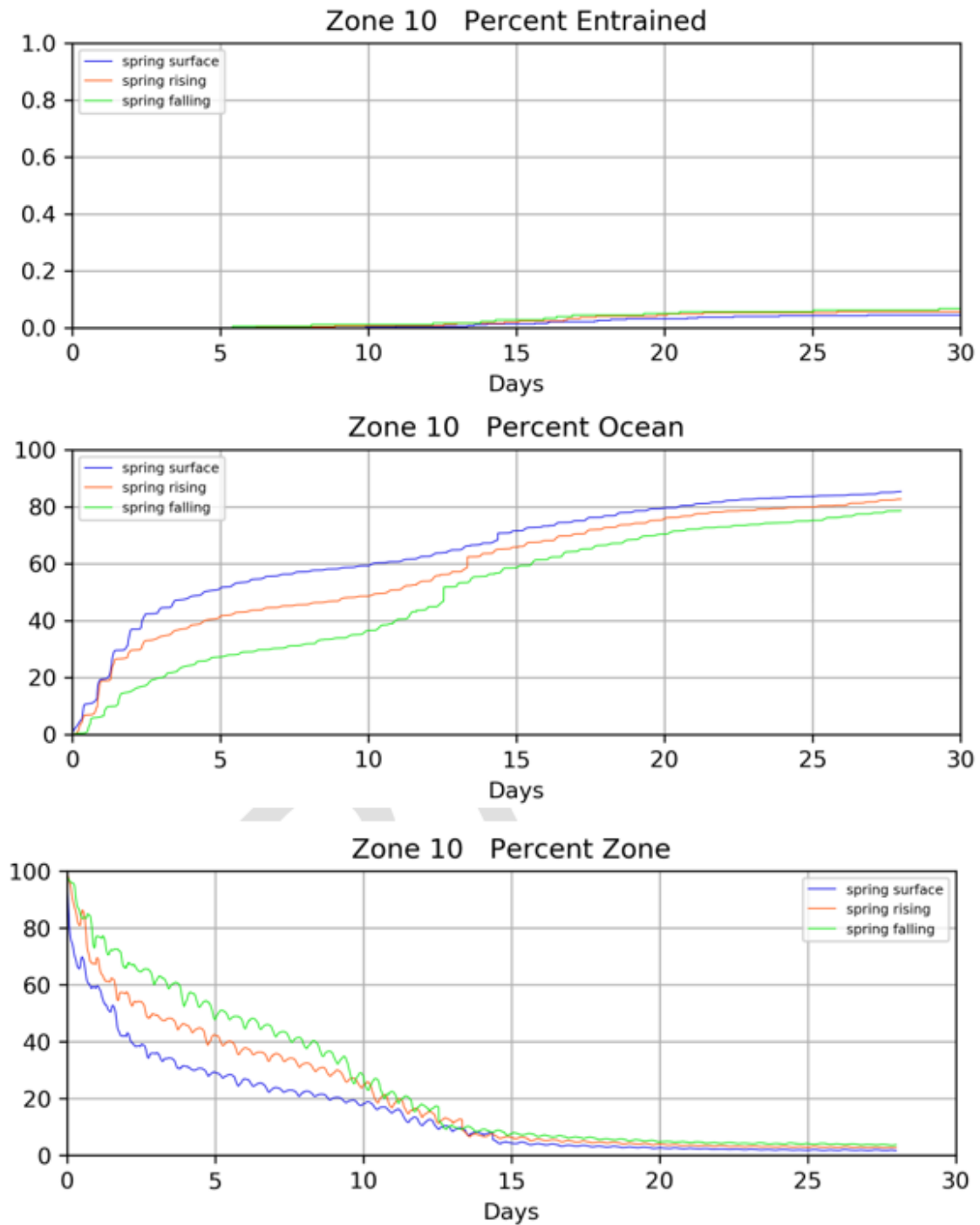


Figure 5.12 Fate of Zone 10 particles over 28 days: percentage entrained into FSRU (top); percentage leaving to Bass Strait (middle); and percentage remaining in zone (bottom).

5.3 Outcomes for Entrainment

The results after 28 days of simulation indicate that the highest entrainment occurs for particles released in the main channel close to Crib Point, where 0.75 % of particles are predicted to be captured. For zones further away, the entrainment ranged between 0.41 % (east of Crib Point) to less than 0.1 % in the western entrance to the bay. The average entrainment rate for North Arm was 0.38% over 28 days at peak production and 0.26% over 28 days for average production.

The entrainment asymptotes towards the end of the 28-day simulation as the particles are flushed to Bass Strait, or dispersed throughout the remainder of the bay, becoming increasingly unlikely to encounter the entrainment zone of the FSRU over time.

The water starting on the mudflats in the north of the Bay drain slowly compared the other zones (in North Arm) so the entrainment percentage continues to increase rather than asymptote over the 28-day period.

Dispersion of particles through the remainder of the bay, including loss to the ocean (which is highest for areas nearer to the entrance to the bay) is the dominant mechanisms for loss of particles from each of the zones.

Cumulative Impact

The results indicate that over the 28-day simulation the flushing of particles from the zones in the North Arm is approximately 80 to 200 times greater than entrainment into the FSRU. Therefore, the entrainment into the FSRU is only a very small contribution to the loss of particles from a particular zone over time. In addition, the entrainment results need to be considered in the context of the biological cycles and life cycle of the populations as the 28-day timeframe considered may be longer than the time taken to renew populations. The biological context and implications of these model results are addressed in the marine risk assessment prepared by CEE.

6 Closed Loop Operation

6.1 Scenario Descriptions

There are a series of warm discharges from engines and generators that would be discharged from a series of pipes at 3 to 5 m/s near the rear of the vessel on the starboard (east) side. The pipe outlets are on average 9 m below the water surface and point downward at angles of 30 to 45 degrees below the horizontal. The discharges will scour a hole about 1.2 to 1.5 m deep, and about 8 m in diameter (CEE, pers. comms, 2019).

This case has been modelled as a discharge into a single 20 m by 20 m cell that is 1 m thick adjacent to the bottom. The location of the cell is indicated in Figure 6.1.

The following closed loop discharge scenarios have been applied continuously over a 28-day simulation for March 2019:

- Peak production discharge of 1.82 m³/s at 4 °C above ambient and 100 µgCl/L;
- 2/3 production discharge of 1.44 m³/s at 5 °C above ambient and 100 µgCl/L; and
- Discharge of 1.82 m³/s at 4 °C above ambient and 100 µgCl/L plus additional west rear discharge of 0.96 m³/s at 4 °C above ambient and 70 µgCl/L.

The results for these scenarios for chlorine concentration are provided in the sections that follow.

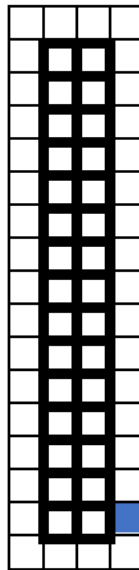


Figure 6.1 Plan view of location of warm water discharge from FSRU (blue square). The dark outlines indicate the location of the FSRU vessel.

6.2 Closed Loop Peak Discharge Results

At peak production a discharge of 1.82 m³/s at 4 °C above ambient occurs over the 28-day duration of the simulation. The mean and 95th percentile contours for the highest concentration of warm water discharge chlorine from the water column (i.e. at any depth from the surface to the bed) are shown in Figure 6.2 and Figure 6.3. The results indicate a small area at the stern

of the vessel on the starboard side where the mean concentrations are greater than $6 \mu\text{g/L}$. There is a significantly larger area of approximately 200 m by 100 m that experiences concentrations above $6 \mu\text{g/L}$ 5% of the time.

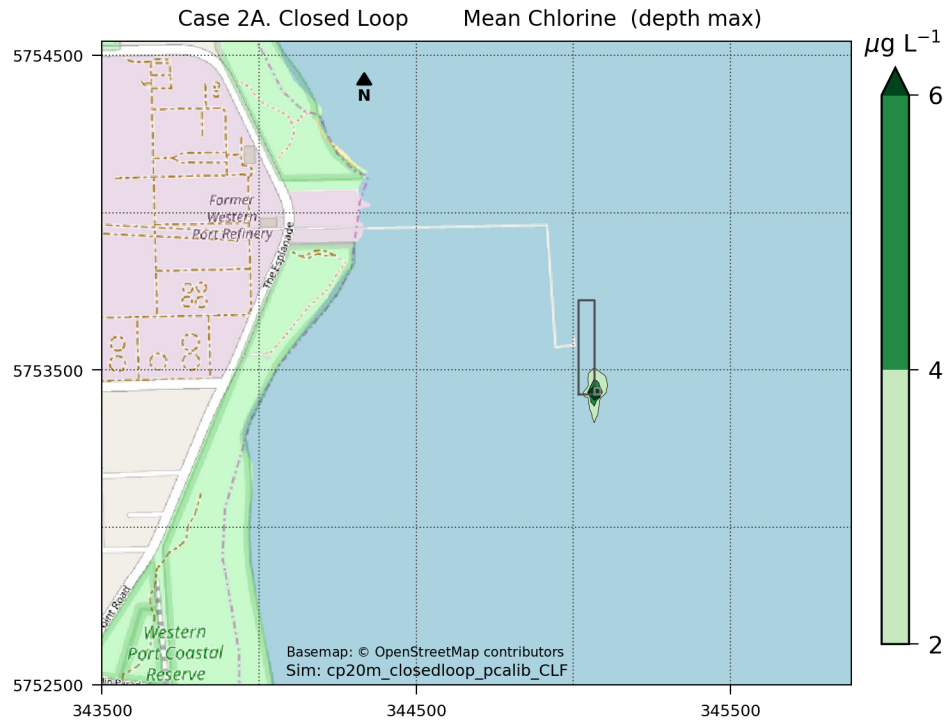


Figure 6.2 Plan view of mean chlorine concentration in the water column (highest for all depths) for a 28-day closed loop peak discharge simulation.

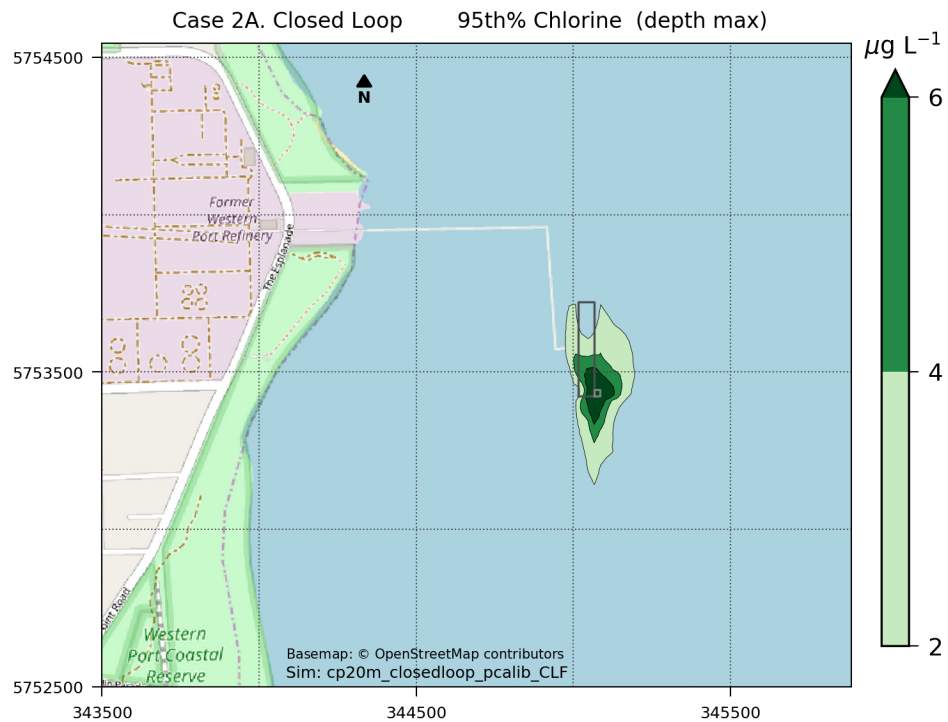


Figure 6.3 Plan view of 95th percentile chlorine concentration in the water column (highest for all depths) for a 28-day closed loop peak discharge simulation.

6.3 Closed Loop 2/3 Discharge Results

At 2/3 production a discharge of $1.44 \text{ m}^3/\text{s}$ at 5°C above ambient occurs over the 28-day duration of the simulation. The mean and 95th percentile contours for the highest concentration of warm water discharge chlorine from the water column (i.e. at any depth from the surface to the bed) are shown in Figure 6.4 and Figure 6.5. The results indicate a small area at the stern of the vessel on the starboard side where the mean concentrations are greater than $6 \mu\text{g}/\text{L}$. There is a significantly larger area of approximately 100 m by 100 m that experiences concentrations above $6 \mu\text{g}/\text{L}$ 5% of the time.

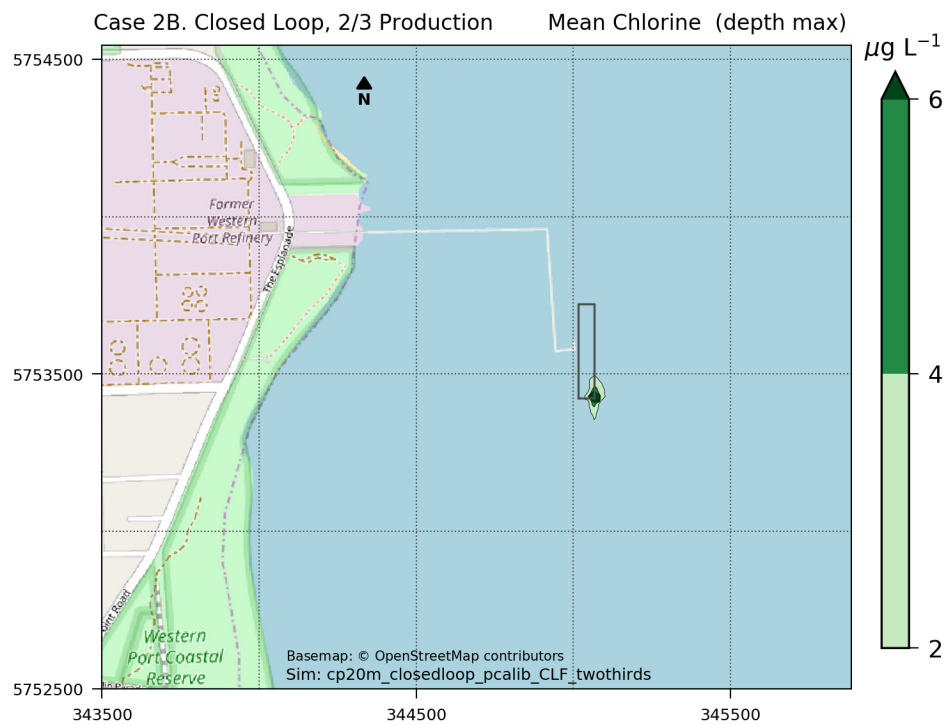


Figure 6.4. Plan view of mean chlorine concentration in the water column (highest for all depths) for a 28-day closed loop 2/3 discharge simulation.

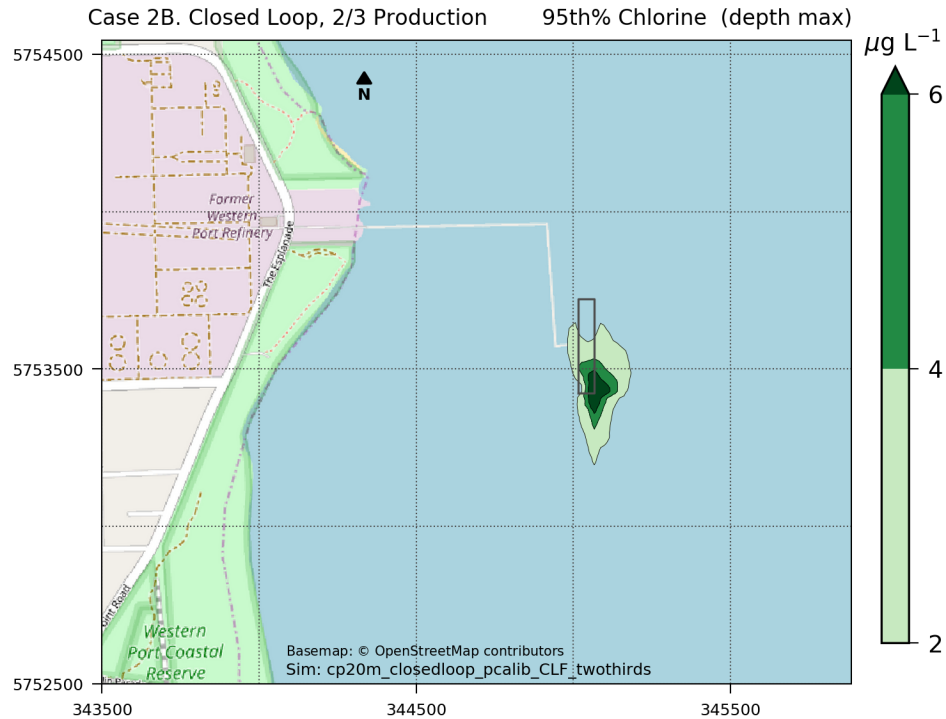


Figure 6.5 Plan view of 95th percentile chlorine concentration in the water column (highest for all depths) for a 28-day closed loop 2/3 discharge simulation.

6.4 Additional West Rear Discharge Results

Combined rear discharges to the east ($1.82 \text{ m}^3/\text{s}$, 4°C above ambient and $100 \text{ }\mu\text{gCl/L}$) and to the west ($0.96 \text{ m}^3/\text{s}$, 4°C above ambient and $70 \text{ }\mu\text{gCl/L}$) were simulated over the 28-day simulation. The small temperature anomalies that are predicted near the discharges are shown in Figure 6.6. The mean and 95th percentile contours for the highest concentration of chlorine from the water column (i.e. at any depth from the surface to the bed) are shown in Figure 6.7 and Figure 6.8. The results indicate small areas at the stern of the vessel on the starboard side where the mean concentrations are greater than $6 \text{ }\mu\text{g/L}$. There is a significantly larger area of approximately 200 m by 100 m that experiences concentrations above $6 \text{ }\mu\text{g/L}$ 5% of the time.

Timeseries at and near the discharge locations are presented in Figure 6.9 to Figure 6.11.

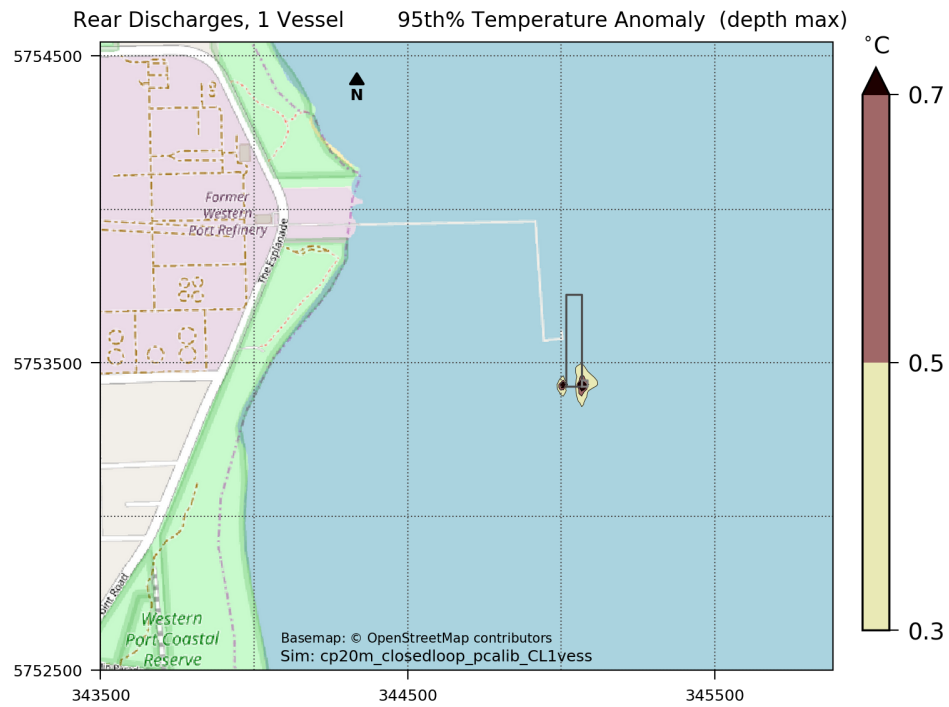


Figure 6.6 Plan view of 5th percentile of temperature change in the water column (highest for all depths) for a 28-day closed loop east and west rear discharge simulation.

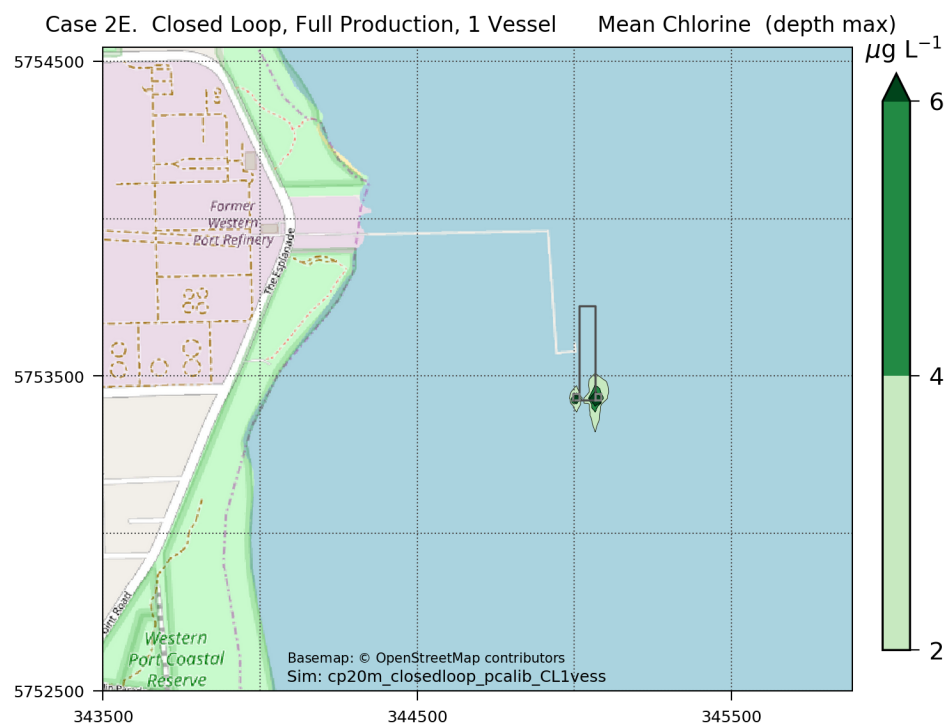


Figure 6.7 Plan view of mean chlorine concentration in the water column (highest for all depths) for a 28-day closed loop east and west rear discharge simulation.

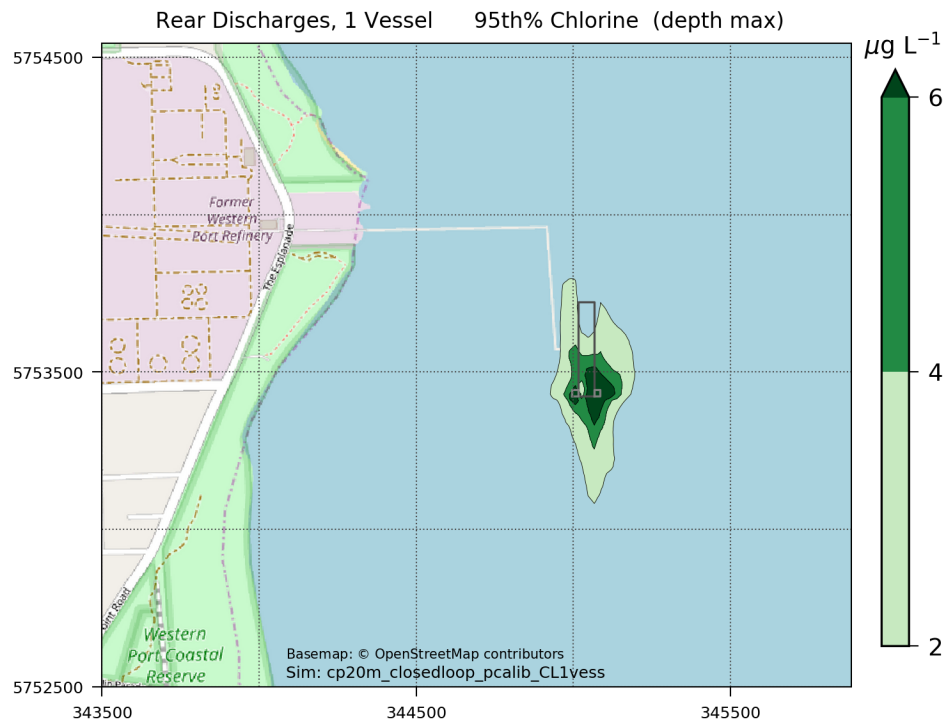


Figure 6.8 Plan view of 95th percentile chlorine concentration in the water column (highest for all depths) for a 28-day closed loop east and west rear discharge simulation.

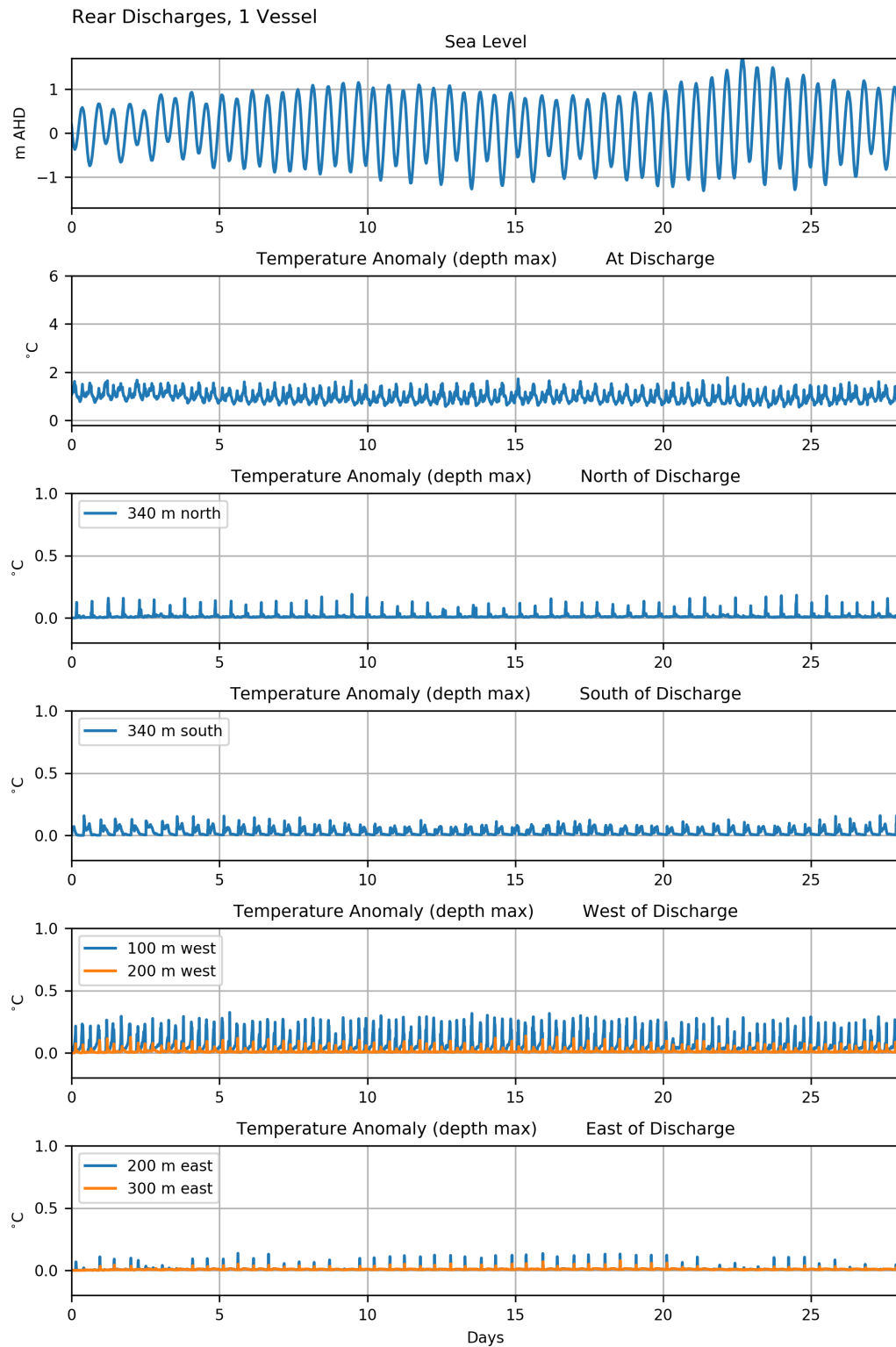


Figure 6.9 Time series of sea level (top panel) and (running down the page) temperature reduction at the seabed below the plume and north, south, west and east of the FSRU during closed loop east and west rear discharge.

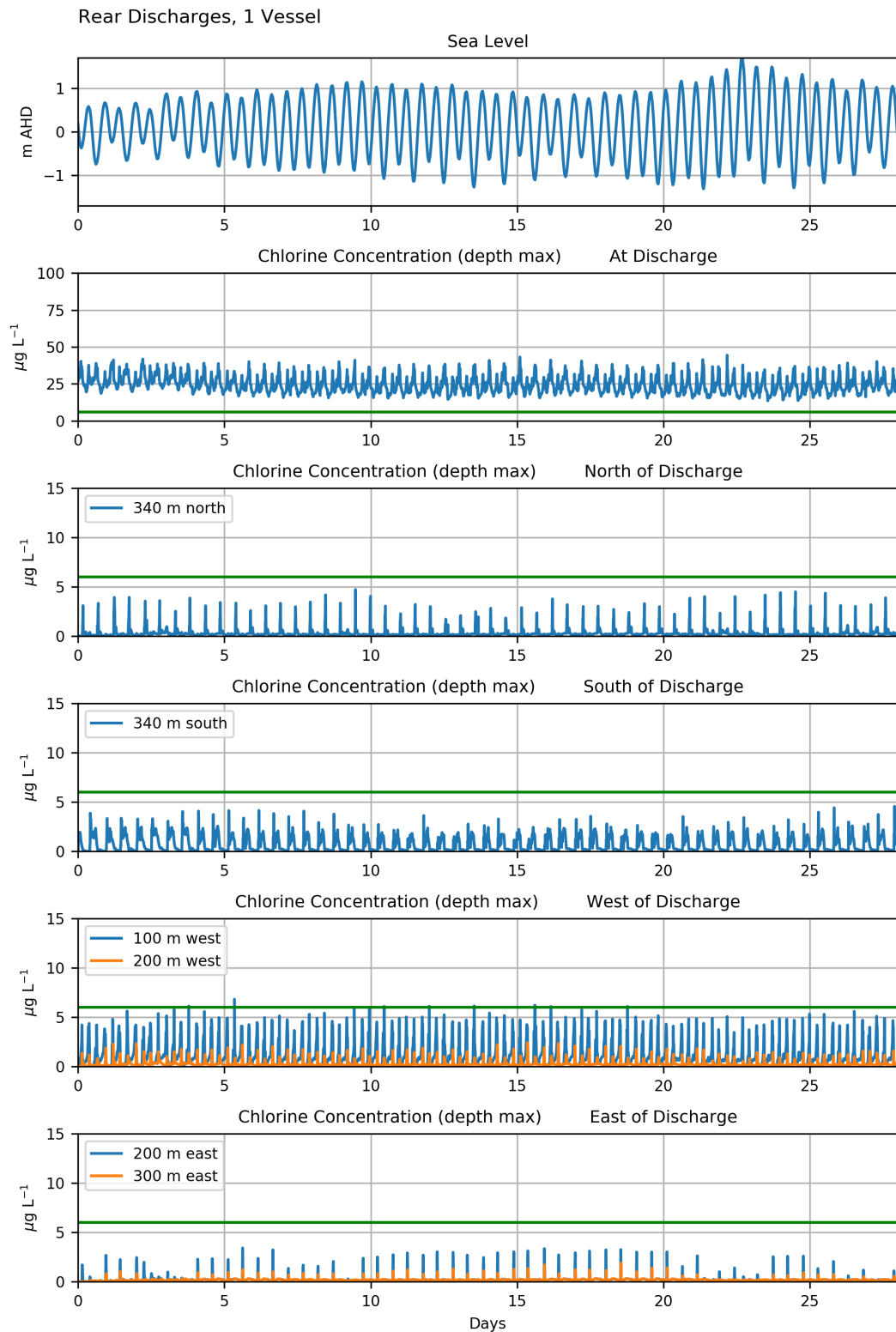


Figure 6.10 Time series of sea level (top panel) and (running down the page) chlorine concentration at the seabed below the plume and north, south, west and east of the FSRU during closed loop east and west rear discharge.

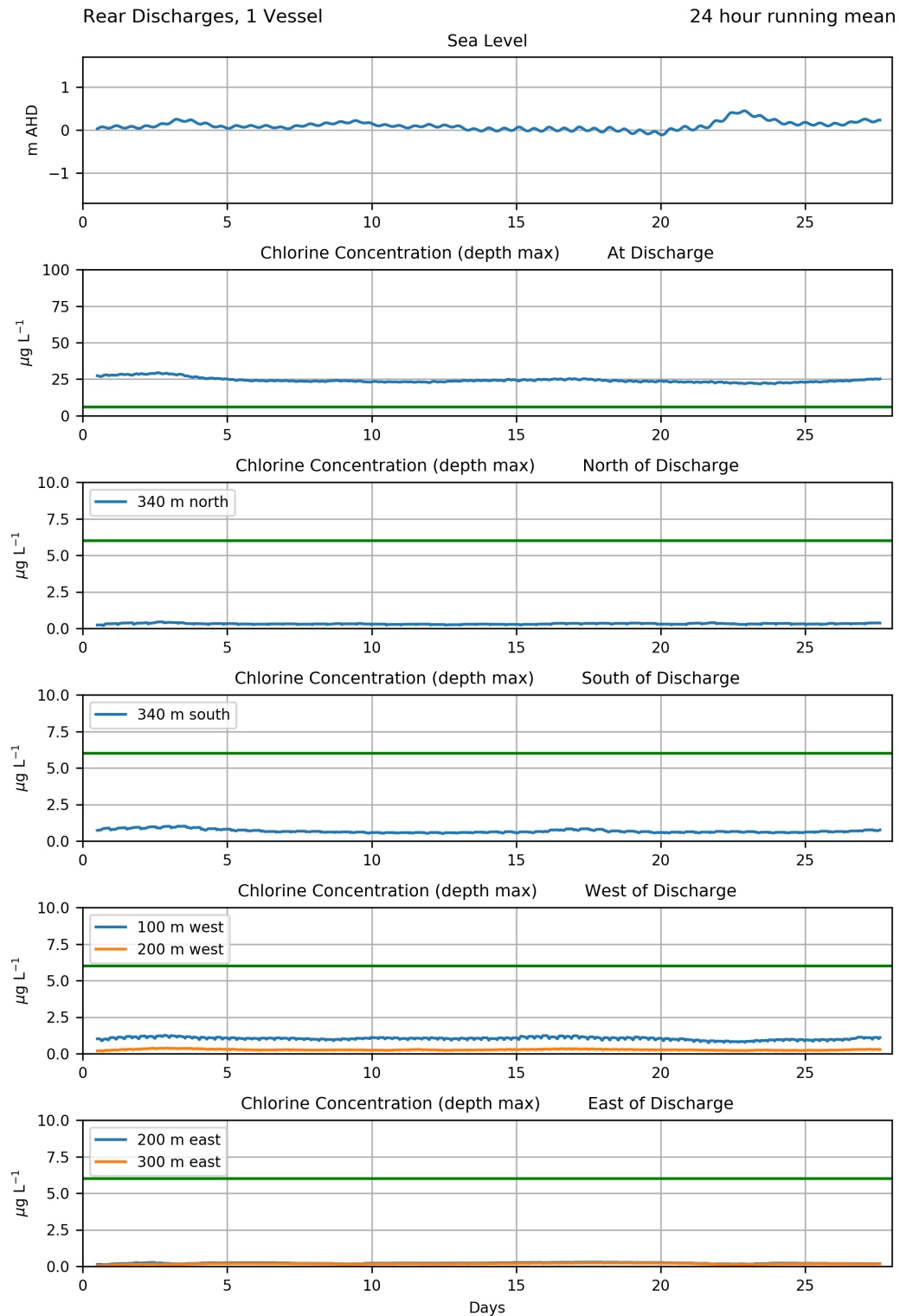


Figure 6.11 24-hr moving average time series of sea level (top panel) and (running down the page) chlorine concentration at the seabed below the plume and north, south, west and east of the FSRU during closed loop east and west rear discharge.

7 Ballast Water Discharge

7.1 Scenario Description

Ballast water will be discharged from pipe near the rear of the vessel on the port side (wharf side). The pipe outlet is on average 9.3 m below the water surface, and points downward at an angle of 30 degrees below the horizontal. The discharge will scour a hole about 1.2 to 1.5 m deep, and about 8 m in diameter (CEE, pers. comms, 2019). Ballast water is discharged on 12 to 40 days per year.

Ballast water discharge has been modelled as an input into a single 20 m by 20 m cell that is 1 m thick adjacent to the bottom. The location of the cell is indicated in Figure 7.1. Chlorine concentrations in the ballast water discharges are assigned to 21 $\mu\text{g/L}$.

Discharge of 1.45 m^3/s at ambient water temperature has been applied 1 hour in every 4 hours over a 28-day simulation for March 2019.

The results for this scenario for chlorine concentration are provided in the section below.

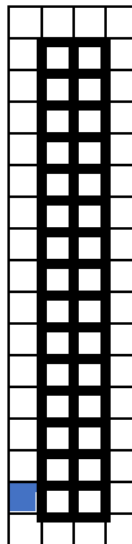


Figure 7.1 Plan view of location of ballast water discharge from FSRU (blue square). The dark outlines indicate the location of the FSRU vessel.

7.2 Ballast Water Discharge Results

The mean chlorine concentration associated with the ballast discharge is less than 2 $\mu\text{g/L}$ in all areas. The 95th percentile contours for the highest concentration of ballast water chlorine from the water column (i.e. at any depth from the surface to the bed) are shown in Figure 7.2. The results indicate a very small area at the stern of the vessel on the port side where concentrations are greater than 6 $\mu\text{g/L}$.

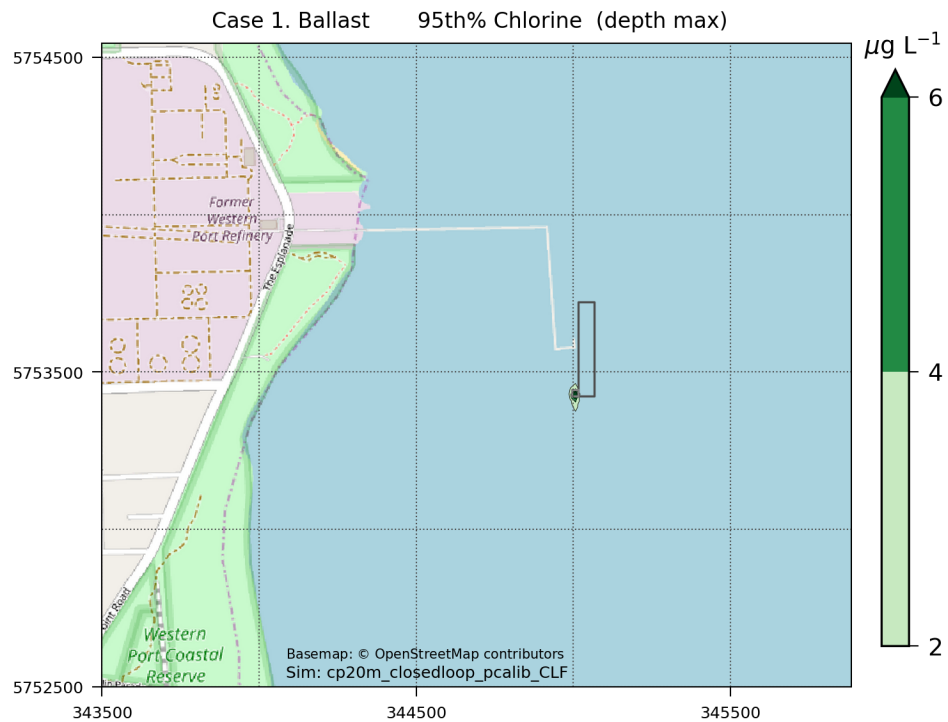


Figure 7.2 Plan view of 95th percentile of highest chlorine concentration in the water column (i.e. over all depths) for a 28-day ballast water discharge simulation.

8 LNG Unloading Scenarios

8.1 Scenario Descriptions

From 12 to 40 deliveries of LNG are anticipated each year to refuel the FSRU. The refuelling LNG tanker will be moored in parallel with the FSRU with a 4.5 m gap between the vessels (CEE, pers. comms, 2019). There is expected to be vigorous mixing in the channel between the boats as the current operating plan is to continue heat exchanger discharges during unloading (CEE, pers. comms, 2019). However, because of the restricted mixing volume the initial dilution of the discharge plume will be greatly reduced. This would not be satisfactory and hence production (and discharge) would need to decrease on the days that an LNG tanker is unloaded. A series of runs to explore the effects of various discharge rates were undertaken, so that a decision can be made by CEE and AGL on the reduced rate of production during LNG unloading.

The following unloading scenarios have been assessed (see Figure 8.1 for graphical depictions) for a continuous discharge over 28-day simulation for March 2019:

- Open loop with peak discharge of $5.4 \text{ m}^3/\text{s}$ at 7°C below ambient temperature and $100 \text{ }\mu\text{g/L}$ chlorine concentration is inserted into six cells directly below the ports, 60 m long and 40 m wide, adjacent to bed with the neighbouring vessel included in the simulation;
- Open loop with 2/3 discharge (4 out of 6 ports operating) of $3.6 \text{ m}^3/\text{s}$ at 7°C below ambient temperature and $100 \text{ }\mu\text{g/L}$ chlorine concentration inserted into four cells directly below the ports, 40 m long and 40 m wide, adjacent to bed with the neighbouring vessel included in the simulation;
- Open loop with 1/3 discharge (2 out of 6 ports operating) of $1.8 \text{ m}^3/\text{s}$ at 7°C below ambient temperature and $100 \text{ }\mu\text{g/L}$ chlorine concentration inserted into two cells directly below the ports, 20 m long and 40 m wide, adjacent to bed with the neighbouring vessel included in the simulation;
- Open loop with peak discharge of $5.4 \text{ m}^3/\text{s}$ at 7°C below ambient temperature and $100 \text{ }\mu\text{g/L}$ chlorine concentration is inserted into cells on west side of FSRU as a mirror image of open loop simulation for single vessel, with the neighbouring vessel included in the simulation;
- Closed loop rear discharges of $1.82 \text{ m}^3/\text{s}$ at 4°C above ambient and $100 \text{ }\mu\text{gCl/L}$ inserted into the rear starboard (east) cell (20 x 20 m) on the bed adjacent to the FSRU, combined with $0.96 \text{ m}^3/\text{s}$ at 4°C above ambient and $70 \text{ }\mu\text{gCl/L}$ inserted into the rear port (west) cell on the bed adjacent to the FSRU, with the neighbouring vessel included in the simulation;
- Closed loop with 2/3 discharge of $1.44 \text{ m}^3/\text{s}$ at 5°C above ambient and $100 \text{ }\mu\text{g/L}$ chlorine concentration inserted into the rear starboard cell adjacent to the FSRU, 20 m long and 20 m wide, adjacent to bed with the neighbouring vessel included in the simulation; and
- Closed loop with 1/3 discharge of $0.72 \text{ m}^3/\text{s}$ at 5°C above ambient and $100 \text{ }\mu\text{g/L}$ chlorine concentration inserted into the rear starboard cell adjacent to the FSRU, 20

m long and 20 m wide, adjacent to bed with the neighbouring vessel included in the simulation.

Given the expected gap between the vessels is small compared to the model grid size it has been assumed that there is no gap between the vessels (Figure 8.1). The results of the scenarios are provided in the sections that follow.

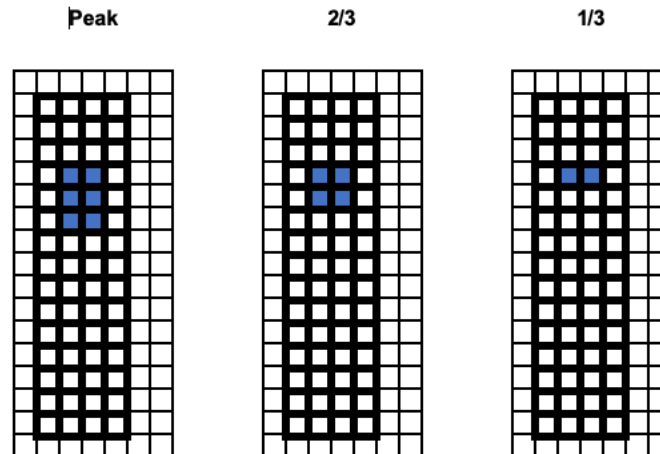


Figure 8.1 Plan view of location of heat exchanger discharge from FSRU (blue squares) for configuration peak (left), 2/3 and 1/3 (right) open loop production. The dark outlines indicate the location of the FSRU and neighbouring vessel.

8.2 Open Loop Peak Production

Temperature and chlorine contours (Figure 8.2 and Figure 8.3) for peak discharge show that the mooring of a second vessel is likely to lead to considerable extension of the seabed areas that have reduced temperatures and increased chlorine concentrations. This is because of the trapping of the plume beneath the vessels during weak currents and subsequent excursions of the plume along the bed as currents increase after slack tide.

Timeseries of temperature and chlorine concentrations at and near the discharge location are presented in Figure 8.4 to Figure 8.6.

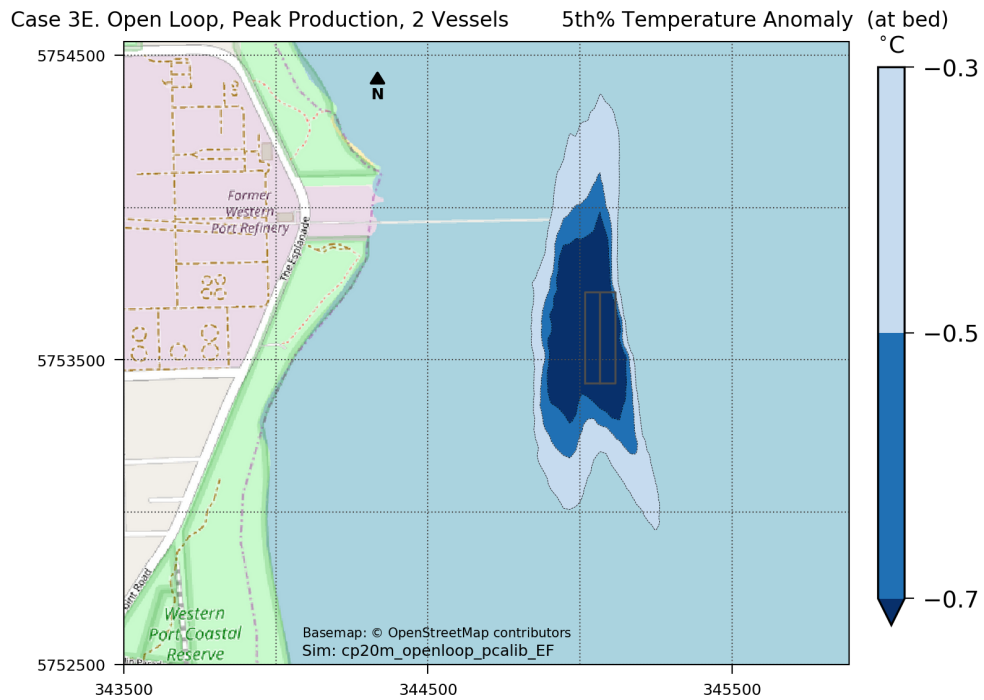


Figure 8.2 Plan view of 5th percentile of temperature decrease at the seabed for a 28-day open loop peak production simulation with neighbouring vessel configuration.

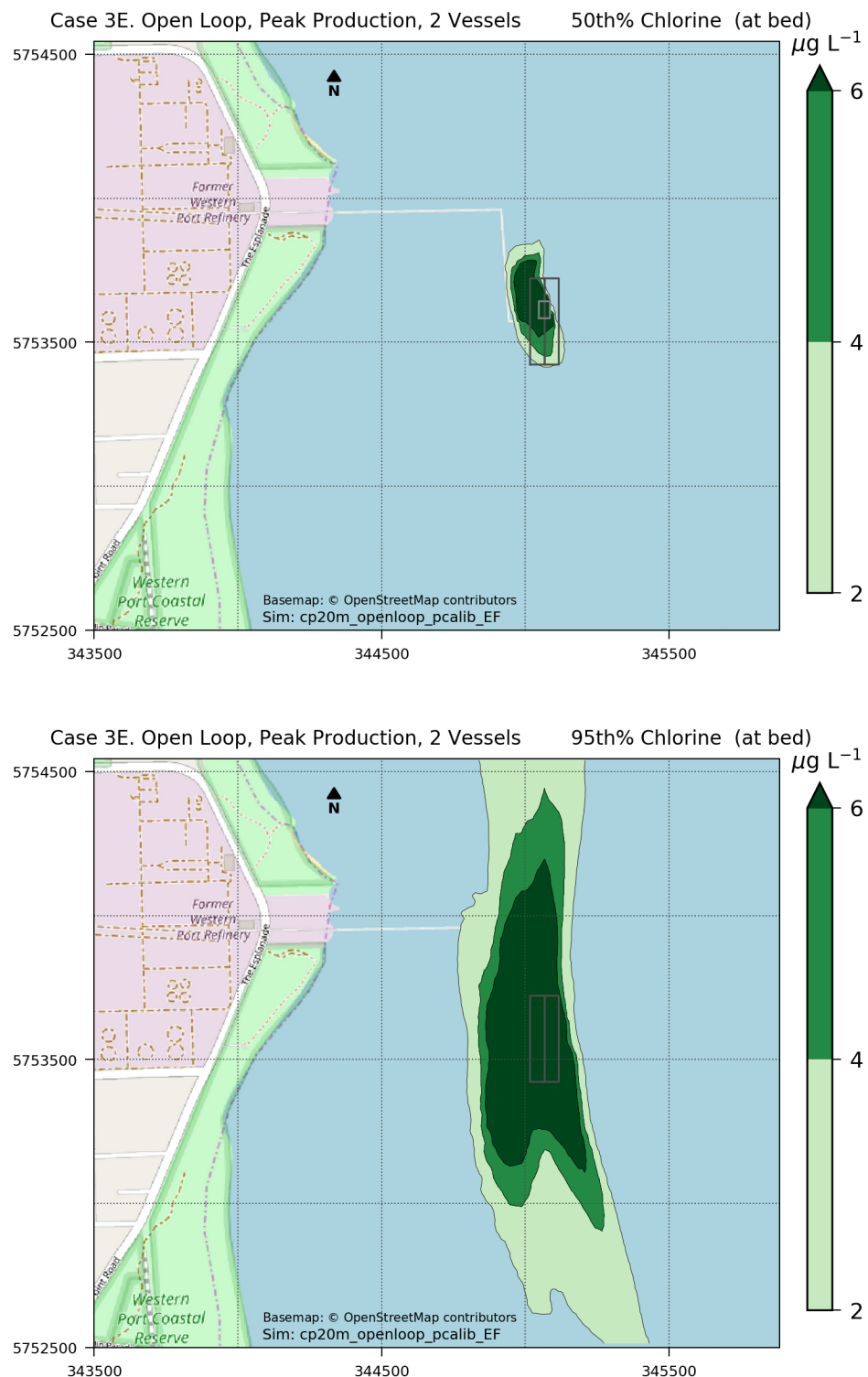


Figure 8.3 Plan view of mean (top) and 95th percentile (bottom) chlorine concentration at the seabed for a 28-day open loop peak production simulation with neighbouring vessel.

Case 3E. Open Loop, Full Production, 2 Vessels
Sea Level

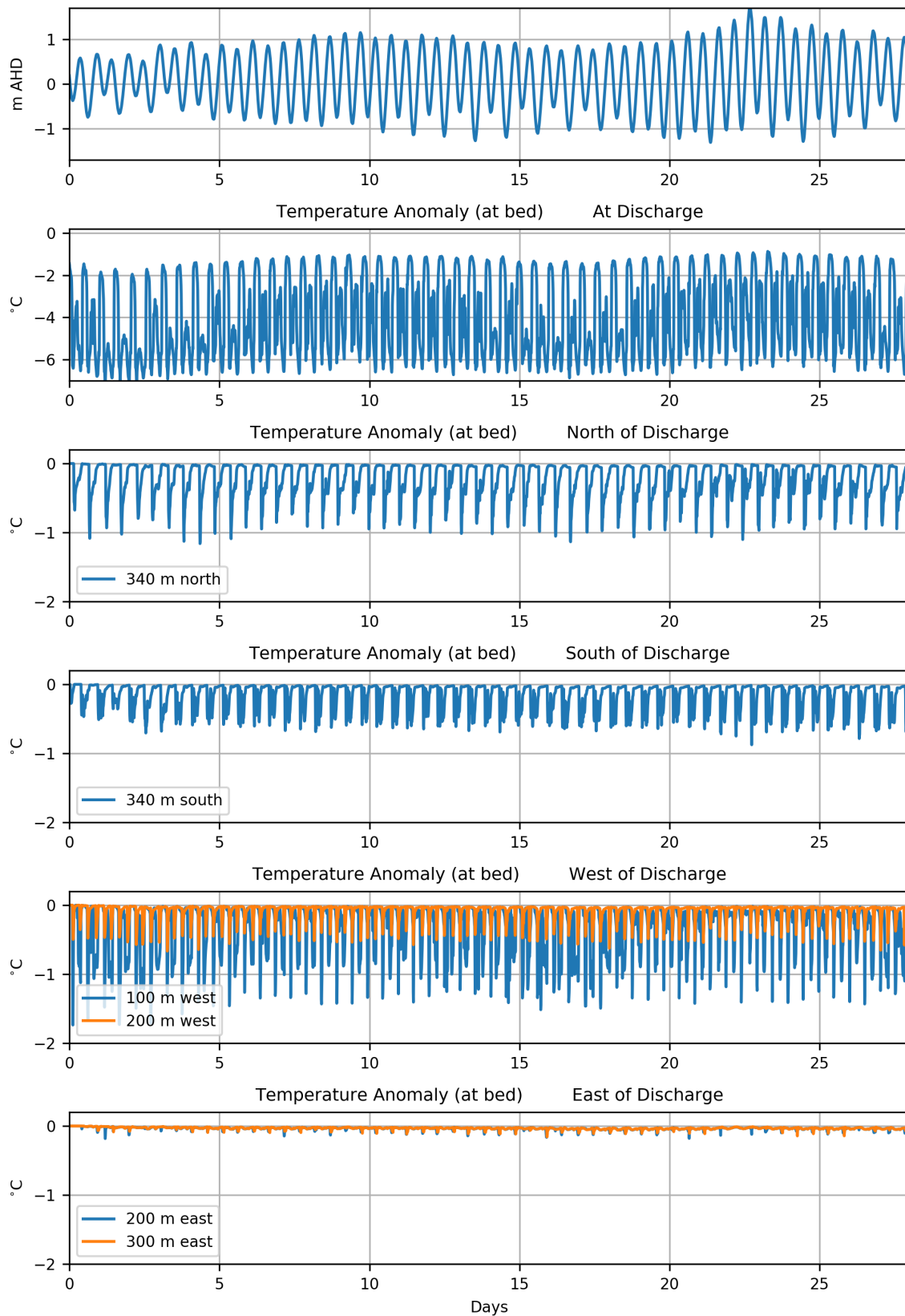


Figure 8.4 Time series of sea level (top panel) and (running down the page) temperature reduction at the seabed below the plume and north, south, west and east of the FSRU during peak discharge simulation with neighbouring vessel.

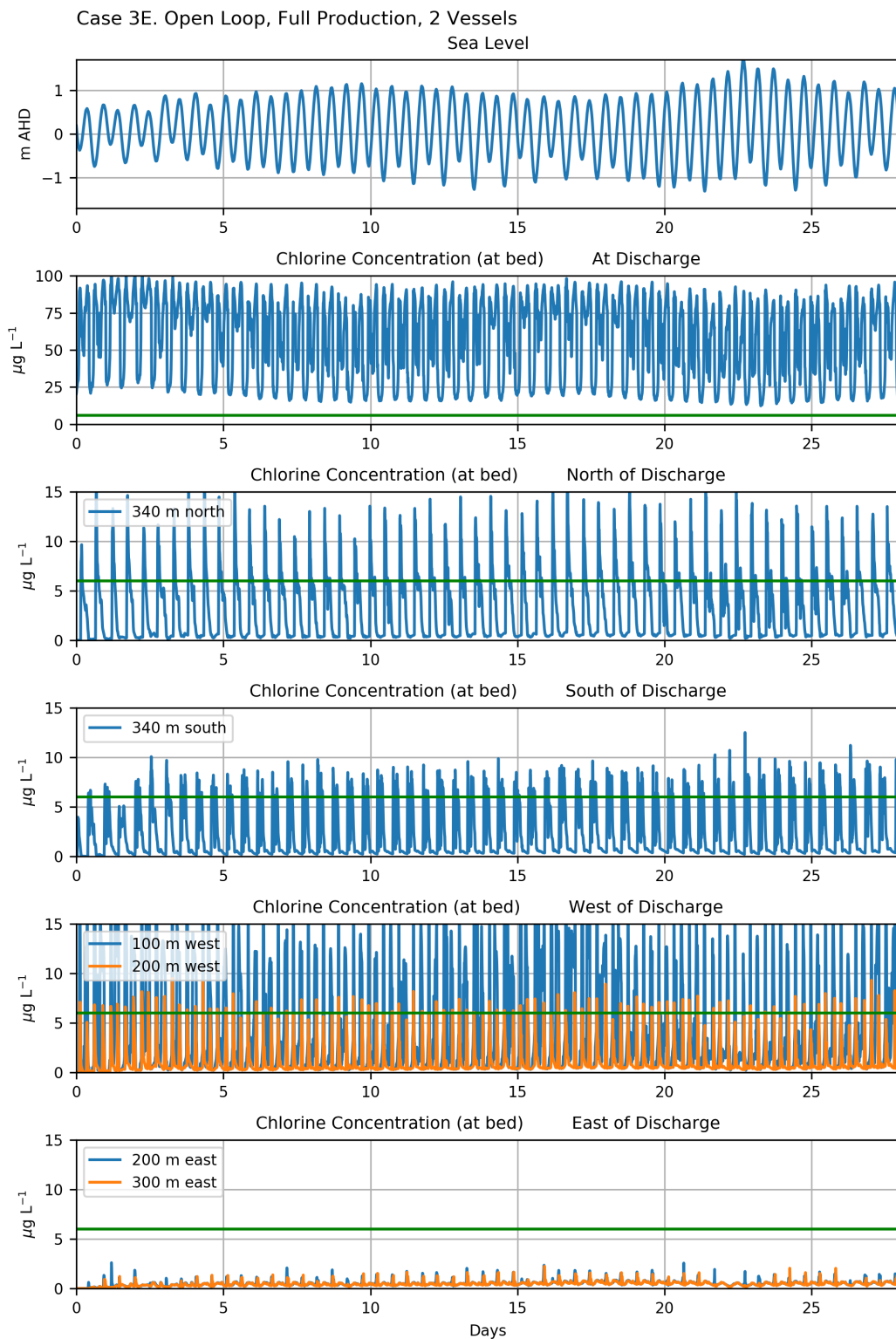


Figure 8.5 Time series of sea level (top panel) and (running down the page) chlorine concentration at the seabed below the plume and north, south, west and east of the FSRU during peak discharge simulation with neighbouring vessel.

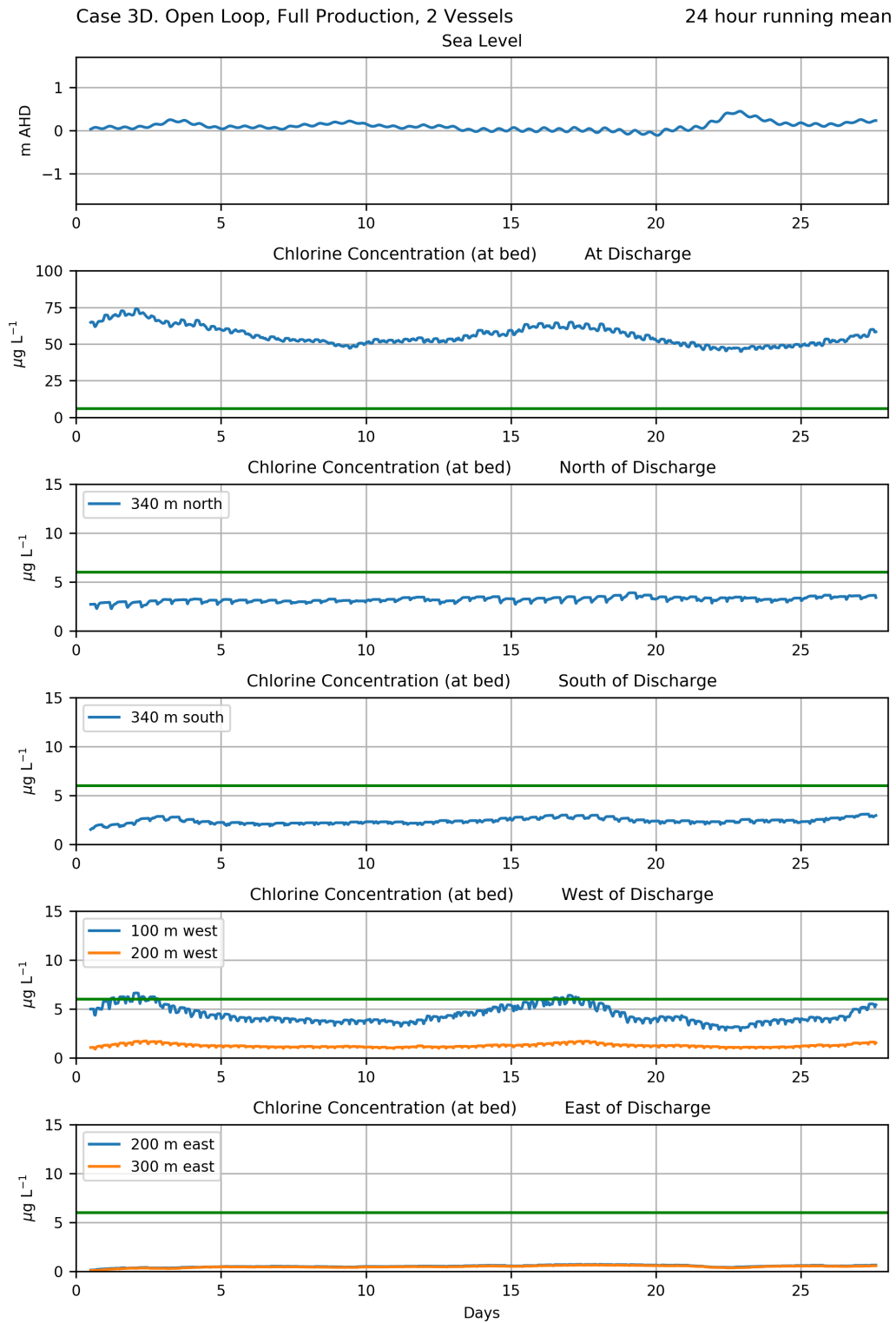


Figure 8.6 24-hr moving average time series of sea level (top panel) and (running down the page) chlorine concentration at the seabed below the plume and north, south, west and east of the FSRU during peak discharge simulation with neighbouring vessel.

8.3 Open Loop 2/3 Production

A decrease in discharge to 2/3 production maintains the shape but reduces the area of the contours shown (Figure 8.7 and Figure 8.8). However, the results indicate that despite the reduced production rate, the lack of initial mixing of the discharge plume that occurs when the second vessel is moored alongside leads to considerably larger areas at the seabed that experience reduced temperatures (-0.3°C or lower) and chlorine concentrations over $6\text{ }\mu\text{g/L}$ and do so more frequently when compared to the single vessel simulations described in the Chapter 3.

Timeseries of temperature and chlorine concentrations at and near the discharge locations are presented in Figure 8.9 to Figure 8.6.

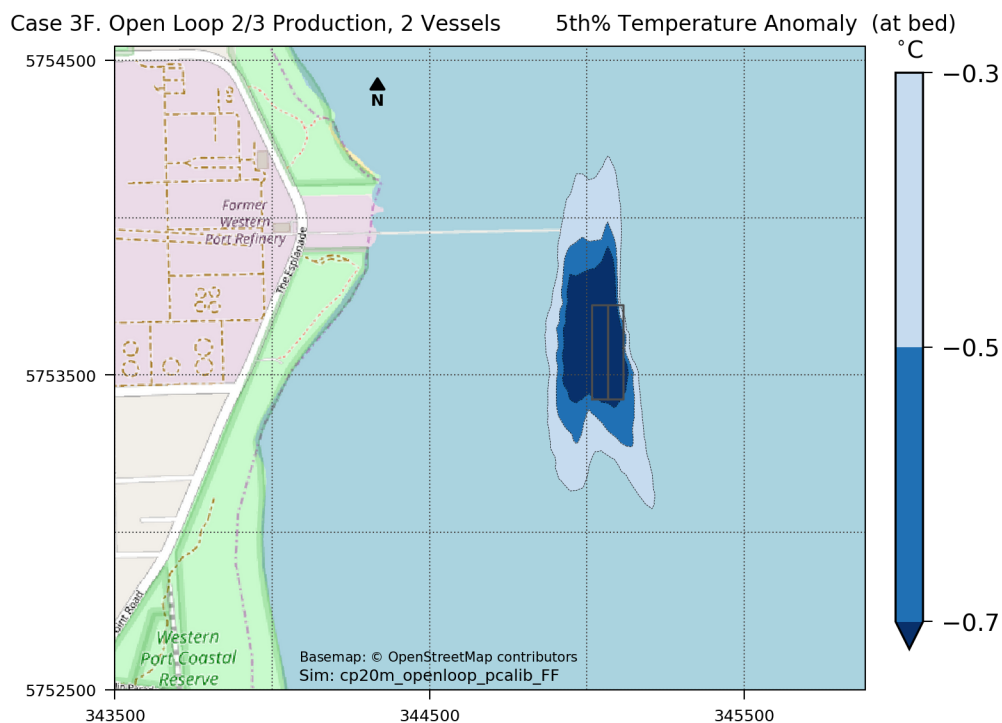


Figure 8.7 Plan view of 5th percentile of temperature decrease at the seabed for a 28-day open loop 2/3 production simulation with neighbouring vessel.

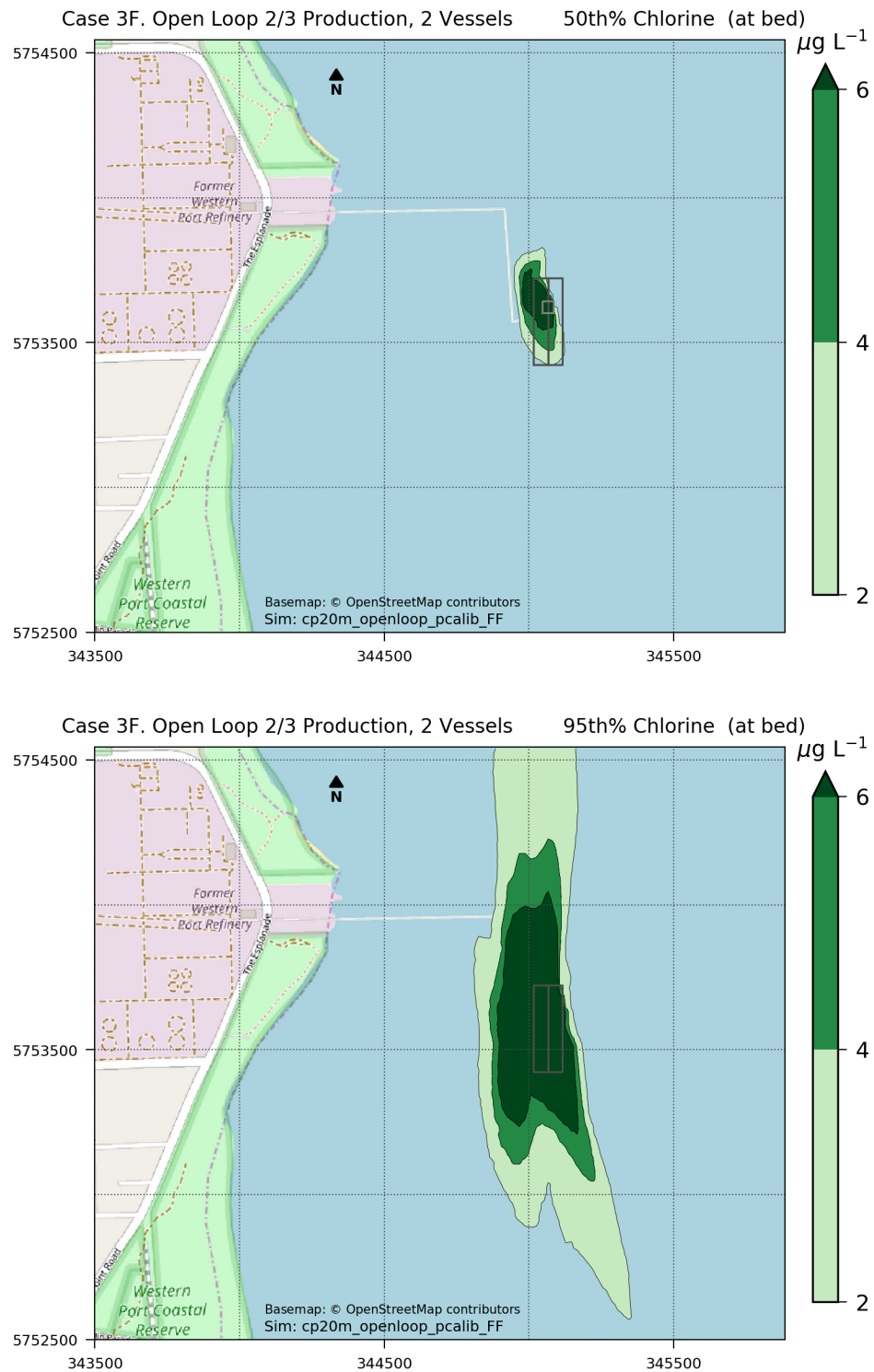


Figure 8.8 Plan view of mean (top) and 95th percentile (bottom) chlorine concentration at the seabed for a 28-day open loop 2/3 production simulation with neighbouring vessel.

Case 3F. Open Loop, 2/3 Production, 2 Vessels
Sea Level

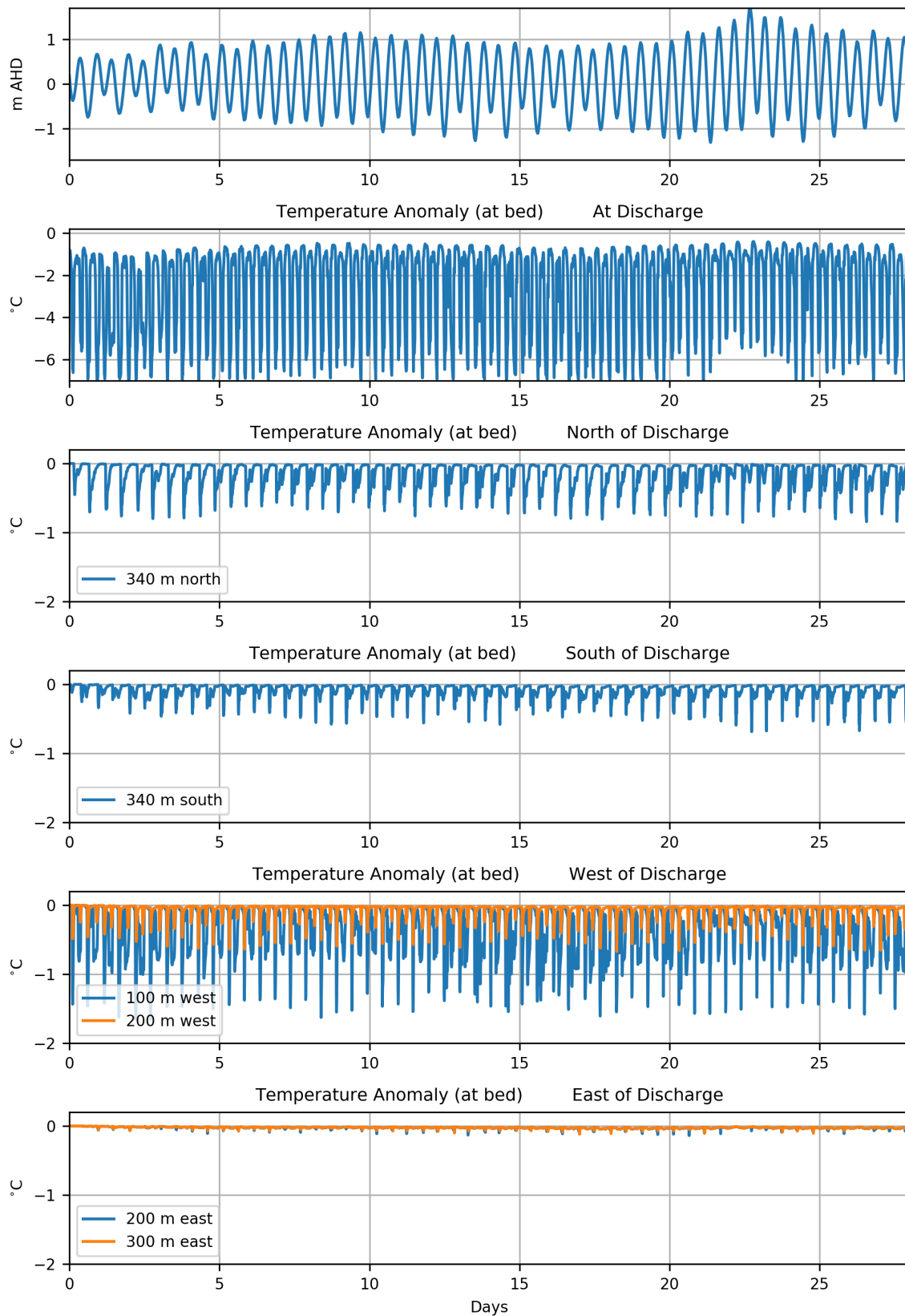


Figure 8.9 Time series of sea level (top panel) and (running down the page) temperature reduction at the seabed below the plume and north, south, west and east of the FSRU during average discharge simulation with neighbouring vessel.

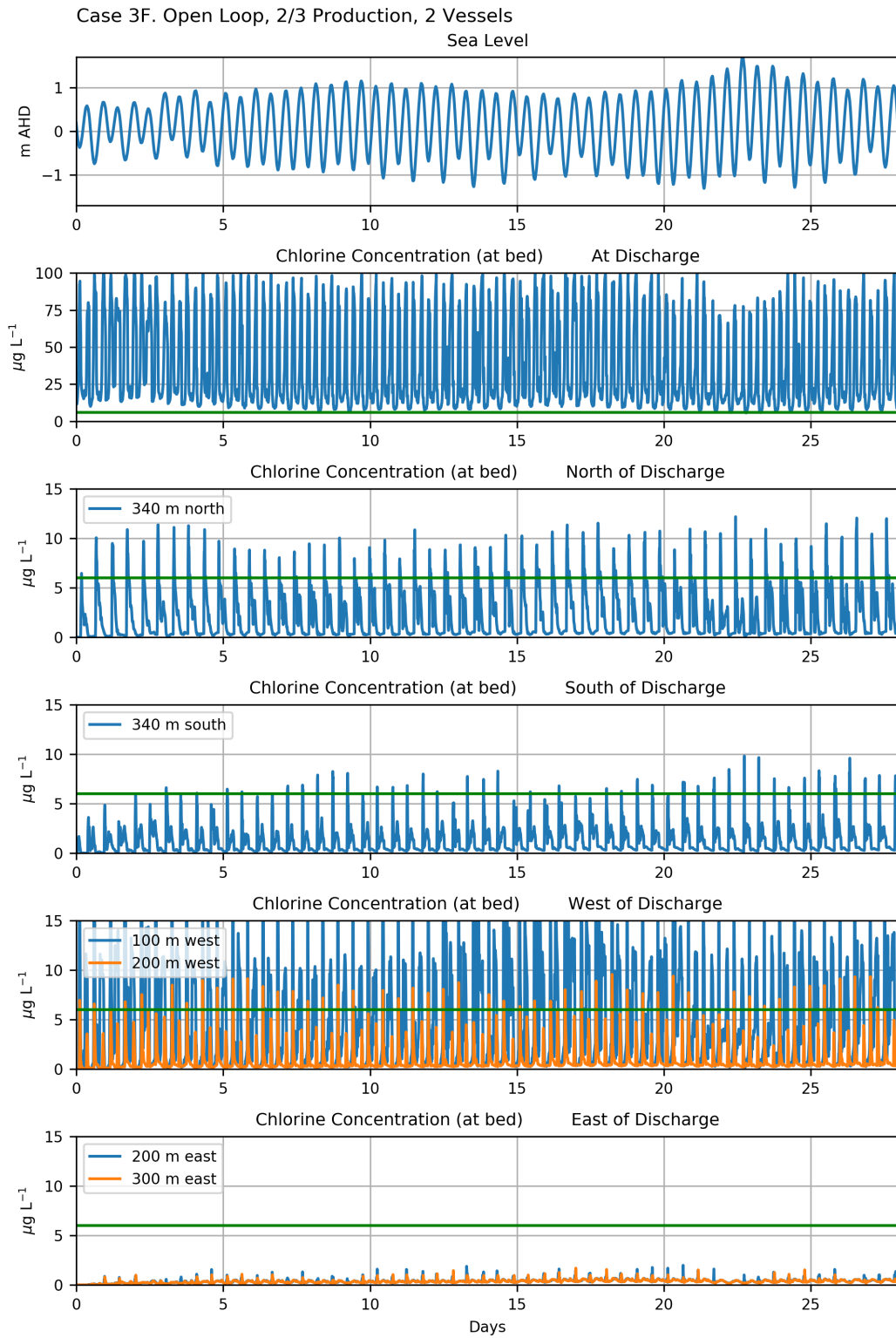


Figure 8.10 Time series of sea level (top panel) and (running down the page) temperature reduction at the seabed below the plume and north, south, west and east of the FSRU during average discharge simulation with neighbouring vessel.

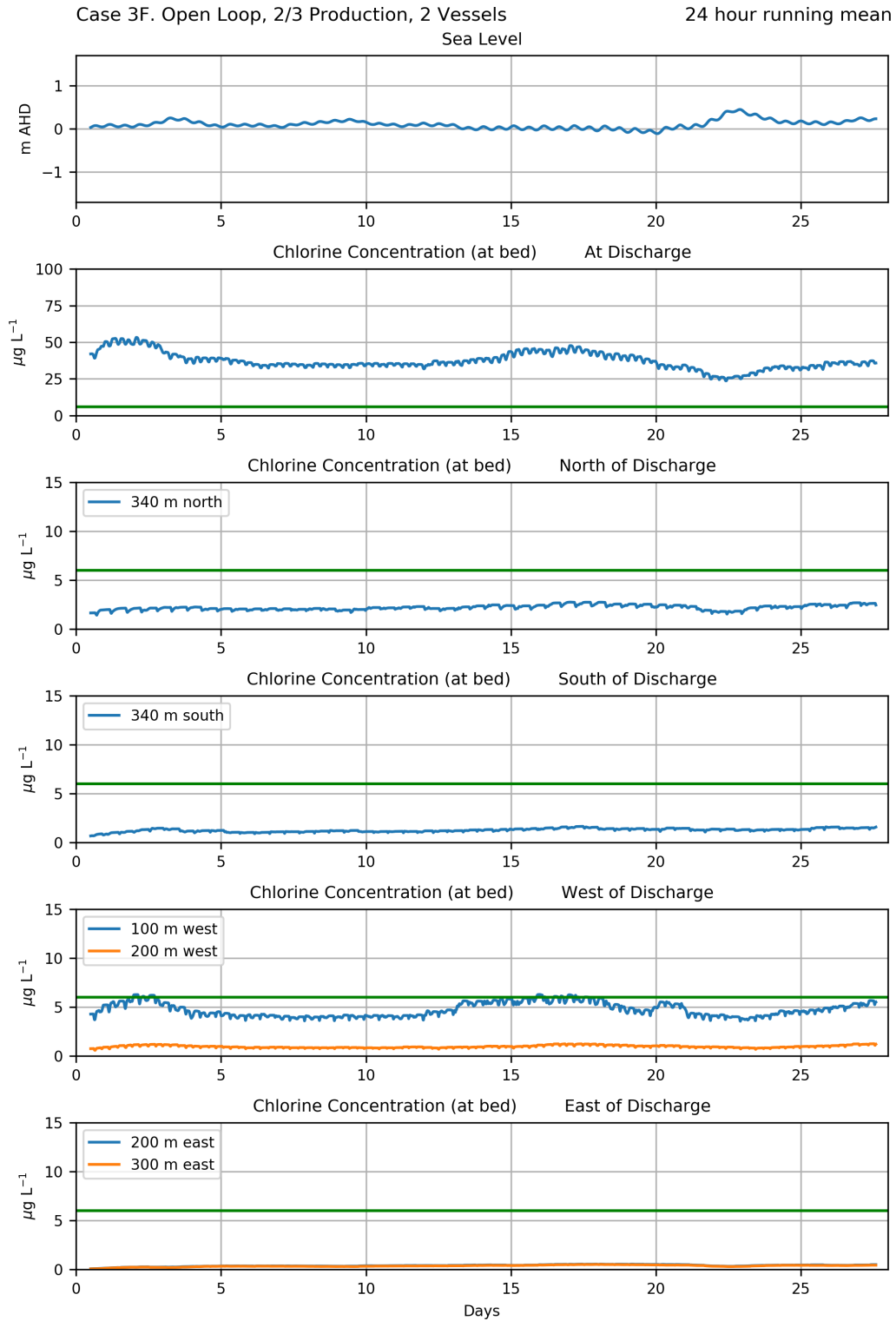


Figure 8.11 24-hr moving average time series of sea level (top panel) and (running down the page) chlorine concentration at the seabed below the plume and north, south, west and east of the FSRU during average discharge simulation with neighbouring vessel.

8.4 Open Loop 1/3 Production

A decrease in discharge to 1/3 production further reduces the area of the contours shown (Figure 8.12 and Figure 8.13). The region of the seabed that experiences reduced temperatures (-0.3°C or lower) for 5 % of the time is approximately $300\text{ m} \times 200\text{ m}$. Part of the seabed beneath the FSRU experiences mean chlorine concentrations over $6\text{ }\mu\text{g/L}$. The area experiencing chlorine concentrations over $6\text{ }\mu\text{g/L}$ for 5 % of the time extends approximately 100 m to the north and west of the vessels at the seabed due to the trapping of the plume beneath the vessels during weak currents and subsequent excursions of the plume along the bed as currents increase after slack tide.

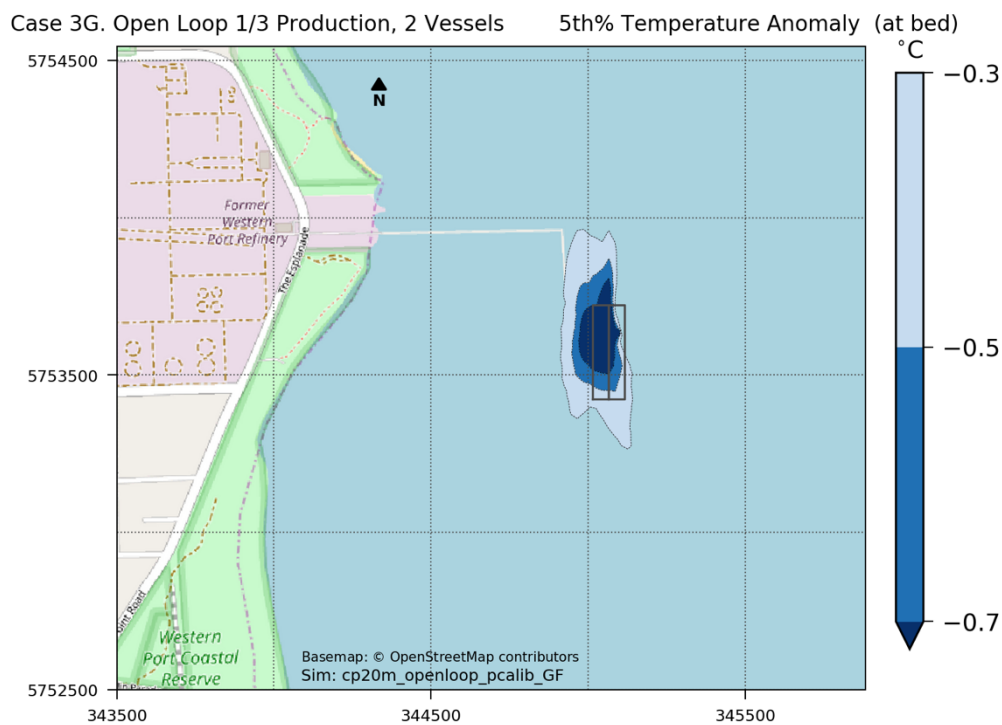


Figure 8.12 Plan view of 5th percentile of temperature decrease at the seabed for a 28-day open loop 1/3 production simulation with neighbouring vessel.

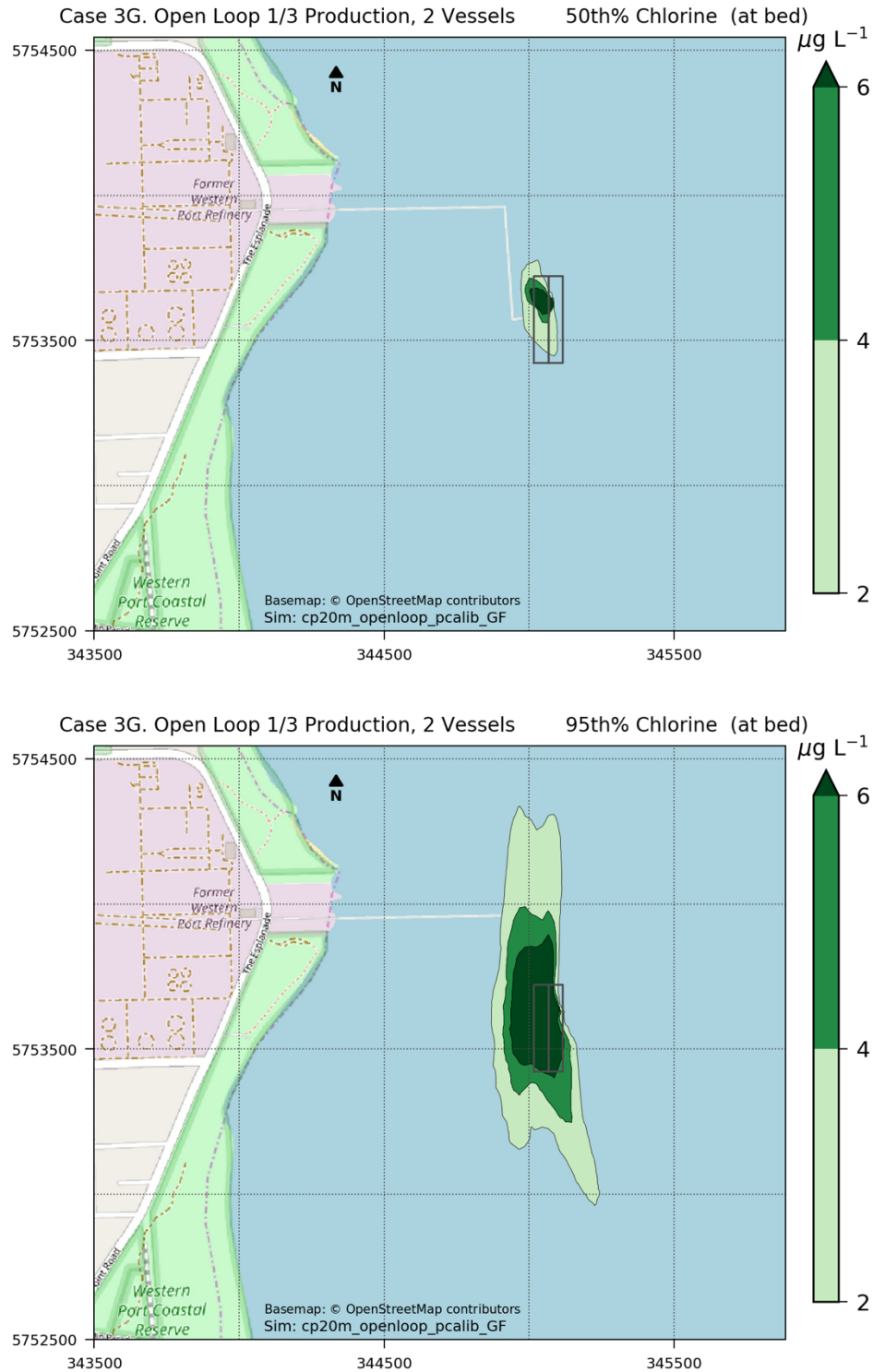


Figure 8.13 Plan view of mean (top) and 95th percentile (bottom) chlorine concentration at the seabed for a 28-day open loop 1/3 production simulation with neighbouring vessel.

8.5 Open Loop, Peak Production, West Facing Ports

This simulation includes open loop operations with peak discharge of $5.4 \text{ m}^3/\text{s}$ at 7°C below ambient temperature and $100 \mu\text{g/L}$ chlorine concentration. The discharge is inserted into cells

to west side of FSRU (i.e. a mirror image of open loop simulation from the east side) with the addition of a neighbouring vessel on the east side.

The area of seabed with a temperature reduction of 0.5°C is about 400 m long north to south and about 110 m wide east to west and smaller than the area with a temperature reduction of 0.5°C for east-side ports with a neighbouring vessel (Figure 8.2). The median and 95th percentile simulated chlorine concentrations contour areas are also reduced (Figure 8.15).

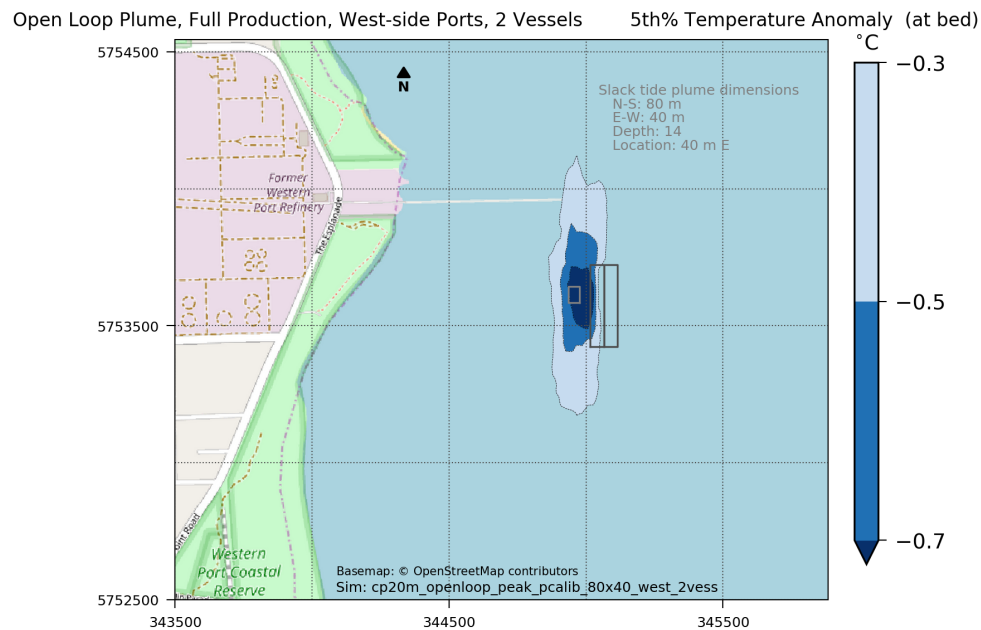
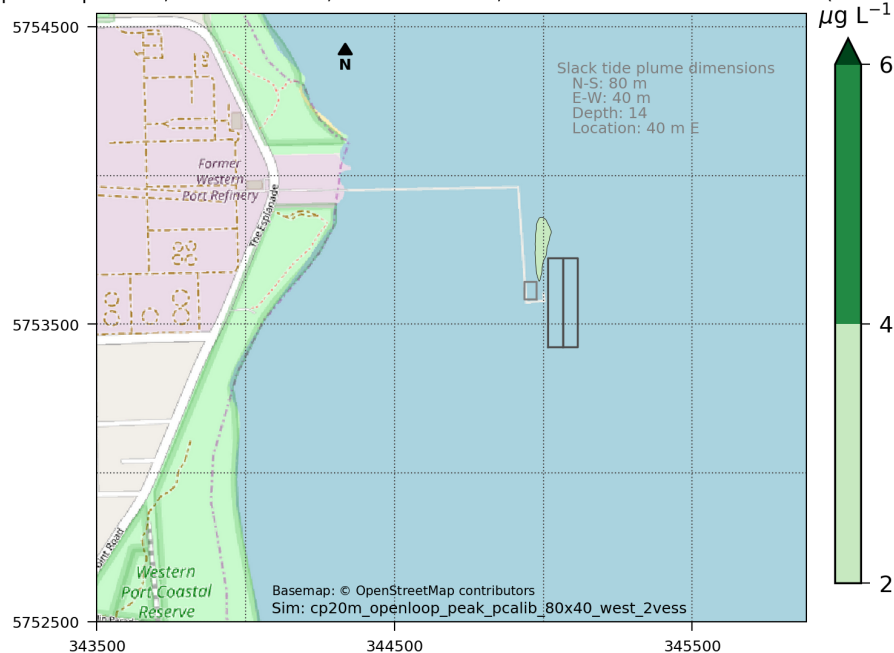


Figure 8.14 Plan view of 5th percentile of temperature decrease at the seabed for a 28-day open loop peak production simulation with discharge from west side of FSRU and neighbouring vessel configuration.

Open Loop Plume, Full Production, West-side Ports, 2 Vessels 50th% Chlorine (at bed) $\mu\text{g L}^{-1}$



Open Loop Plume, Full Production, West-side Ports, 2 Vessels 95th% Chlorine (at bed) $\mu\text{g L}^{-1}$

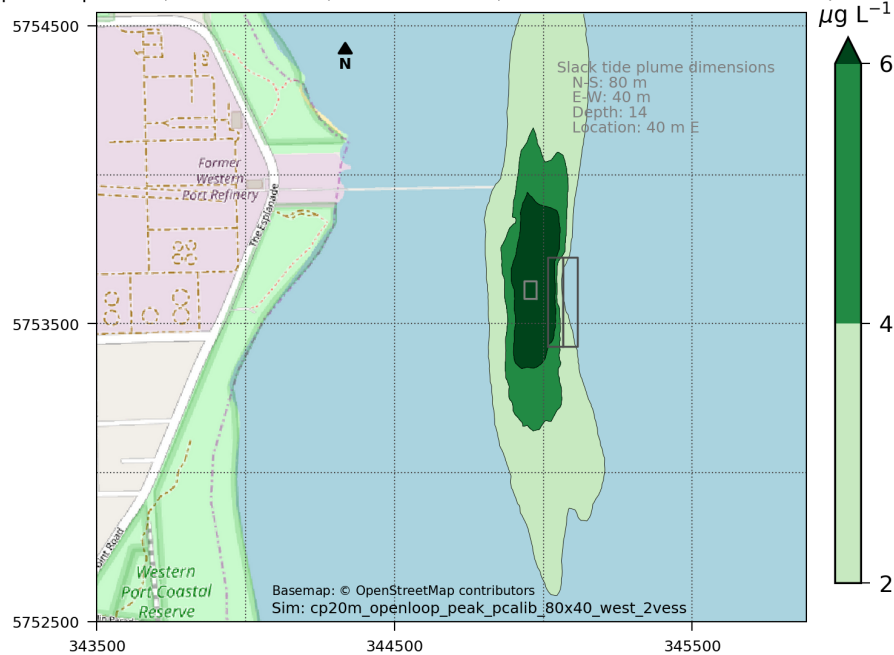


Figure 8.15 Plan view of mean (top) and 95th percentile (bottom) chlorine concentration at the seabed for a 28-day open loop peak production simulation with discharge from west side of FSRU and neighbouring vessel.

8.6 Closed Loop East and West Rear Discharge

This simulation considered closed loop rear discharges of $1.82 \text{ m}^3/\text{s}$ at 4°C above ambient and $100 \mu\text{gCl/L}$ inserted into the rear starboard (east) cell ($20 \times 20 \text{ m}$) on the bed adjacent to the FSRU, combined with $0.96 \text{ m}^3/\text{s}$ discharge at 4°C above ambient and $70 \mu\text{gCl/L}$ inserted into the rear port (west) cell on the bed adjacent to the FSRU, with the neighbouring vessel included in the simulation.

The simulation results illustrate small areas at the rear of the FSRU with temperature increases of more than 0.3°C (Figure 8.16). Mean chlorine concentration contours (Figure 8.17) are above $6 \mu\text{g/L}$ over small areas near the discharges at the rear of the FSRU and the 95th percentile chlorine concentration contours (Figure 8.18) indicates a larger area with chlorine concentrations above $6 \mu\text{g/L}$ to the rear, west and underneath the vessels.

Timeseries of temperature and chlorine concentrations at and near the discharge locations are presented in Figure 8.19 and Figure 8.20.

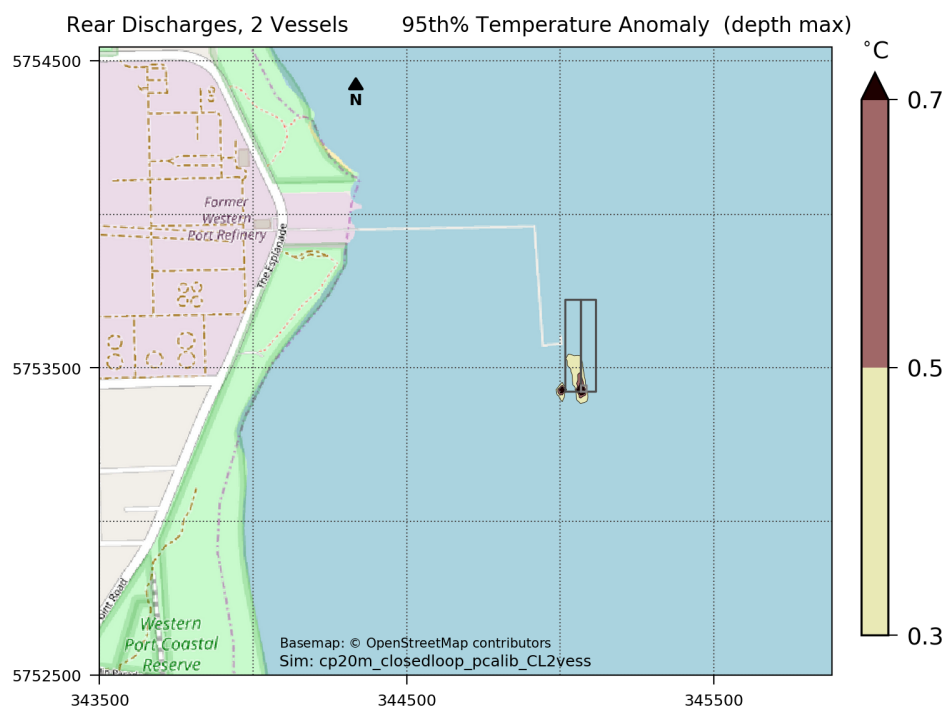


Figure 8.16 Plan view of 5th percentile of temperature change in the water column (highest from all depths) for a 28-day closed loop east and west rear discharge simulation with neighbouring vessel.

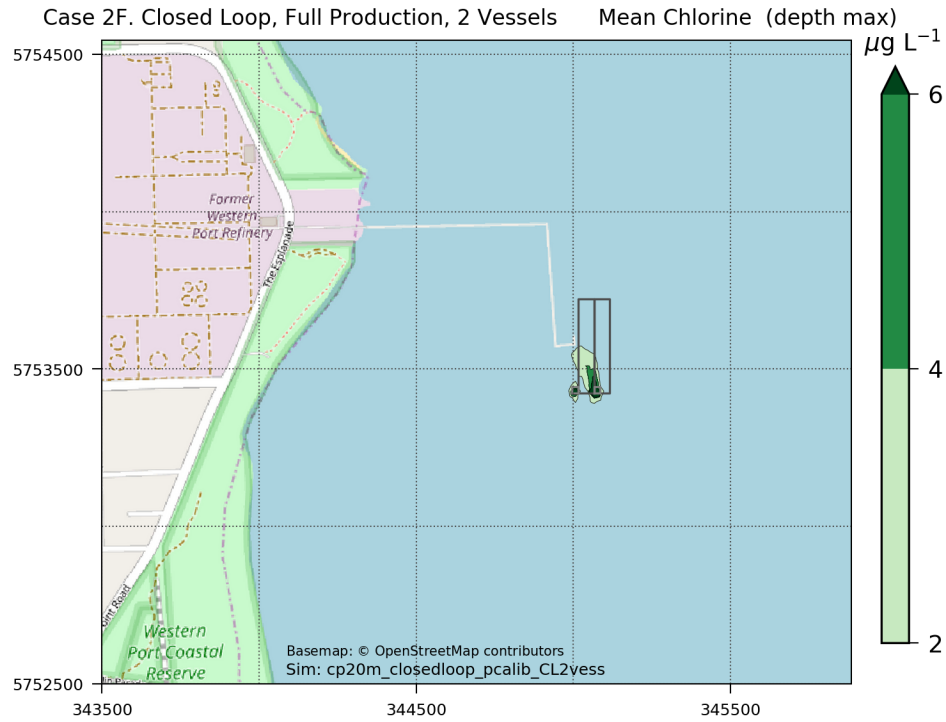


Figure 8.17 Plan view of mean chlorine concentration in the water column (highest from all depths) for a 28-day closed loop east and west rear discharge simulation with neighbouring vessel.

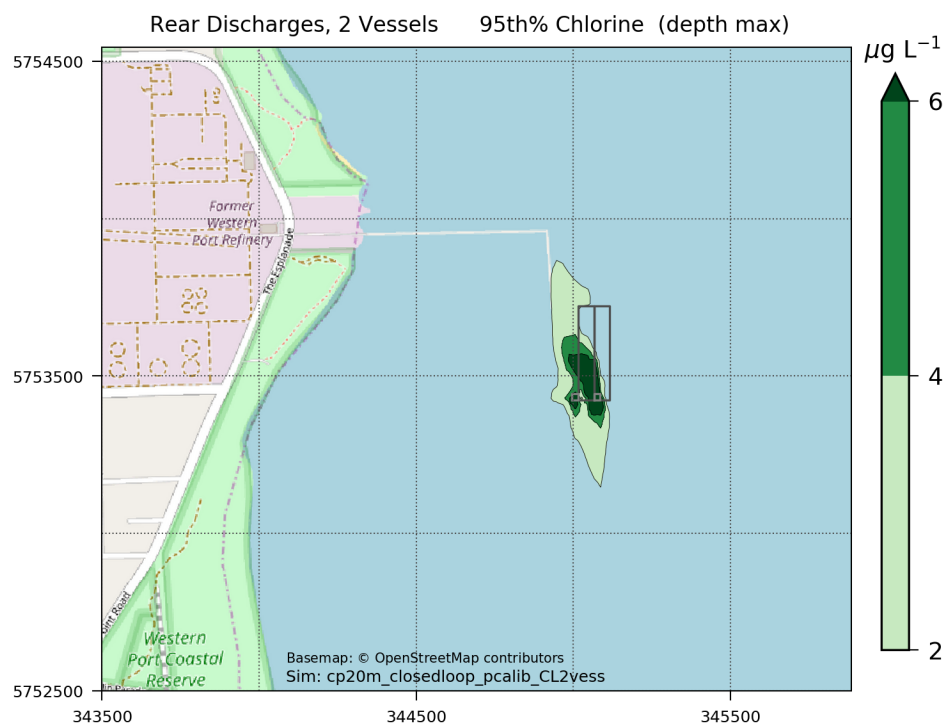


Figure 8.18 Plan view of 95th percentile chlorine concentration in the water column (highest from all depths) for a 28-day closed loop east and west rear discharge simulation with neighbouring vessel.

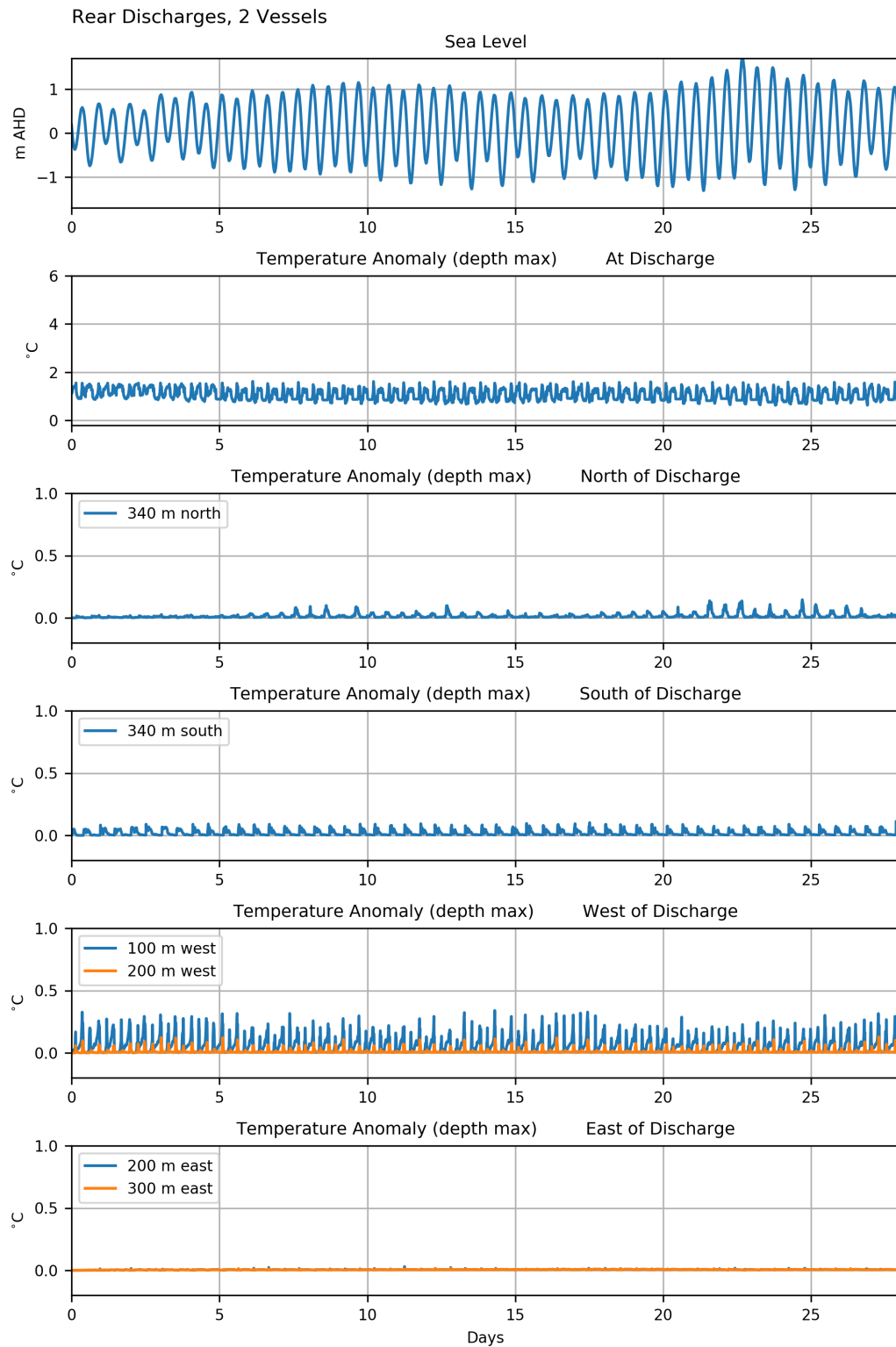


Figure 8.19 Time series of sea level (top panel) and (running down the page) temperature reduction at the seabed below the plume and north, south, west and east of the FSRU during closed loop east and west rear discharge with neighbouring vessel.

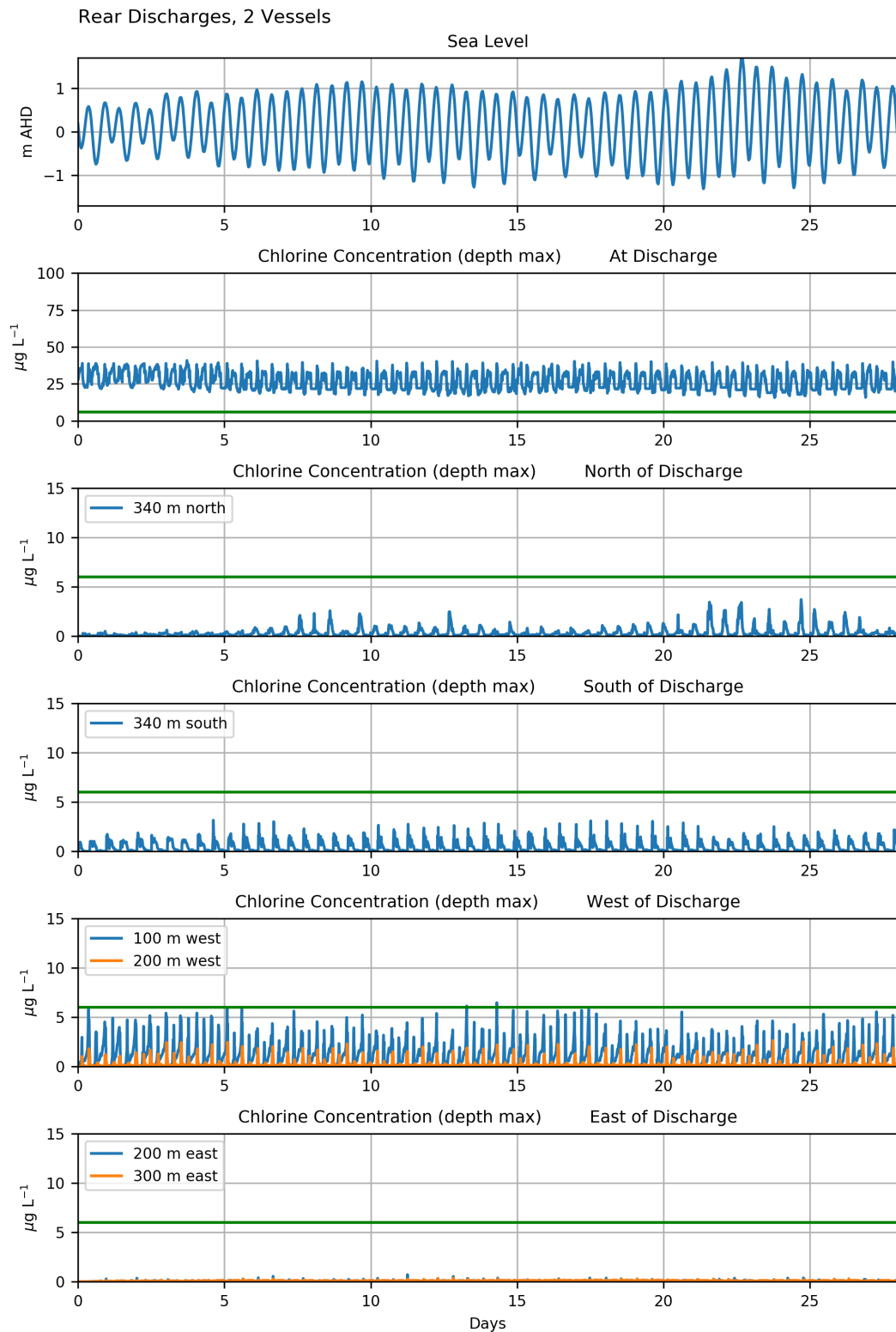


Figure 8.20 Time series of sea level (top panel) and (running down the page) chlorine concentration at the seabed below the plume and north, south, west and east of the FSRU during closed loop east and west rear discharge with neighbouring vessel.

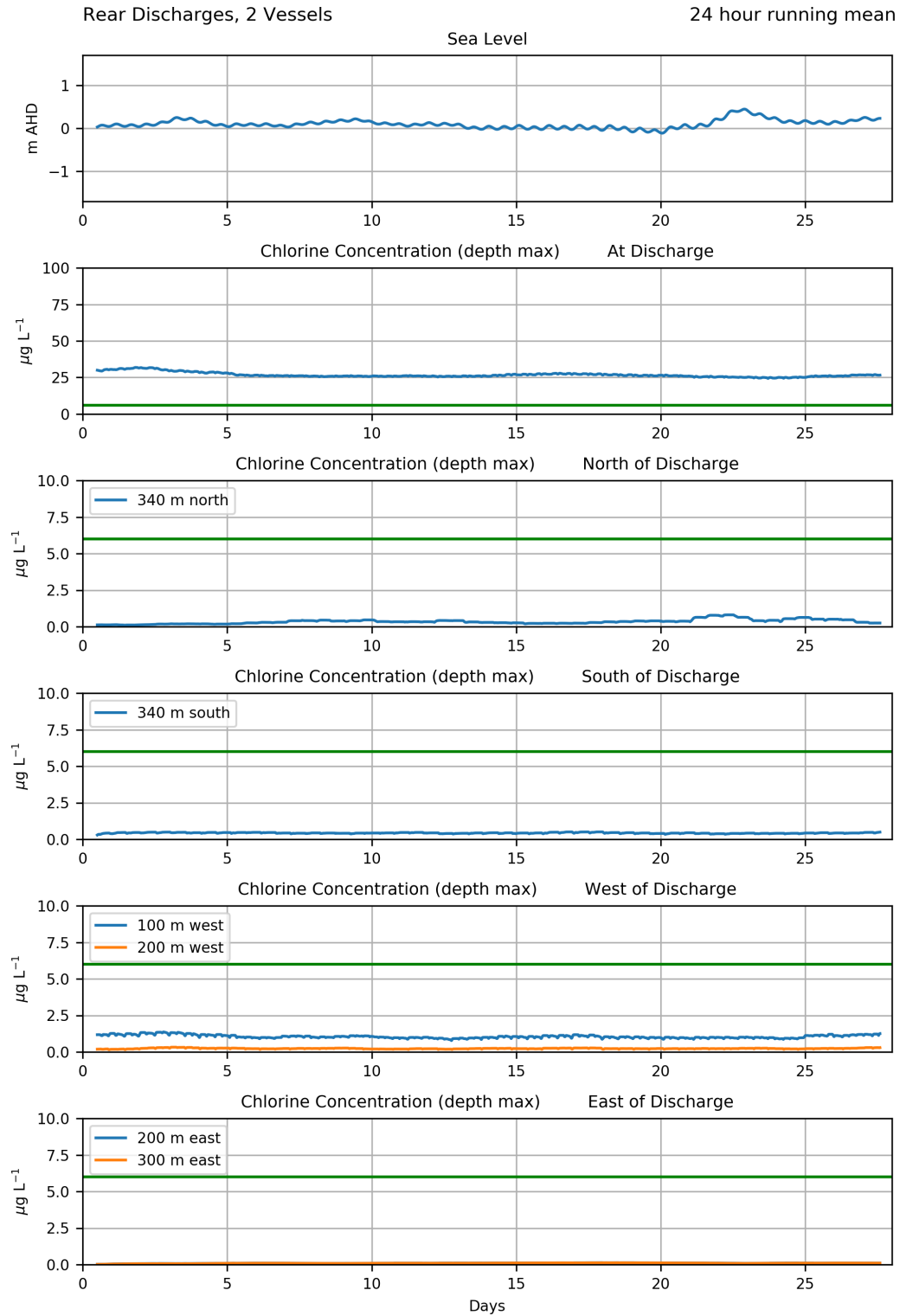


Figure 8.21 24-hr moving average time series of sea level (top panel) and (running down the page) chlorine concentration at the seabed below the plume and north, south, west and east of the FSRU during closed loop east and west rear discharge simulation with neighbouring vessel.

8.7 Closed Loop 2/3 Production

This simulation considered a scenario of closed loop with 2/3 discharge of $1.44 \text{ m}^3/\text{s}$ at 5°C above ambient and $100 \text{ }\mu\text{g/L}$ chlorine concentration inserted into the rear starboard cell (20 m long and 20 m wide at the bed) adjacent to the FSRU with the neighbouring vessel included in the simulation.

Results show (Figure 8.22) a small region experiences mean chlorine concentrations over $6 \text{ }\mu\text{g/L}$ at the rear of the FSRU. The area experiencing chlorine concentrations over $6 \text{ }\mu\text{g/L}$ for 5 % of the time is approximately 150 m by 75 m.

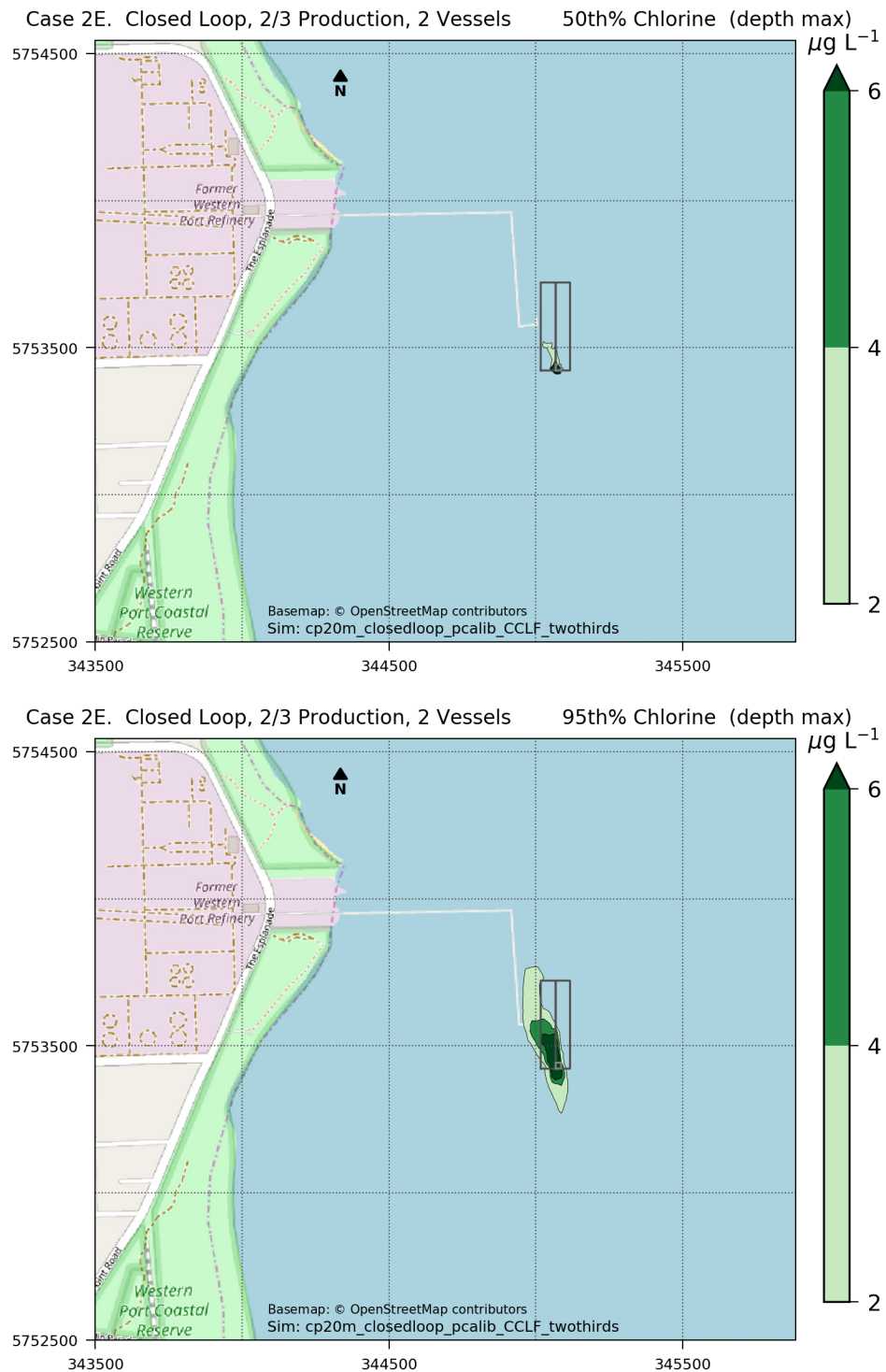


Figure 8.22 Plan view of mean (top) and 95th percentile (bottom) chlorine concentration in the water column (i.e. over all depths) for a 28-day closed loop 2/3 production simulation with neighbouring vessel.

8.8 Closed Loop 1/3 Production

Closed loop with 1/3 discharge with $0.72 \text{ m}^3/\text{s}$ at 5°C above ambient and $100 \text{ }\mu\text{g/L}$ chlorine concentration reduces the area experiencing chlorine concentrations over $6 \text{ }\mu\text{g/L}$ (Figure 8.23) compared to the results of the cool open loop 1/3 production discharge shown above. A small region experiences mean chlorine concentrations over $6 \text{ }\mu\text{g/L}$. The area experiencing chlorine concentrations over $6 \text{ }\mu\text{g/L}$ for 5 % of the time is approximately 100 m by 50 m.

Mean and 95th percentile chlorine concentrations due to simultaneous ballast water and closed loop discharges are shown in Figure 8.24.

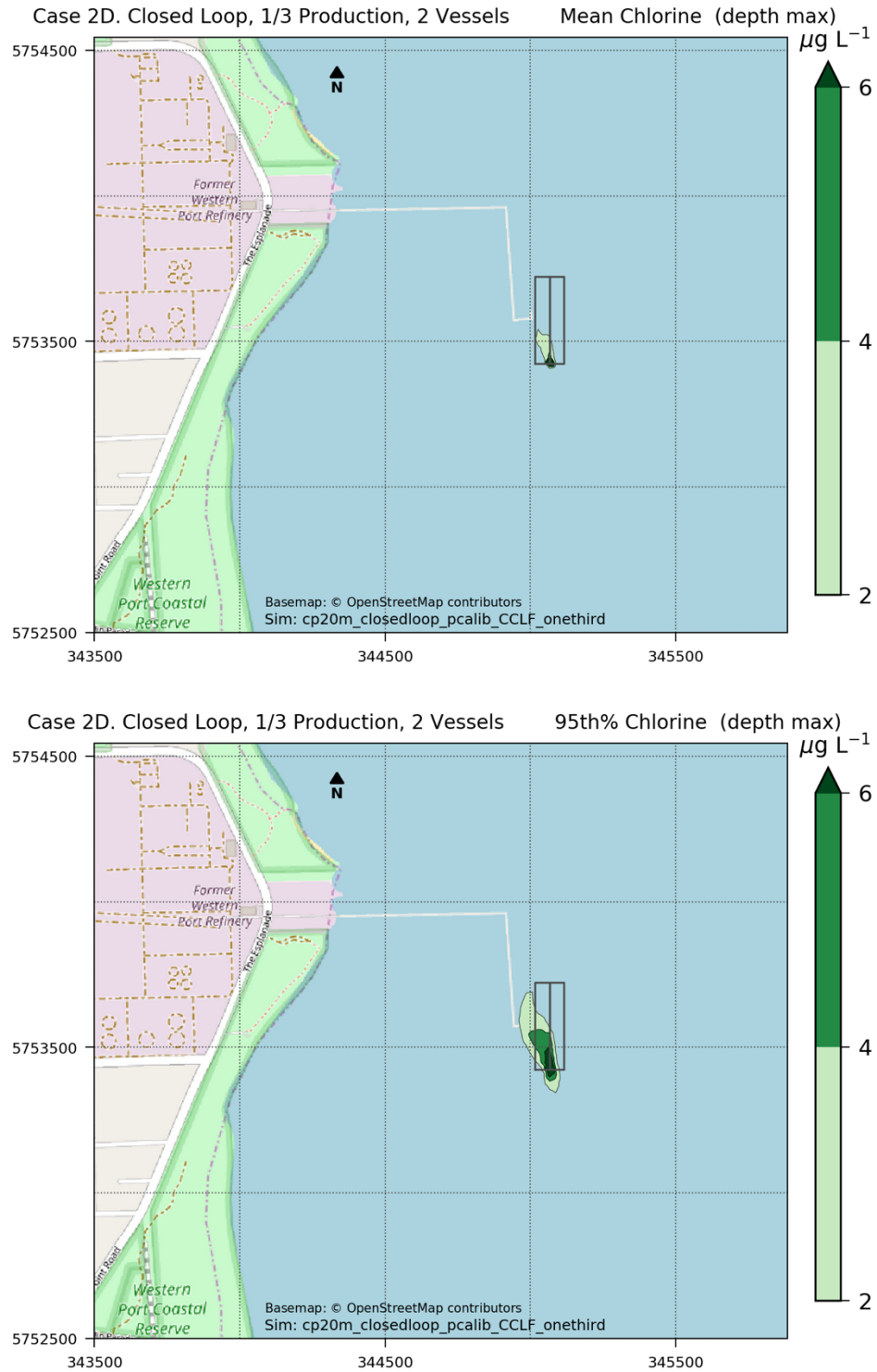


Figure 8.23 Plan view of mean (top) and 95th percentile (bottom) chlorine concentration in the water column (i.e. over all depths) for a 28-day closed loop 1/3 production simulation with neighbouring vessel.

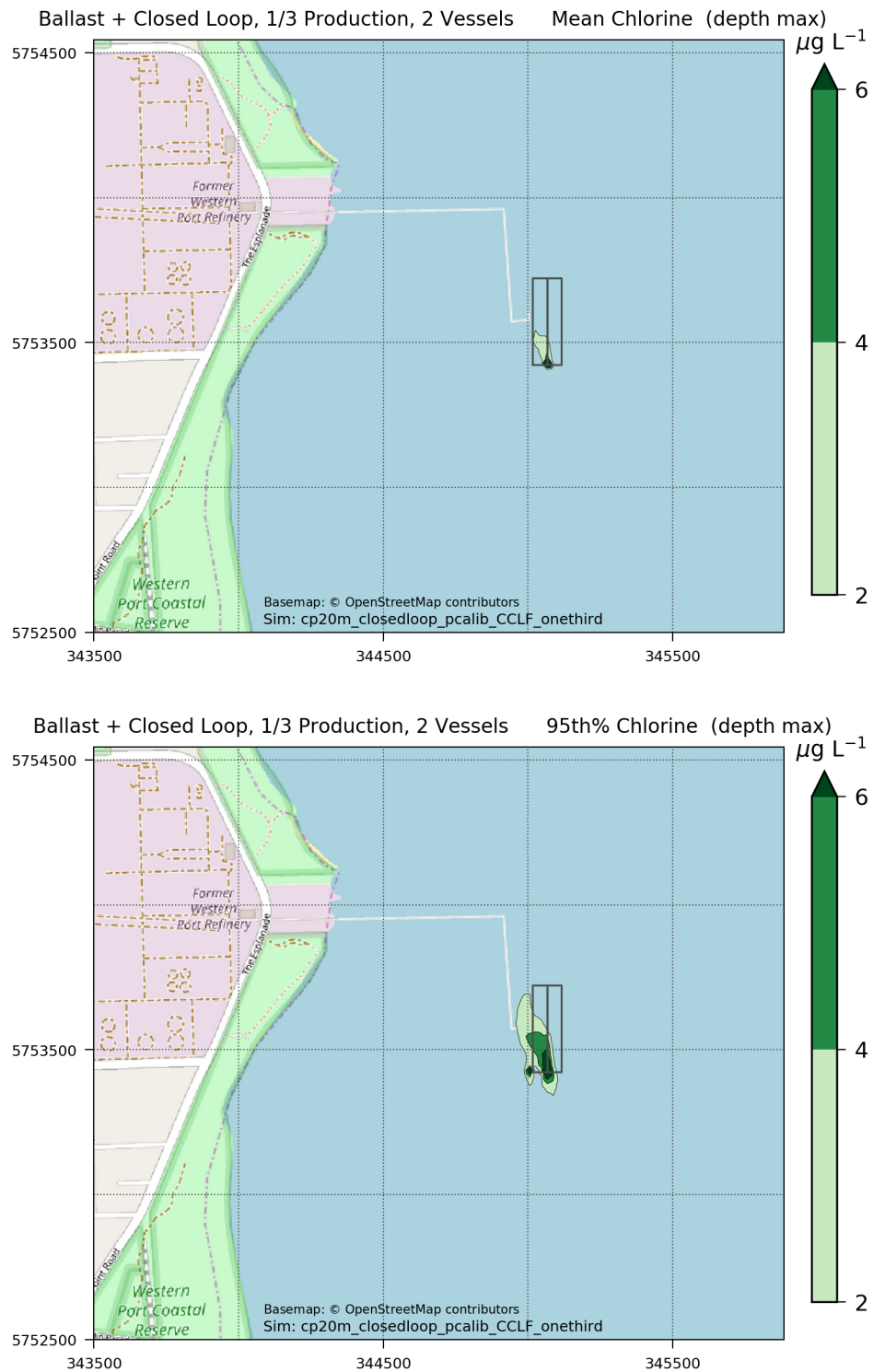


Figure 8.24 Plan view of mean (top) and 95th percentile (bottom) chlorine concentration in the water column (i.e. over all depths) from ballast and closed loop discharges for a 28-day closed loop 1/3 production simulation with neighbouring vessel.

9 Assumptions, Limitations and Model Sensitivity

9.1 Assumptions and Limitations

The modelling outcomes in this report are based on the project information and data available at the time of the modelling study. As such, the outcomes of the modelling are limited to being valid only for the description of the project that has been provided. This includes the description of the FSRU vessel, the mooring position and the intake discharge rates, temperature and chlorine concentrations. Key assumptions and limitations associated with the modelling are as follows:

- The available bathymetric data used to undertake the modelling provides a sufficient depiction of the current bathymetry of WPB at a resolution that is appropriate for the modelling;
- The ocean and atmospheric information that has been used from BoM resources is of sufficient temporal and spatial resolution to use as boundary conditions into the model. Previous modelling of WPB has shown that spatial heterogeneous boundary conditions are likely to provide the best simulation results for WPB. The BoM data represents the best available source of heterogeneous data for the whole of WPB;
- The selected simulation periods are representative of the range of conditions that are expected and that changes due to climate change, or other unknown long-term environmental trends, do not create significant differences in terms of entrainment and plume dispersion;
- It has been assumed that the configuration of the model that has been applied contains the necessary descriptions of the key processes that influence the distribution of the FSRU discharge and larvae capture into the FSRU. Care has been taken with the application of AEM3D to ensure that the required processes (see Section 2.1.2) have been included. Moreover, the calibration demonstrates that there is good agreement between the model and observations, thus providing confidence in the model capability. The model sensitivity exercise that is discussed below has been used to assess the potential impact that assigned model parameters and configurations have on the overall findings;
- The accuracy of the model is limited by the grid size. The grid scales applied have been selected to appropriately resolve the flow field at the project site and in the boarder WPB. Finer resolution grids are limited by excessively long simulation times of the model;
- The model grid size limits the ability of the model to capture sub-grid scale process in the background flow, such as the detail of flow characteristics around the jetty and the influence of the FSRU and other vessels on the detailed flow behaviour. It has been assumed that the selected grid size of 20 m by 20 m by 1 m deep is sufficiently fine to adequately represent mixing of discharges; and
- In terms of the simulation of FSRU intake and discharge it has been assumed that the near-field modelling provided by CEE adequately captures the required processes that occur at scales less than the far field model grid and that the outcomes of the near-field modelling have been appropriately translated into the far-field model inputs.

9.2 Model Sensitivity

The model was calibrated against observed ADCP data as described in Chapter 2. Based on the calibration a model configuration was selected and applied to obtain the results described above (Simulation P). However, a key discrepancy between the Simulation P and observed ADCP data that may have implications for the accuracy of the prediction of the FSRU impact is weaker modelled near-bottom currents at the western ADCP near Crib Point. Whilst this is not symptomatic of the whole model domain (as evidenced by outputs at nearby locations) it is related to the resolution of the complex bathymetry in the project area and potential discrepancies between the present bottom elevations and the time of the bathymetric data survey.

To examine the sensitivity with regards to the FSRU discharge and intake additional scenario simulations were repeated using two alternative model configurations. The first configuration was a moderate constant drag ($C_D = 5 \times 10^{-3}$) with high dissipation rate and slow vertical mixing ($C_\epsilon = 1.15$, $C_{TT} = 50$). This simulation (Simulation A, see Appendix A) produced higher velocities at Crib Point than Simulation P (gradient 0.99, $R^2 = 90\%$ at the bottom when compared to data from the ADCP). Current speeds near the surface and mid-depth were higher than observed at the Crib Point ADCP (gradient of 1.02 and 1.04 at the surface and mid-depth, respectively), and 12 to 38% higher at the other ADCPs.

In the second additional configuration (Simulation X, see Appendix A) a constant low drag coefficient of $C_D = 2 \times 10^{-3}$ was applied, with high dissipation rate but rapid mixing ($C_\epsilon = 1.15$, $C_{TT} = 8$). This model produced similar results to Simulation P described in the results above using a different set of parameters. These results are compared below to the calibrated model described in Chapter 2 (Simulation P).

Whilst there is likely to be a combination of drag application and mixing parameters that further reduce the discrepancies between the observed and modelled currents at the ADCP locations that are presented in Chapter 2, the heterogeneous nature of the drag (given the different benthic cover in WPB) and uncertainty in the drag map make further refinement of the model difficult. Assessing the sensitivity of the FSRU scenario outcomes over a range of model configurations is considered a more efficient and informative processes.

In addition to these alternative model configurations, alternate configurations of the near-field plume implementation were also tested for the FSRU discharge assessment.

9.2.1 FSRU Discharge

Hydrodynamics

Figure 9.1 illustrates seabed temperature reductions over time for the different model configurations. Despite the differences in modelled currents, the changes to the seabed temperature are largely consistent. This is because the development of the plume is dependent on the slack tide characteristics and the movement of the pooled plume water that occurs for only a limited time before mid-tide. During this phase of the tide the modelled velocities are low and similar for the model configurations (aside from some notable phase differences). The pooled water is dispersed prior to when Simulation A produces significantly higher mid-tide current speeds.

Contour maps of 5th percentile of temperature reduction at the seabed are shown in Figure 9.2 and Figure 9.3 for a 28-day simulation in March 2019 for the different model configurations. The figures illustrate that while simulation P and X produce very similar statistical plume results, simulation A, which has higher ambient velocities, produced a smaller plume. Therefore, simulation P, which has been used for the discharge assessments and underpredicts velocities near the bottom at Crib Point, is likely to provide a conservative estimate of the plume dispersion. The contour maps also illustrate that repeating the simulation for June 2018 using configuration P produces very similar results to the March 2019 period despite differences in the boundary conditions (see Section 2.2.4). This is because both tidal series, which dominate the flow field and hence plume dispersion, contain comparable periods of neap and spring tide over the 28-day of simulation.

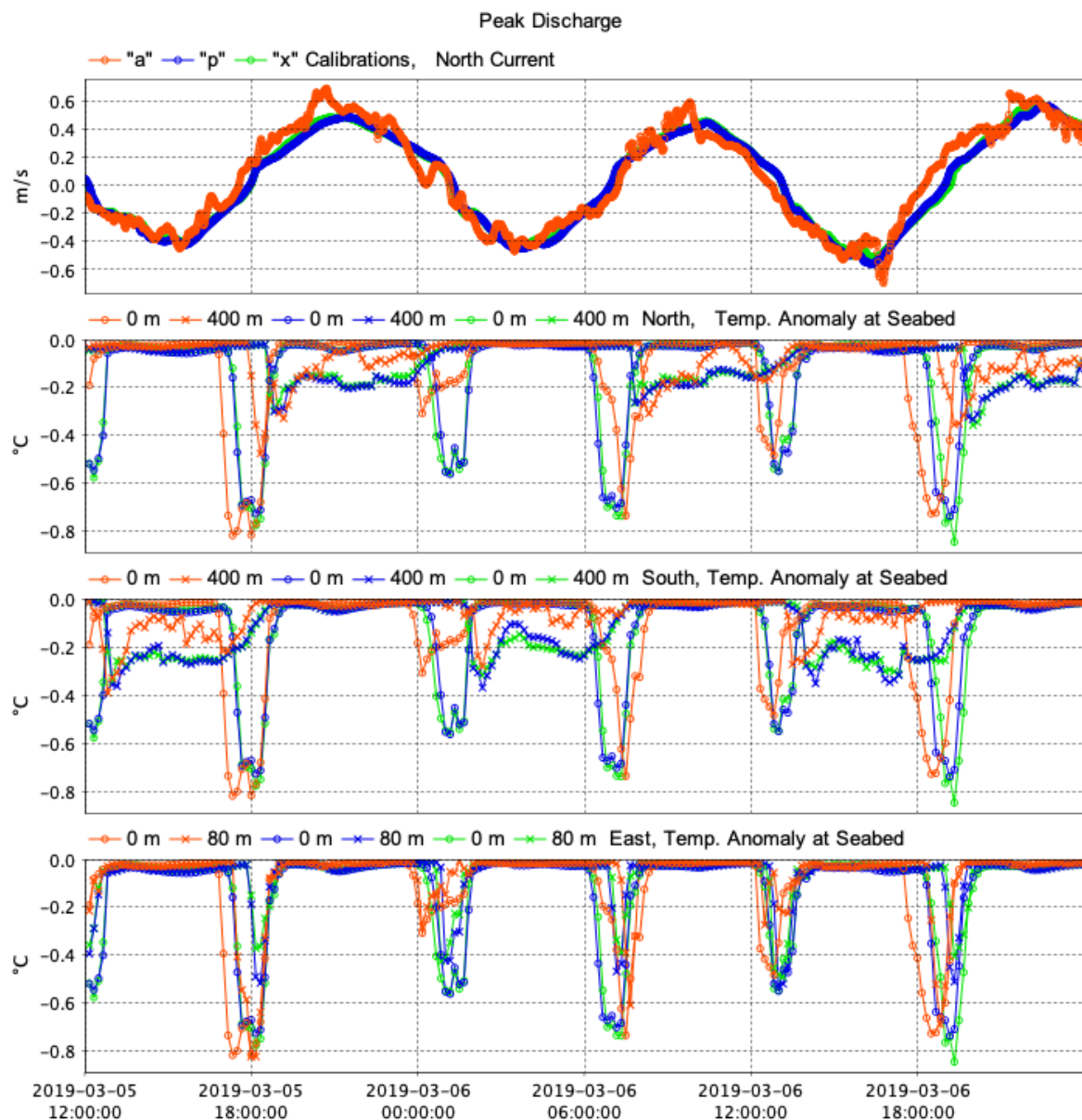


Figure 9.1 Timeseries of current at the FSRU ports (top panel), temperature reduction at sites at and north of FSRU (second panel), temperature reduction at sites at and south of FSRU (third panel) and temperature reduction at sites at and east of the FSRU during peak discharge for three different model configurations.

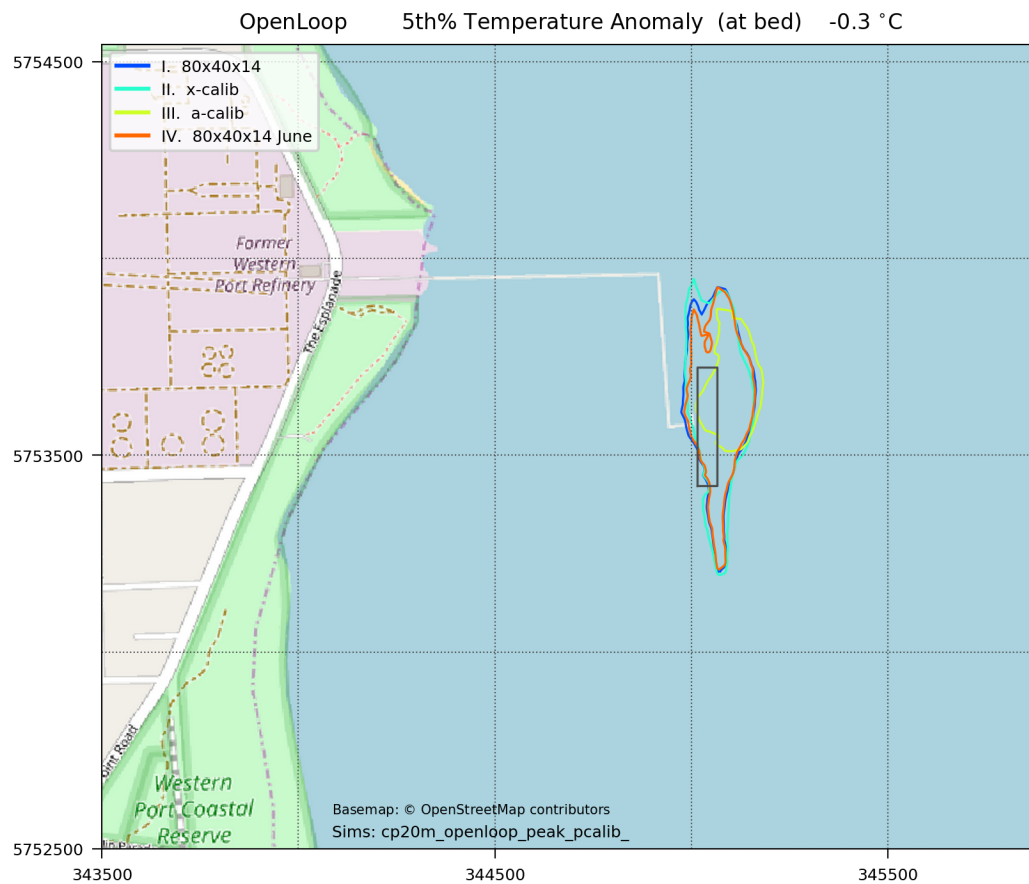


Figure 9.2 -0.3 °C contour of 5th percentile of temperature decrease at the seabed during over a 28-day simulations at peak FSRU discharge. Simulation P is shown in dark blue.

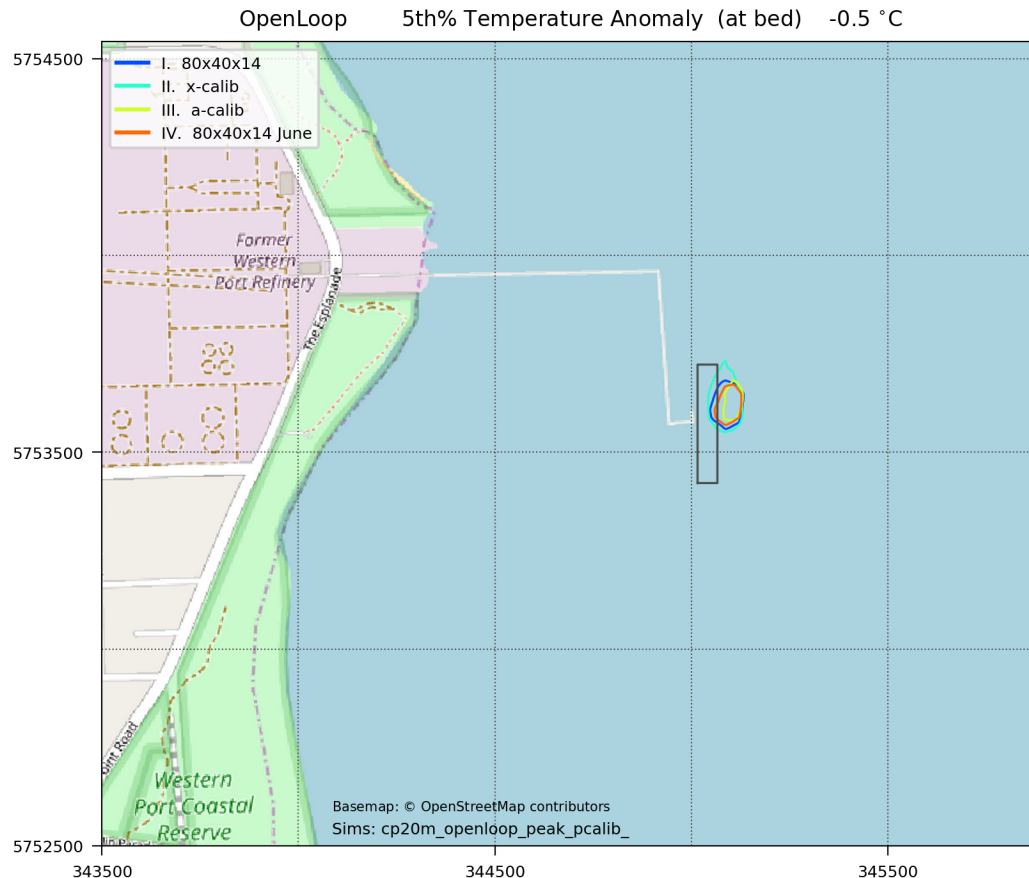


Figure 9.3 -0.5 °C contour of 5th percentile of temperature decrease at the seabed during over a 28-day simulations at peak FSRU discharge. Simulation P is shown in dark blue.

Near-field Plume Configuration

A series of simulations were performed using a range of alternative configurations for the discharge plume that was represented in the far-field model (i.e. size, shapes and location). A detailed list of the set-up and the results for each of these configurations is provided in Appendix B. The results are summarised in Figure 9.4 and Figure 9.5 for the 5th percentile temperature decrease at the seabed of -0.3 °C and -0.5 °C respectively.

The results indicate that whilst there is a general consistency between the simulations, larger plumes were created when there was less lateral near-field pre-dilution (i.e. those with 60 m N-S length compared to 80 m and 20 m E-W width compared to 40 m). The largest plume was created when the initial plume size was 60 x 20 m and remained alongside the boat under all flow conditions. This suggests that dilution offered by the momentum associated with the discharge water (as it travels out from the vessel and entrains ambient fluid) is an important process in limiting the extent of the temperature decrease on the seabed.

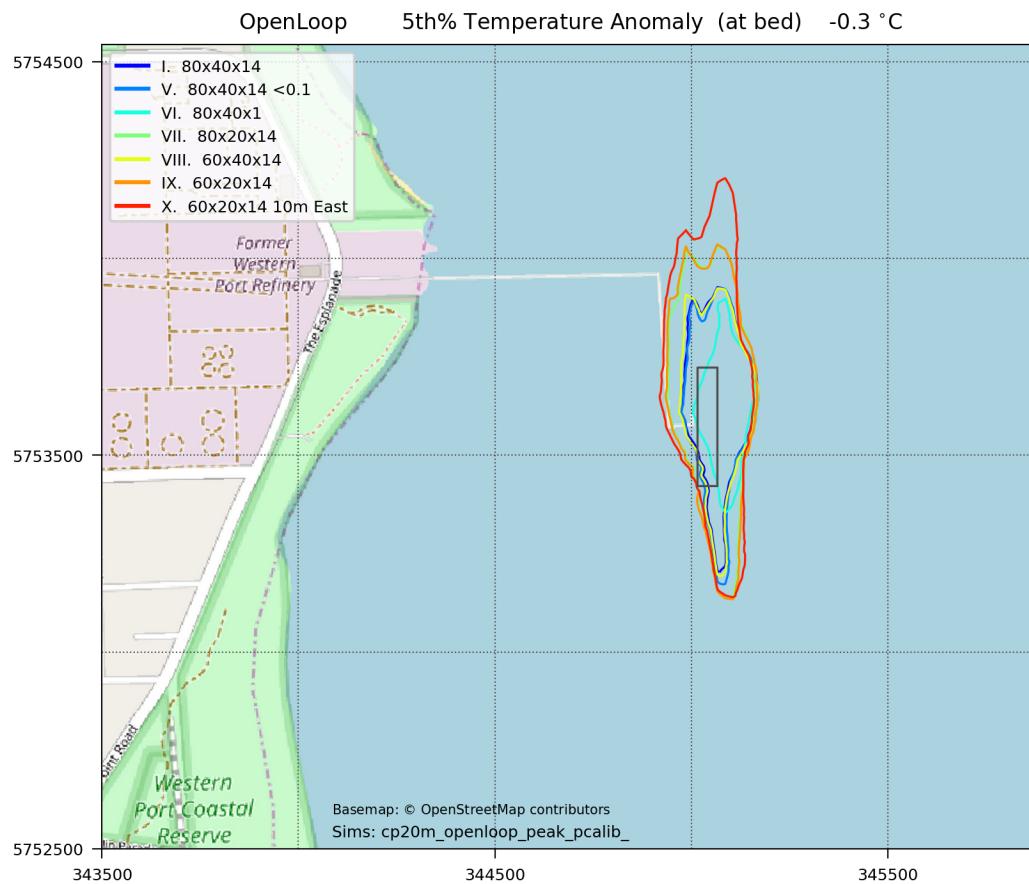


Figure 9.4 -0.3 °C contour of 5th percentile of temperature decrease at the seabed during over a 28-day simulation at average FSRU discharge. Simulation P is shown in dark blue.

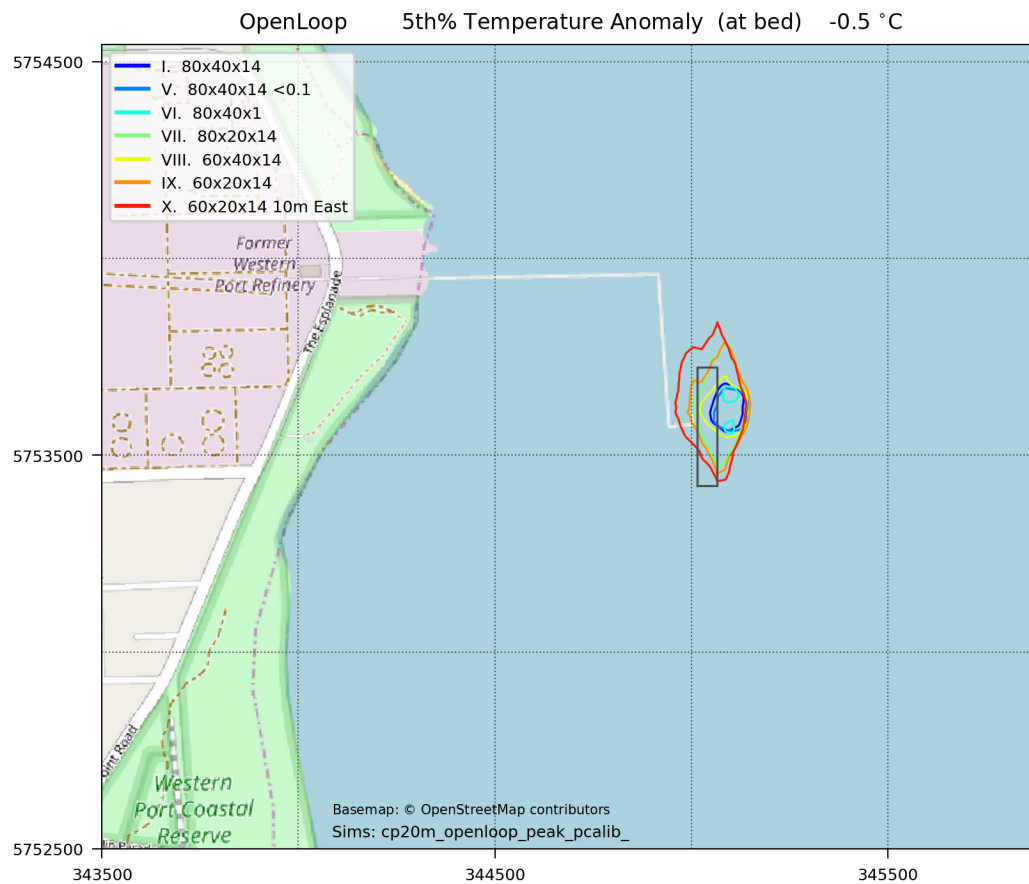


Figure 9.5 -0.5 °C contour of 5th percentile of temperature decrease at the seabed during over a 28-day simulation at average FSRU discharge. Simulation P is shown in dark blue.

9.2.2 FSRU Intake

Hydrodynamics

Re-simulating the release and entrainment of particles from zones 2, 3 and 7 using the alternative model configurations (Simulation A and X) produced the time series illustrated in Figure 9.6 over a 28-day simulation starting 11 November 2018. The higher velocities produced by Simulation A generated larger initial entrainment rates in zones 2 and 3. Simulation X produced entrainment figures within a range similar to the range associated with alternative particle release time and position. The high velocities and therefore larger tidal excursions produced by Simulation A lead to higher initial entrainment as a greater number of particles are advected past the FSRU during the early stages of the simulation. After this time the entrainment slows as the particles are dispersed.

Simulation P and X, which produce comparable particle capture results are likely to be more reliable given they produce a better comparison with the observations than Simulation A. Despite Simulation A producing the higher levels of entrainment from zones 2 and 3, the capture after 28 days remains less than 1% in zone 2.

A different period of release with boundary conditions from June 2018 was also undertaken. The results from this period (Figure 9.6) show that initial entrainment rates from zone 2 are lower for the June 2018 simulation, in response to the smaller tidal amplitude at the time of particle release (Figure 2.8). This reduction in entrainment is consistent with simulated neap tide surface release in Simulation P (Figure 5.5).

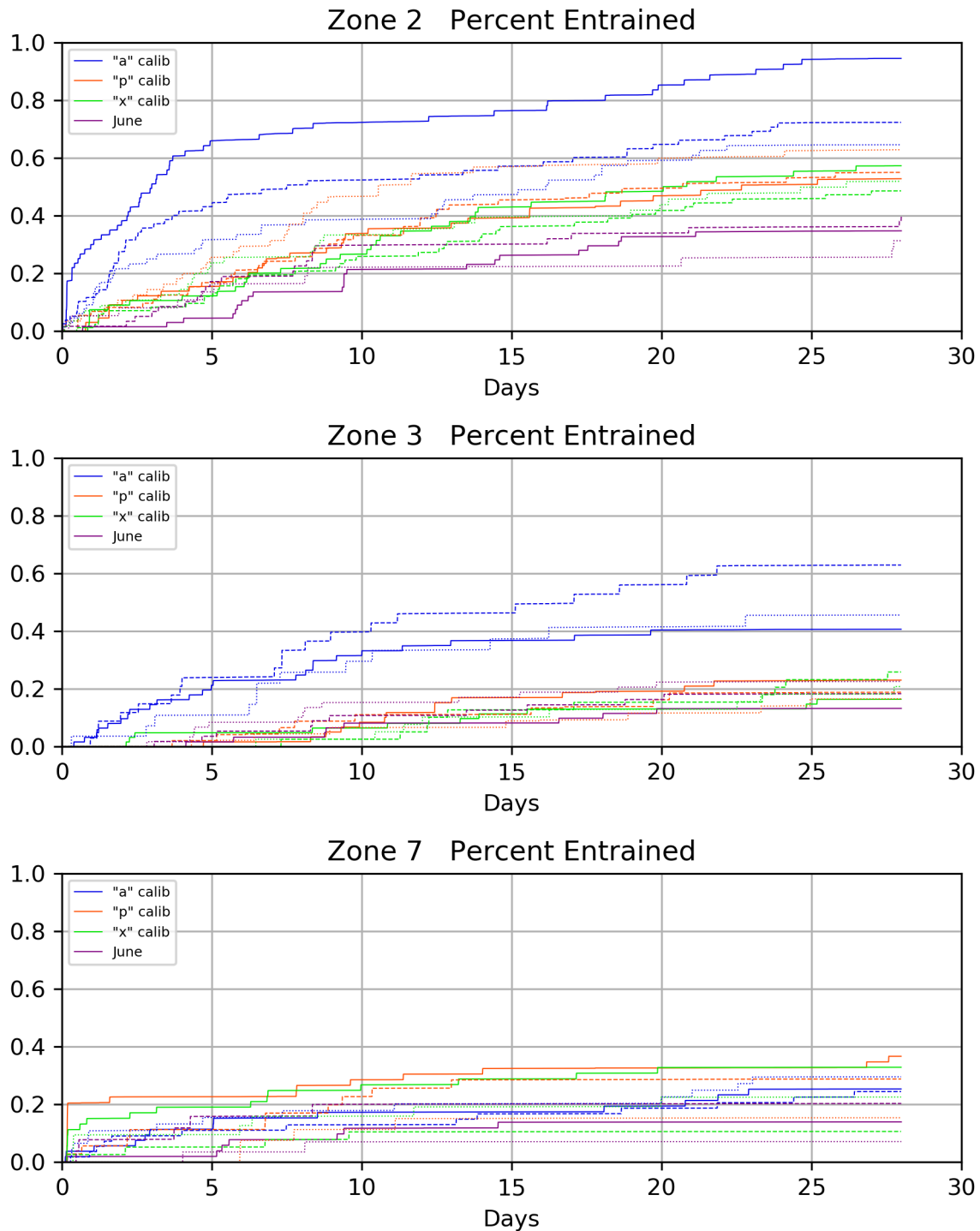


Figure 9.6 Entrainment of particles over 28 days from Zone 2 (top); Zone 3 (middle); Zone 7 (bottom) for different model hydrodynamics (colours) and different release times (solid, dashed and dotted lines are for initial conditions of uniform surface distribution on rising tide, mixed distribution on rising tide and mixed distribution on falling tide, respectively)

Model Configuration

Sensitivity tests were undertaken to assess how sensitive the entrainment results are to different model initial conditions and output timesteps (Figure 9.7). The results indicate that for a particular initial distribution and time of release (e.g. surface distribution on a rising tide) the output interval (10 minutes compared to 5 minutes) and the initial spacing (50 m compared to 35 m) do not significantly change the simulation entrainment estimates. There is comparable variation in entrainment numbers between simulations with different initial releases distributions but the same temporal and spatial resolution as there is between simulations with different spatial and temporal resolutions.

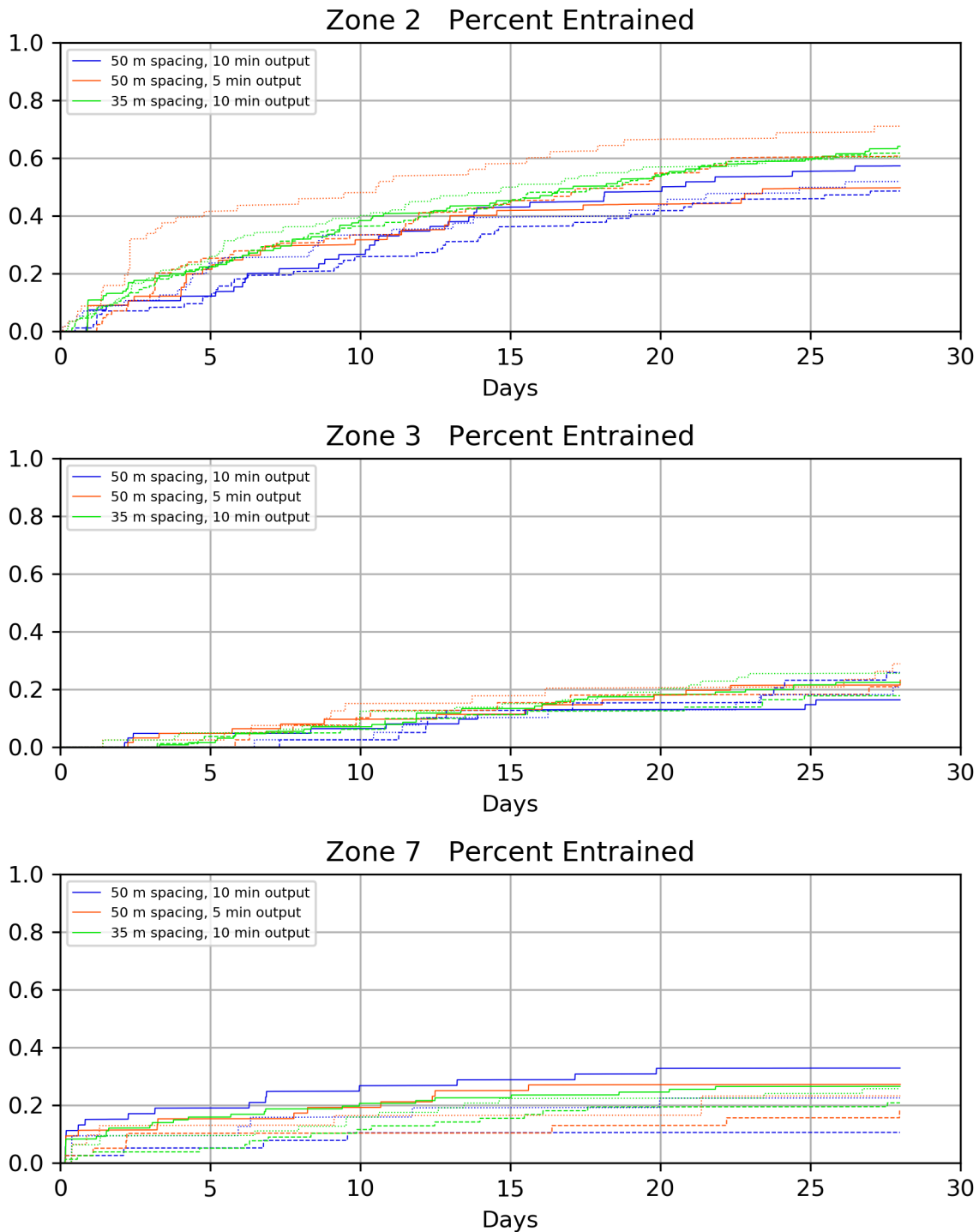


Figure 9.7 Entrainment of particles over 28 days from Zone 2 (top); Zone 3 (middle); Zone 7 (bottom) for different model set-up (colours) and different release times (solid, dashed and dotted lines are for initial conditions of uniform surface distribution on rising tide, mixed distribution on rising tide and mixed distribution on falling tide, respectively)

10 Conclusions

10.1 Temperature Outcomes

There is very small east-west movement of the plume due to the dominance of the north-south flow. As the patches of cooler water travel along the seabed under the action of the currents, the pooled water is diluted by vertical and lateral mixing as shear increases, until mixing erodes the plume completely. Within approximately 1.5 hours of slack water, temperature reductions are less than -0.3°C at the FSRU and at sites 200 and 400 m north (during flood tide) and south (during ebb tide).

As a consequence, the following summary can be drawn for temperature changes at the seabed during peak FSRU discharge rate of $5.4\text{ m}^3/\text{s}$.

- For 10 % of the time there is a small area of seabed beside the FSRU (and extending for less than the dimensions for the FSRU) that experiences cooling of -0.3 to -0.5°C from ambient; and
- For 5 % of the time there is:
 - A region beneath the plunging zone of the plume (approx. 100 m by 100 m) that experiences cooling of -0.5 to -0.7°C from ambient; and
 - An outer region that extends up to 300 m north and south of the FSRU that experiences cooling of -0.3 to -0.5°C from ambient. The width of the elongated plume is approximately 50 to 200 m, and widest near the FSRU.

For the average FSRU discharge rate of $3.6\text{ m}^3/\text{s}$:

- For 5 % of the time there is region beneath the plunging area of the plume (approx. 100 m by 100 m) that experiences cooling of -0.3 to -0.5°C from ambient.

At the bay-wide scale, heat fluxes are dominated by exchanges with the ocean and atmosphere (on diurnal and seasonal cycles and during events such as storms) so that the dispersed cool water has a local effect but a negligible large scale or cumulative effect on the water temperatures in the remainder of the bay.

10.2 Chlorine Outcomes

The FSRU produces chlorine in the seawater used for cooling and other purposes by electrolysis of the sodium chloride in the seawater drawn into the vessel. There is rapid decay of the chlorine as it passes through the pipes and heat exchangers. At the discharge ports, the chlorine level will be a maximum concentration of 100 µg/L. Over the same 28-day simulation for cool-water discharge the concentrations of chlorine at the seabed were assessed.

Consistent with CSIRO's report (Batley and Simpson, 2019), CEE has adopted a CPO (chlorine produced oxidants) guideline value of 6 µg Cl/L for 99% species protection for assessing potential impacts at Crib Point where strong tidal reversals in currents result in intermittent exposure of biota to dispersing discharge. For the great majority of the time the chlorine is dispersed and diluted to concentrations less than 6 µg/L in the vicinity of the FSRU and lower concentrations beyond the project area.

The modelling indicated for the peak FSRU discharge rate of 5.4 m³/s, 5% of the time there is a patch on the seabed (approx. 200 m N-S by 150 m E-W) where the discharge plume plunges and chlorine concentrations at the seabed are higher than 6 µg/L.

For average discharge of 3.6 m³/s, 5% of the time there is a patch on the seabed (approx. 50 m by 50 m) where the discharge plume plunges and chlorine concentrations at the seabed are higher than 6 µg/L.

These percentile results reflect short-duration concentration peaks. The time-weighted average chlorine concentration near the FSRU is below 2 µg/L which is below the guideline value of 6 µg/L recommended by the CSIRO.

Because there is rapid chemical change, and because of the large exchange of waters between the project area and the remainder of the bay (and ultimately with Bass Strait), the cumulative effects of chlorine discharge from the FSRU in the project area and more broadly over the remainder of the bay are expected to be negligible. The chlorine created by electrolysis of seawater returns to the chloride (as part of sodium chloride) in seawater in a day or so, so there is no long-term accumulation of chlorine in the bay (CEE 2018d).

10.3 FSRU Entrainment

The potential entrainment of plankton into the FSRU (e.g. plankton and fish larvae) from different regions of the bay was simulated in the model by releasing neutrally buoyant particles into various zones in the western and northern parts of the bay. The position of each particle was determined in the model every 10 minutes. To allow a 28 days run time, the 50 x 50 m model grid was used for the particle release and capture simulations.

The dimensions of the entrainment volume associated with seawater intake by the FSRU were determined as a function of the current speed (CEE, 2018b). These dimensions were applied to determine the number of the released particles from each zone that travel into the intake entrainment zone. As a sensitivity analysis, a series of counts were made based on particle release at different stages of the tide (spring, neap, rising and falling) and with different initial distributions (vertical and horizontal).

The simulation results indicate that the highest entrainment occurs for particles released in the main channel close to Crib Point, where 0.75% of particles are predicted to be captured over a 28-day period. For zones further away, the entrainment ranged between 0.41 % (east of Crib Point) to less than 0.1 % in the western entrance to the bay. The average entrainment rate for North Arm was 0.38% over 28 days at peak production and 0.26% over 28 days for average production.

The entrainment asymptotes towards the end of the 28-day simulation as the particles are flushed to Bass Strait, or dispersed throughout the remainder of the bay, becoming increasingly unlikely to encounter the entrainment zone of the FSRU over time. The water on the mudflats in the north of the Bay drains slowly compared the other zones (in North Arm) so the entrainment percentage continues to increase rather than asymptote over the 28-day period.

Dispersion of particles through the remainder of the bay, including loss to the ocean (which is highest for areas nearer to the entrance to the bay) are the dominant mechanisms for loss of particles from each of the zones.

The entrainment results need to be considered in the context of the biological cycles and life cycle of the populations as the 28-day timeframe considered may be longer than the time taken to renew populations. The biological context and implications of these model results are addressed in the marine risk assessment prepared by CEE.

10.4 Model Sensitivity

The differences in seabed temperature reductions between alternative far-field model configurations were small, despite the inclusion of a higher ambient velocity case. This occurs because the development of the discharge plume is dependent on the slack tide characteristics and the movement of the pooled plume water that occurs for only a limited time before mid-tide, when dilution increases. The simulated velocities from the different model configurations are largely consistent over this period (aside from some phase differences).

Simulations of an alternative 28-day period, with alternate weather and ocean conditions, indicated little change in the discharge plume characteristics. This occurs because of the dominance of the tidally driven flow on the dispersion of the plume so that provided comparable periods of neap and spring tide are included the simulation results are expected to be largely consistent.

Model sensitivity simulations indicated that there is a consistency between the simulations of the discharge plume with the exception of the cases with less lateral pre-dilution in the near-field plume. This suggests dilution that is offered by the momentum associated with the discharge water (as it travels out from the vessel and entrains ambient fluid) is an important process in limiting the extent of the temperature decrease and chlorine concentration on the seabed.

Re-simulating the release and entrainment of particles from a select number of zones using alternative model configurations produced some notable differences. The higher velocity configuration produced larger initial entrainment rates for zones near to Crib Point. After the initial periods the entrainment slows as the particles are dispersed more rapidly. For zones further from Crib Point the simulated differences between the different configurations of the model become less. However, it should be noted that the higher velocity model configuration, whilst informative, produces velocities and tidal excursions that are significantly higher than observed and thus less reliable than the other configurations in terms of accuracy of predictions.

Results from sensitivity tests with different initial spatial distributions of particles and output frequency showed a similar range of results as simulations with the same configurations but different initial particle distributions.

10.5 Discharge Scenarios

Additional discharge scenarios were assessed for closed loop discharges, ballast water and the impact of an unloading LNG vessel moored beside the FSRU.

The outcomes of these scenarios are described in Chapter 6 to 8.

11 References

- Batley, G. and Simpson, S. 2019. Behaviour and regulation of chlorine in waters associated with the AGL Gas Import Jetty Project. CSIRO Report No. EP192435. Prepared for CEE Pty Ltd.
- Bothelo, D. and Imberger, J., 2007. *Dissolved-oxygen response to wind-inflow interactions in a stratified reservoir*. Limnology and Oceanography, vol. 52 (5), pp. 2027 – 2052.
- Cardno, Hydrodynamics - Second Container Port Advice. Report prepared for Infrastructure Victoria, May 2017.
- CEE, 2018a, AGL Gas Import Jetty Project Crib Point, Western Port: Plume Modelling of Discharge from LNG Facility, Prepared for Jacobs Group (Australia) Pty Ltd.
- CEE, 2018b, AGL Gas Import Jetty Project Crib Point, Western Port: Modelling and Assessment of Biological Entrainment into Seawater Heat Exchange System, Prepared for Jacobs Group (Australia) Pty Ltd.
- CEE, 2018c, AGL Gas Import Jetty Project Crib Point, Western Port: Chlorine in seawater heat exchange process at Crib Point, Prepared for Jacobs Group (Australia) Pty Ltd.
- CEE, 2018d. Chlorine in FSRU Seawater Processes - AGL Gas Import Jetty and Pipeline Project. Report for AGL.
- Chan, T., Hamilton, D., Robson, B., Hodges, B. and Dallimore, C., 2002, *Impacts of hydrological changes on phytoplankton succession in the Swan River, Western Australia*. Estuaries, 25(6B): 1405-1415
- Cinque K., Okely P. and Yeates P., 2018. *Hydrodynamic and sediment modelling to forecast seagrass coverage and recovery in Western Port*. In: Understanding the Western Port Environment 2018 - A summary of research findings from the Western Port Environment Research Program 2011-2017 and priorities for future research, Melbourne Water.
- Dallimore, C., Hodges, B. and Imberger, J., 2003. *Coupling and underflow model to a three-dimensional hydrodynamic model*. Journal of Hydraulic Engineering, 129 (10), pp. 748 – 757.
- Harrison S., Black K., Bosserelle C. and Lee R., 2011. *Port Phillip and Western Port receiving water quality modelling: hydrodynamics*. ASR technical report 2007-EPA1. Published as EPA publication No. 1377.
- Hancock G., Olley J. and Wallbrink P., 2001. *Sediment transport and accumulation in Western Port*. Report on Phase, 1. CSIRO Land and Water Technical Report 47/01.
- Hillmer, I. and Imberger, J., 2007. *Influence of advection on scales of ecological studies in a coastal equilibrium flow*. Continental Shelf Research, 27 (1), pp. 134-153
- Hinwood J. and O'Brien, 1974. *Water Quality Mathematical Model Volume 1 – Theory*. Prepared for the Westernport Bay Environmental Study.
- Hinwood J., 1979. Hydrodynamic and transport models of Western Port, Victoria. Marine Geology, Vol. 30, 117–30.

- Hodges, B., Imberger, J., Saggio, A. and Winters, K., 2000. *Modeling basin-scale internal waves in a stratified lake*. Limnology and Oceanography, 45 (7), 1603 – 1620.
- Hughes, A., Prosser, I., Wallbrink, P. and Stevenson, J., 2003. *Suspended sediments and bedload budgets for the Western Port Bay Basin*. Technical Report 4/03, CSIRO Land and Water.
- Hurst T, 2018. *Restoration of temperature mangrove ecosystem*. PhD Thesis, Deakin University.
- Hydronumerics, 2016. Western Port SEPP Loads Modelling Strategy, Development and Scenarios. Technical report prepared for EPA Victoria.
- Lee R., 2011. Chapter 4, Physical and chemical setting. In: Understanding the Western Port Environment: a summary of current knowledge and priorities for future research. Melbourne Water Corporation.
- Marsden M., Mallett C. and Donaldson A., 1979. Geological and Physical Setting, Sediments and Environments, Western Port, Victoria. Marine Geology, 30:11-46.
- Marsden, M. and Mallett, C., 1974. *Morphology and sediment distribution, Western Bay*. Prepared for the Westernport Bay Environmental Study.
- Melbourne Water, 2011. Understanding the Western Port Environment – A summary of current knowledge and priorities for future research. Melbourne Water.
- Romero, J., Antenucci, J. and Imberger, J., 2004. *One- and three-dimensional biogeochemical simulations of two differing reservoirs*. Ecological Modelling, 174 (1 – 2), pp. 143 – 160.
- Royal HaskoingDHV, 2019. Current Monitoring Crib Point: ADCP Deployment and Data Analysis. Draft report prepared for AECOM.
- Shapiro, 1975. *Westernport Bay Environmental Study 1973-1974*. Ministry for Conservation, Victoria, Australia.
- Silva, C., Marti, C. and Imberger, J., 2014. *Physical and biological controls of algal blooms in the Río de la Plata*. Environmental Fluid Mechanics, 14, pp. 1199-1228
- Spillman, C., Imberger, J., Hamilton, D., Hipsey, M. and Romero, J., 2007. Modelling the effects of Po River discharge, internal nutrient cycling and hydrodynamics on biogeochemistry of the Northern Adriatic Sea, Journal of Marine Systems, 68 (1-2), pp. 167-200.
- Symonds A., Vijverberg T., Post S., van der Spek, B., Henrotte, J. and Sokolewicz M. *Comparison between MIKE 21 FM, DELFT3D and DELFT3D FM flow models of Western Port Bay, Australia*. Coastal Engineering Conference, 2016.
- Wallbrink P., Martin C. and Wilson C., 2003. Quantifying the contributions of sediment, sediment-P and fertiliser-P from forested, cultivated and pasture areas at the landuse and catchment scale using fallout radionuclides and geochemistry. Soil and Tillage Research. 69, pp. 53-68.